Title
Spin Torques in Magnetic and Superconducting Tunnel Junctions

Author
Hoffman, Silas Eli

Publication Date
2012

Peer reviewed|Thesis/dissertation

University of California

Los Angeles

Spin Torques in Magnetic and Superconducting Tunnel Junctions

A dissertation submitted in partial satisfaction

of the requirements for the degree

Doctor of Philosophy in Physics

by

Silas Hoffman

2012

Abstract of the Dissertation

Spin Torques in Magnetic and Superconducting Tunnel Junctions

by

Silas Hoffman

Doctor of Philosophy in Physics

University of California, Los Angeles, 2012

Professor Yaroslav Tserkovnyak, Chair

The main text is presented in four parts. In chapter 2, we develop a phenomenological theory of voltage induced torques in magnetic tunnel junctions. The reciprocal of this effect and spin-transfer torque can pump charge into an attached circuit when the magnet precesses. We calculate the resulting change in impedances due to this pumping as a function of applied magnetic field and thickness of tunneling spacer. Because the impedances due to voltage and current pumping are qualitatively distinct under variation of the magnetic field, we suggest that this measurement could be used as experimental differentiation between these effects.

In chapter 3 we study magnetic Josephson junctions wherein spin polarized Ohmic and supercurrent exert a torque on the magnetic layer. As a result, there is a nonlinear dynamic interplay between the magnetic order parameter and the phase of the superconducting parameter. This results in a modified stability diagram for both the magnet and superconductor. In particular, we find a non-monotonic dependence of the critical current on the applied magnetic field and current. When the temperature is raised above the superconducting critical temperature, the leads become metallic and the equations of motion coincide with those of chapter 2.

In contrast to the monodomain models studied in other chapters, chapter 4 examines the effects of micromagnetics on the thermal stability of a typical MRAM bit. In addition to noting that a finite stiffness parasitically effects bit stability, we find that domain-wall nucleation and propagation is the dominant mode of thermal bit flipping.

Finally, in chapter 5 we derive a nonequilibrium expression for spin current between two magnetic leads biased by voltage, temperature or spin. The interaction on the dot is left general and the equation for current can be written as a function of the full retarded Green's function on the dot. We apply this methodology to a dot with large on-site Coulomb interaction.

The dissertation of Silas Hoffman is approved.

Alexander Levine

Sudip Chakravarty

Stuart Brown

Louis Bouchard

Yaroslav Tserkovnyak, Committee Chair

University of California, Los Angeles

2012

To my father for his encouragement and my mother for telling me it's not a stick.

Table of Contents

List of Figures

Acknowledgments

I am grateful to my advisor, Yaroslav Tserkovnyak, who guided me to becoming a better scientist through endeavor, persistence, and intellect. His countless hours of helping me revise and edit contributed to the bulk of this manuscript and my ability to write. Without his patience to guide and mentor, I fear that this day work would not come to fruition.

Vita

2004	B.Sc., Physics University of Illinois at Urbana-Champaign
2004–2010	Teaching Assistant University of California, Los Angeles
2007	M.Sc., Physics University of California, Los Angeles

Publications

S. Hoffman, Ya. Blanter, and Y. Tserkovnyak, "Nonlinear dynamics in a magnetic Josephson junction," *Phys. Rev. B* **86**, 054427 (2012)

S. Hoffman, Y. Tserkovnyak, P. K. Amiri, and K. L. Wang, "Magnetic bit stability: Competition between domain-wall and monodomain switching," *Appl. Phys. Lett.* **100**, 212406 (2012)

CHAPTER 1

Introduction

1.1 Preliminaries

According to the standard model of particle physics, there are three forces that mediate the interaction between twelve elementary particles. Owing to the abundance and experimental accessibility, we focus on a single particle, the electron. The charge and spin of the electron facilitate the detection and manipulation by both electric and magnetic potentials. This interplay between magnetism and electricity and charge and spin induce equilibrium and nonequilibrium interactions that engender a utilitarian and academic study of electrons and is the focus of this manuscript.

In chapter 2 we detail our work on current and voltage induced torques in magnetic tunnel junctions. Charge current can be magnetically polarized due to the exchange interaction separating the majority and minority bands in a magnet [Slo96, Ber96]. Likewise, passing current through a magnetic layer in the presence of spin-orbit interaction induces a torque proportional to the current and strength of the interaction [MZ08, COL09, HBT10]. These effects are can induce flipping of a bistable ferromagnet and therefore have become increasingly important for information storage in computing applications. A major inspiration for the work in chapter 2 was the discovery that voltage, in the absence of current, can likewise induce a torque on ferromagnets in magnetic tunnel junction. We propose two distinct phenomenological models that individual examine these effects and cal-

culate the corresponding reciprocal of these torques whereby magnetic dynamics pumps electrons through our circuit, shifting the impedance. When superconducting rather than normal metal leads are used, such as in a Josephson junction, the magnet can effectively pump and thereby manipulate phase in addition to charge. The resulting nonlinear coupling between magnet and superconductor is studied in chapter 3. We find that magnetic dynamics can induce a "foldover region" where superconductor has multiple critical currents.

In many applications a single domain magnetic model is sufficient to capture the essential physics of a magnet. However when the exchange energy is comparable to the dipole interaction, the effect of magnetic texture must be taken into account. Although micromagnetics are sometimes the focus of study (e.g. skyrmion lattices, domain-walls, etc.), they often become an added complication in developing nanomagnets for memory storage applications. To this end, we consider the effect of micromagnetics on the robustness of a bit against thermal fluctuations in chapter 4. We find that the formation and propagation of a domain-wall is energetically (and therefore thermally) advantageous as compared with coherent monodomain switching.

As made apparent by the Born-Van Leeuwen theorem quantum mechanics is essential for the existence of ferromagnetism. When the spin of the magnets is large, the quantum fluctuations are obscured. In these cases, as in much of this work, the magnet is treated as a macroscopic parameter. However in the microscopic regime, correlation and tunneling effects must be taken into account. This is the primary topic considered in chapter 5. This study was initiated by the experimental data indicating an anomalously large exchange interaction between two ferromagnets separated by an insulating layer [FTB02]. The exchange interaction is known to be mediated by the equilibrium spin current and could naturally be enhanced by an impurity, as modeled by a quantum dot, in the insulating region [ZTV05, ZVV06]. To this end, we calculate the equilibrium spin

current between two canted leads separated by an intermediate quantum dot. We extend this treatment to the nonequilibrium regime and obtain an expression for spin and charge current under voltage, temperature, or spin bias.

Although this document is not fundamentally pedagogical, we hope it can be used as a reference and stimulant for future spintronics research. We will spend the remainder of the introduction setting the stage for the aforementioned subjects while motivating the necessity of their study. In Sec. 1.2 we introduce equilibrium and dynamic properties of ferromagnets. We discuss the basic properties of Josephson junctions and the effect of ferromagnets in proximity to superconductors in Sec. 1.3. We conclude the introduction in Sec. 1.4 by reviewing Keldysh formalism necessary to construct nonequilibrium tunneling currents.

1.2 Magnetoelectronics

1.2.1 Energetic considerations

In determining the equilibrium direction of a magnet, there are typically four interactions that one must take into account: external magnetic field, magnetocrystalline anisotropy, exchange interaction between micromagnetic domains, and dipole-dipole interactions. Each of these interactions compete to form a configuration that minimize the free energy F of a magnet. The direction of equilibrium magnetization is along the effective magnetic field, determined by the functional derivative of the free energy with respect to the magnetization, $\mathbf{M}$, $\mathbf{H}^{\text{eff}}(\mathbf{x}) = -\mathcal{V}^{-1}\partial F/\partial \mathbf{M}(\mathbf{x})$ with $\mathcal{V}$ the volume of the magnet. Magnetocyrstalline anisotropy is induced by the spacial anisotropy of the crystalline structure coupled to magnetic domains by the spin-orbit interaction. Because the ferromagnetic crystalline structures are periodic on the scale of the lattice, which is often much smaller than the size of a magnet, the magnetocyrstalline anisotropy is regarded as a function of local magnetization. The exchange interaction describes the ten-

dency for neighboring magnetic domains to align parallel in a ferromagnet and antiparallel in an antiferromagnet. As this interaction increases, the energy cost to align in a different direction from micromagnetic neighbors increases and the magnetic configuration tends to a single domain. In contrast to the first two short range energy contributions, the dipole-dipole interaction reflects the magnetic dipole of the individual domains interacting with the overall magnetization over long distances. Summing the energy of these interactions determines the magnetic contribution to the free energy (in CGS units)

$$F[\mathbf{M}] = -\int \mathrm{d}^3\mathbf{x}\mathbf{M}(\mathbf{x})\cdot\mathbf{H}_a - \frac{K_u}{2}\int \mathrm{d}^3\mathbf{x}(\mathbf{M}(\mathbf{x})\cdot\mathbf{n})^2 + \frac{A_{\mathrm{xc}}}{M_s^2}\int \mathrm{d}^3\mathbf{x}(\nabla\mathbf{M}(\mathbf{x}))^2 - \frac{1}{8\pi}\int \mathrm{d}^3\mathbf{x}\int \mathrm{d}^3\mathbf{x}'\mathbf{M}(\mathbf{x})\cdot\frac{3(\mathbf{M}(\mathbf{x}')\cdot(\mathbf{x}-\mathbf{x}'))(\mathbf{x}-\mathbf{x}') - \mathbf{M}(\mathbf{x}')|\mathbf{x}-\mathbf{x}'|^2}{|\mathbf{x}-\mathbf{x}'|^5}, \tag{1.1}$$

where $\mathbf{H}^a$ is an external magnetic field, K_u is the uniaxial crystalline anisotropy constant along $\hat{\mathbf{n}}$, and A_{xc} is the exchange constant or stiffness. The atomic energies responsible for the splitting of majority and minority bands of the electrons is large compared to the above energies and therefore the magnitude of $\mathbf{M}(\mathbf{x})$ is taken to be constant. We often use to the unit direction of the magnetic field $\mathbf{m} = \mathbf{M}/M_s$ where M_s is called the magnetic saturation.

The competition between long and short range order engenders equilibrium configurations that depend on the size of the magnetic structure. Long range order tends to align magnetic domains antiparallel with respect to each other due to the magnetostatic field. Conversely, neighboring micromagnetic domains minimize the exchange interaction when aligned parallel to eachother. The onset of inhomogeneous magnetization typically occurs when the length of the structure is larger than $\lambda = \sqrt{A_{\mathrm{xc}}/4\pi M_s^2}$ (i.e., when the exchange energy and magnetostatic energy are comparable). The mediation region patching together two domains of opposite magnetization is known as a domain-wall. There are several types of domain-walls. In thin films the orientation tends to remain in-plane. When the

major and minor axes of the cross section are comparable to λ, a vortex forms to connect the two regions of opposite magnetization. If the cross section is elliptical with one dimension larger than λ, a Néel wall can form in which the texture rotates 180° in the plane of the ellipse between the domains. The formation of domain-walls may be energetically favorable. We discuss the equilibrium generation of a Néel wall in an elliptical magnetic and the effect on thermal stability in chapter 4.

Owing to the complexity of multidomain structures and ensuing many body problem of interaction via the magnetostatic field, equilibrium micromagnetic configurations are difficult to determine analytically except in the simplest cases. Many physical effects can be analyzed in the single domain limit wherein the exchange stiffness is infinite, locking all magnetizations parallel to one another. The magnetostatic energy takes a particularly simple form $(N_x M_x^2 + N_y M_y^2 + N_z M_z^2)\mathcal{V}$ where $N_x + N_y + N_z = 4\pi$, known as demagnetization factors, are shape dependent anisotropies. For example, in the case of a thin film, these reflect the tendency of magnetization to orient in the plane of the film and along the major axis of non-circular samples. This monodomain limit will be used ubiquitously in chapter 2 and chapter 3.

When a magnet is attached to an external circuit, voltage can induce anisotropy [WFM07, MSN09]. In lieu of any ab initio calculation of this effect, the prevailing understanding is that an electric field across the junction causes an excess of electrons at the interface which populate the $3d$ orbital [MSN09]. This results in a magnetic anisotropy if a spin-orbit interaction is present at the surface of the magnet. In addition, there is likely some reshuffling and hybridization of orbitals that enhances this effect. The strength of this voltage controlled anisotropy can compete with and overpower the above free energy contributions, as to bring an in-plane equilibrium magnetization out-of-plane. The free energy is proportional to Qm_z^2 where Q is the charge residing on the interface of the magnet. This is our first example of magnetoelectric torques, that is a torque exerted on the magnet

as a result of the circuit. In chapter 2, we investigate the Onsager reciprocal of this torque, charge pumping induced by dynamic magnetization, and calculate the change in ac impedance of the circuit.

1.2.2 Magnetization Dynamics

Because the magnitude of the magnetization is held constant, the time evolution of the magnetic configuration away from equilibrium must be perpendicular to the instantaneous direction. In the absence of dissipation, the second law of thermodynamics requires that $\dot{\mathbf{M}} \cdot \mathbf{H}^{\text{eff}} = 0$, where $\dot{G} \equiv dG/dt$ for any function G. The magnet thus precesses around the effective field along constant energy contours according to $\dot{\mathbf{M}} \sim \mathbf{M} \times \mathbf{H}^{\text{eff}}$. Damping must bring the system back to the equilibrium configuration, parallel to $\mathbf{H}^{\text{eff}}$, and has two mathematically equivalent expressions formuated by Landau and Lifshitz [PL80] and Gilbert [Gil04]. Using the damping proposed in the latter, the equation of motion of a magnetic configuration is

$$\dot{\mathbf{M}} = -\gamma \mathbf{M} \times \mathbf{H}^{\text{eff}} + \frac{\alpha}{M_s} \mathbf{M} \times \dot{\mathbf{M}}\,, \tag{1.2}$$

known as the Landau-Lifshitz-Gilbert (LLG) equation. Here γ is the electron gyromagnetic ratio and α quantifies the strength of the damping. Because the damping is perpendicular to the direction of motion and $\mathbf{M}$, for $\alpha > 0$ the magnet is torqued towards $\mathbf{H}^{\text{eff}}$, decaying to the equilibrium position as expected.

Application of spin current to a magnet induces a torque when the polarization of the current and magnet are misaligned. The filtering of the spin current through the magnet, transfers a net angular momentum and rotates the magnet. This phenomena, known as spin-transfer torque, was predicted independently by Slonczewski [Slo96] and Berger [Ber96]. In the approach by Slonczewksi [Slo05], one static magnet, $\mathbf{M}_s$, and one free magnet, $\mathbf{M}_f$ are oriented at angle θ with respect to each other. By Fermi's golden rule, one may calculate the spin current

transferred between the leads. The difference between the spin transferred from one lead to the other determines the torque on the magnet to be proportional to $\mathbf{M}_f \times \mathbf{M}_s \times \mathbf{M}_f$. The dynamics of the magnet are now governed by the LLG equation plus spin-transfer torque

$$\dot{\mathbf{M}} = -\gamma \mathbf{M} \times \mathbf{H}^{\text{eff}} + \frac{\alpha}{M_s} \mathbf{M} \times \dot{\mathbf{M}} + \frac{\mu I}{M_s} \mathbf{M} \times \mathbf{m}_s \times \mathbf{M}\,, \tag{1.3}$$

where μ depends on the magnetic and geometric properties of the leads and $\mathbf{m}_s$ is the direction of the polarized current.

This torque can induce magnetic precession and reversal. To illustrate this, consider a single domain magnetic rod along the z axis with no crystalline anisotropy. In the absence of an external applied field, the effective field becomes $\mathbf{H}^{\text{eff}} = 4\pi M_z \mathbf{z}$ where M_z is the component of the magnet along the z axis. When no spin current is incident on the magnet, there are two bimodal stable configurations along the z axis. Flipping occurs when one of these fixed points in the differential equation becomes unstable (i.e., when the spin-torque overcomes the geometric anisotropy). One can show that the equation of motion of the magnet projected along the z axis is

$$(1+\alpha^2)\dot{M}_z = \mathbf{z} \cdot \left(\frac{4\pi\alpha\gamma M_z}{M_s} \mathbf{M} \times \mathbf{z} \times \mathbf{M} + \frac{\mu I}{M_s} \mathbf{M} \times \mathbf{z} \times \mathbf{M} \right). \tag{1.4}$$

Because $\mathbf{z} \cdot \mathbf{M} \times \mathbf{z} \times \mathbf{M}$ is positive, the equilibrium position is determined by the magnitude and sign of the current. That is, when the magnet is oriented along the z axis, $\mathbf{m} = \mathbf{z}$ is no longer stable if for a negative applied current $\mu|I| > 4\pi\alpha\gamma$. Any infinitesimal fluctuation will thereby flip the orientation of the magnet. Similar arguments can be made when the magnet is in the opposite orientation.

Because applying a current can induce magnetic dynamics, magnetic dynamics can likewise induce current. For instance suppose in a system of two ferromagnets, one is subjected to a microwave field, inducing FMR precession. A net spin and charge will be transferred through the circuit as a result of this precession

[TBB05]. This contribution to current can be calculated microscopically, however, the form of the pumping can be immediately determined from reciprocity considerations to be proportional to $\mu\dot{\mathbf{m}} \cdot \mathbf{m} \times \mathbf{m}_s$ as discussed in chapter 3. In that chapter we further extend spin torque on the magnet due to ohmic currents to superconducting currents. In addition to pumping current the system is analogously able to pump phase. This coupling allows for manipulation of the magnet by the superconducting order and vice versa.

1.3 Josephson Junctions

The microscopic description of superconductivity is well accounted for by the theory put forth by Bardeen, Cooper, and Schrieffer (BCS theory) but is complicated when the condensate function is spatially inhomogeneous. A simple macroscopic alternative, valid at temperatures near but below the critical temperature, is the Ginzburg-Landau theory [PL80]. The formulation of this theory is derived under the same considerations of the general theory of phase transitions. One useful application of Ginzburg-Landau is to the case of a Josephson junction, wherein two superconductors are separated by a non-superconducting interlayer. The two signature effects in such a junction, the dc and ac Josephson effect, were predicted by their namesake Brian Josephson. The dc Josephson effect predicts that when there is a difference in phase between the superconducting wave functions in two superconductors, a supercurrent proportional to the sine of the difference in phases will flow between them. The ac Josephson effect states that the time derivative of the phase difference is proportional to the voltage difference between the junctions. Underlying these physical effects is a wealth of properties as a result of the highly nonlinear interplay between supercurrent, ohmic current, and displacement current. Below we describe the basic framework of Josephson junctions that is most relevant for the discussion in later chapters. An exhaustive description of

effects can found in [Lik86].

1.3.1 Derivation of GL theory and josephson current

The Ginzburg-Landau free energy is a phenomonological, macroscopic treatment of the superconductor derived from a general model of second order phase transitions. The philosophy is to write the free energy as a function of a classical order parameter, ψ called the pseudowavefunction, which at some finite critical temperature is minimized at a nonzero value. The gap of a superconductor, Δ, characterizes the coherence of a Cooper pair and thus a nonzero value signifies a phase transition to superconducting order. Although it is natural to identify ψ with the gap, it is normalized to the density of superconducting electrons[1], i.e. Cooper pair density, and therefore proportional to the gap. The superconducting contribution to the free energy near the critical temperature is

$$F[\psi] = \int \mathrm{d}V a|\psi|^2 + \frac{b}{2}|\psi|^4 + \left|\left(\nabla - \frac{2ie}{\hbar c}\mathbf{A}\right)\psi\right|^2 , \tag{1.5}$$

where b, which must be greater than zero for finite ψ, and $a \sim (T - T_c)$, T_c the critical temperature, are phenomenological coefficients and $\mathbf{A}$ the vector potential. e and m are the (dressed) electron charge and mass, respectively. When the temperature is above the critical temperature, $\psi = 0$ minimizes the free energy. Below this temperature, the gauge symmetry is broken and the pseudowavefunction acquires a nonzero value resulting in a finite gap. Varying with respect to the vector potential gives the probability current and the associated boundary condition

$$\begin{aligned} \mathbf{j} &= -\frac{ie\hbar}{2m}(\psi^*\nabla\psi - \psi\nabla\psi^*) - \frac{2e^2}{mc}|\psi|^2\mathbf{A}\,, \\ \mathbf{n}\cdot\left(-\hbar\nabla - \frac{2e}{c}\mathbf{A}\right)\psi &= 0\,, \end{aligned} \tag{1.6}$$

[1]The wording of "superconducting electrons" is somewhat ambiguous as the nomenclature is a relic from the superfluid description where the number of bosons in the ground state per volume corresponds to the density of superfluid bosons.

where $\mathbf{n}$ is the vector normal to the surface of the body.

A natural application of these expressions is to two slabs of the same metal, below their critical temperature, separated by insulator . For a sufficiently thin barrier, the probability that the condensate wave functions overlap is finite. This facilitates the flow of supercurrent, I_s even in the absence of bias, i.e. in equilibrium. Because the leads are the same material at the same temperature, the magnitude of the gap is the same and the pseudowavefunctions in the leads, ψ_L and ψ_R, differ only by a phase. As the left and right leads would be identical if the phases were equal, the current must be proportional to their difference in phases, $\phi = \phi_L - \phi_R$. Changing ϕ by an integral multiple of 2π is physically indistinguishable and therefore the current must be periodic in phase difference. Because current and phase both change sign under time reversal, equilibrium supercurrent must be an odd function of the phase difference. These conditions require the supercurrent to take the form $I_S = I_c \sin\phi + \sum_{n=2}^{\infty} I_n \sin n\phi$. Using Eq. 1.6, all but the first term in the current is zero and we ultimately arrive at the dc Josephson effect

$$I_S = I_c \sin\phi \,, \tag{1.7}$$

where the critical current, $I_c \sim |\psi|^2$, is the maximum supercurrent through this junction.

When there is a difference in voltage between the two leads, V, the phase acquires time dependence. To understand this, consider a gauge transformation under which the scalar potential transforms $V \to V - (1/c)\dot{\chi}(t)$ and $\phi \to \phi + (2e/\hbar c)\chi(t)$. The ac Josephson effect is a gauge invariant combination of these two quantities that respects the dc Josephson effect in the absence of voltage (i.e. $\dot{\phi} = 0$ when $V = 0$)

$$\dot{\phi} = \frac{2e}{\hbar} V \,. \tag{1.8}$$

Substituting this expression into Eq. 1.7, results in $I_S = I_c \sin[(2e/\hbar)Vt]$. Hence, the supercurrent acquires an alternating current component with frequency $(2e/\hbar)V$

when a voltage difference is applied between the leads.

1.3.2 Characteristics of the Resistively Shunted Junction

In general, the supercurrent is only part of the contribution to the overall current. There are three essential additional currents: normal current, displacement current, and fluctuating current. The normal current is the result of the quasiparticle tunneling across the insulating interlayer and is written following ohms law $I_N = \sigma V$ where σ is the normal conductance of the junction. If a potential difference applied to the leads is much greater than the gap, it is energetically favorable for the Cooper pairs to break into quasiparticles and the ohmic current dominates over the supercurrent. Displacement current in a Josephson junction, $I_D = C\dot{V}$, is the same above and below the critical temperature. The capacitance, C, is determined by the geometry of the structure. The dimensionless parameter $\beta \equiv (2e/\hbar)(I_c C/\sigma^2)$, known as the Stewart-McCumber parameter, determines the relative importance of the displacement current to the normal current. Junctions with $\beta \ll 1$ are called high damping, whereas when $\beta \gg 1$ are referred to as low damping. The final contribution to the current, I_F, represents any noise present in the system, e.g. thermal noise or shot noise. The total current through the junction is thus given by the sum of the individual currents

$$I = I_S + I_N + I_D + I_F \,. \tag{1.9}$$

Supplementing this with Eq. 1.8, the current-voltage relation of the Josephson junction can be determined.

Because the exact description of a Josephson junction for an arbitrary set of parameters is unknown, simplifying approximations are accordingly made. A rather general description of the current through the circuit known as the Tunnel-Junction-Microscopic (TJM) is determined from the microscopic Green's function of BCS theory. Although this model captures nearly all of the physical nuances of

a Josephson junction, there is no exact analytic solution and numerical methods are computational intensive. A major simplification may be made in a narrow range of temperatures in which the current is taken to be energy independent. This is the case in the Resistively Shunted Junction (RSJ) model which takes the simplest expressions for the contributions to the current and is modeled by the equation

$$I = \frac{\hbar}{2e}\left(C\ddot{\phi} + \sigma\dot{\phi}\right) + I_c \sin\phi + I_F\,, \tag{1.10}$$

along with the ac Josephson effect. As this is the primary model for our interest, we detail some basic properties below in the absence of stochastic processes ($I_F = 0$).

First consider the case when the dc current through the circuit is less than critical current, $|I| < I_c$. Eq. 1.10 allows solutions for stationary ϕ given by

$$\begin{aligned} \phi_0 &= \sin^{-1}\frac{I}{I_c} + 2\pi n\,, \\ \phi_\pi &= \pi - \sin^{-1}\frac{I}{I_c} + 2\pi n\,, \end{aligned} \tag{1.11}$$

where n is integer. Because all of the equations in the RSJ model are invariant under 2π translations of ϕ, all ϕ_0 solutions are equivalent and we choose $n = 0$ without loss of generality. This is likewise true for ϕ_π. In the literature, a junction with $\phi = \phi_0$ is a 0-junction and $\phi = \phi_\pi$ is a π-junction. According to the ac Josephson effect, if ϕ is constant there is no voltage across the junction, $\dot{\phi} = V = 0$. This state is thus referred to as the stationary state, superconducting state, or simply the S state. The differential equation defined in Eq. 1.10 is equivalent to a particle of mass $(\hbar C/2e)$ at position ϕ with damping $(\hbar\sigma/2e)$ in a potential $U(\phi)$ corresponding to the energy stored in the junction.[2] In this picture, the

[2]In the absence of applied current, Eq. 1.10 also maps identically onto the equation of motion for a pendulum excited at an arbitrary angle away from equilibrium.

nomenclature of low and high damping in the large and small limits, respectively, of Stewart-McCumber parameter is now transparent. The potential can be found by integrating the associated power of the circuit over time

$$\begin{aligned} U(\phi) &= \int (I_S + I) V \mathrm{d}t = \frac{\hbar}{2e} \int (I_S + I) \dot{\phi} \mathrm{d}t = \frac{\hbar}{2e} \int (I_S + \sin\phi) \mathrm{d}\phi \,, \\ &= -E_c \cos\phi + \frac{\hbar}{2e} I\phi + \text{const.} \,, \end{aligned} \tag{1.12}$$

where $E_c \equiv (\hbar/2e) I_c$. The superconducting phase is in a "washboard" potential in which ϕ_0 are minimums and ϕ_π are maximums. Thus when $|I| < I_c$, 0-junctions are stable and π-junctions unstable. As the current is slowly increased from 0, the cosinosoidal potential tilts, such that the potential barrier between consecutive minimum decreases until $I = I_c$. At this point, the derivative of the potential at $\phi = \pi/2$ is zero and neither ϕ_0 nor ϕ_π are stable. This is the onset of the resistive (R) state of the superconductor where the phase difference is no longer stationary, inducing a finite voltage and therefore an ohmic current.

When the dc current exceeds the critical current, $|I| > I_c$, the maximum supercurrent is not sufficient to transport charge across the circuit and must be supplemented by ohmic current. The dynamics are, in general, difficult to characterize and therefore we consider the low and high damping limits. When $\beta \to 0$, Eq. 1.10 reduces to

$$I = \frac{\hbar\sigma}{2e} \dot{\phi} + I_c \sin\phi \,, \tag{1.13}$$

which admits an exact solution

$$\phi(t) = 2 \tan^{-1} \left(\sqrt{\frac{I - I_c}{I + I_c}} \tan \frac{\omega_J t}{2} \right) - \frac{\pi}{2} \,. \tag{1.14}$$

The characteristic frequency of oscillation, $\omega_J = (2e/\sigma\hbar)\sqrt{I^2 - I_c^2}$ when $|I| > I_c$ and zero otherwise, determines the current-voltage relation as $\bar{V} = (\hbar/2e)\omega_J$ where the bar denotes the average voltage. Near the critical current, the voltage across the junction is small and the current is primarily transported by the superconducting component. When $I \gg I_c$, the current-voltage relation is nearly linear

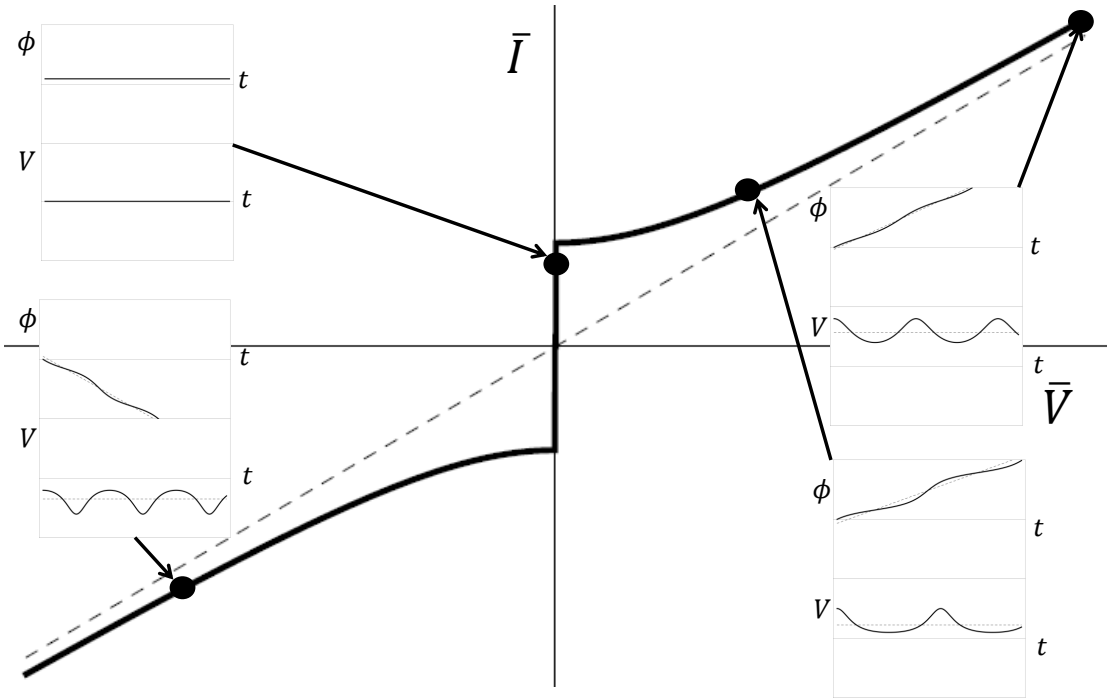

Figure 1.1: Schematic graph of the current-voltage relation for in the RSJ model (solid line) that approaches an ohmic current-voltage relation (dashed line) for large voltage. Insets show oscillations of voltage and phase as a function of time for various values of current indicated on the curve.

reflecting the almost entirely dissipative nature of the current. In the high damping limit, the inertia of the phase is very low. Regardless of the initial conditions, if a minimum of the potential exists (i.e. $|I| < I_c$) the phase will eventually relax into an S state. When the current exceeds the critical current no minimums exist and the superconductor is in the R state. We graph the current-voltage relation as well as the time dependence of the phase and voltage for representative currents in Fig. 1.1.

Conversely, in the limit of small damping $\beta \gg 1$, the inertia of the phase is very large. For current finite but smaller than the critical current, the periodic potential $U(\phi)$ is titled but there still exist local minimums. Suppose that the current is sufficiently large so that the energy lost due to damping is compensated by the change in potential energy, $U(\phi + 2\pi) - U(\phi) \sim -2\pi I$. If the initial energy of the system is large enough to overcome the barrier separating consecutive minimums, the phase will slide down the potential indefinitely. Otherwise, the phase will relax into a minimum as in the high damping case. Thus, in the low damping limit, we may realize both an S state and R state for currents less than the critical current. This coexistence of two states at the same current results in a hysteretic current-voltage relation. The phase portraits of the RSJ equation, Fig. 1.2, illustrate the properties of the high and low damping RSJ models.

1.3.3 Proximity Effects at Superconducting Interfaces

When a superconductor is brought into contact with a normal (non-magnetic) metallic material, the properties of both can change. This is known as the proximity effect. For instance, leakage of Cooper pairs into the normal material can induce superconducting correlations on the metallic side. This results in a decrease in the density of states in the metal and, similarly, a decrease in the density of Cooper pairs on the superconducting side which decreases the critical temperature. In the range of validity of the Ginzburg-Landau equations, the penetration

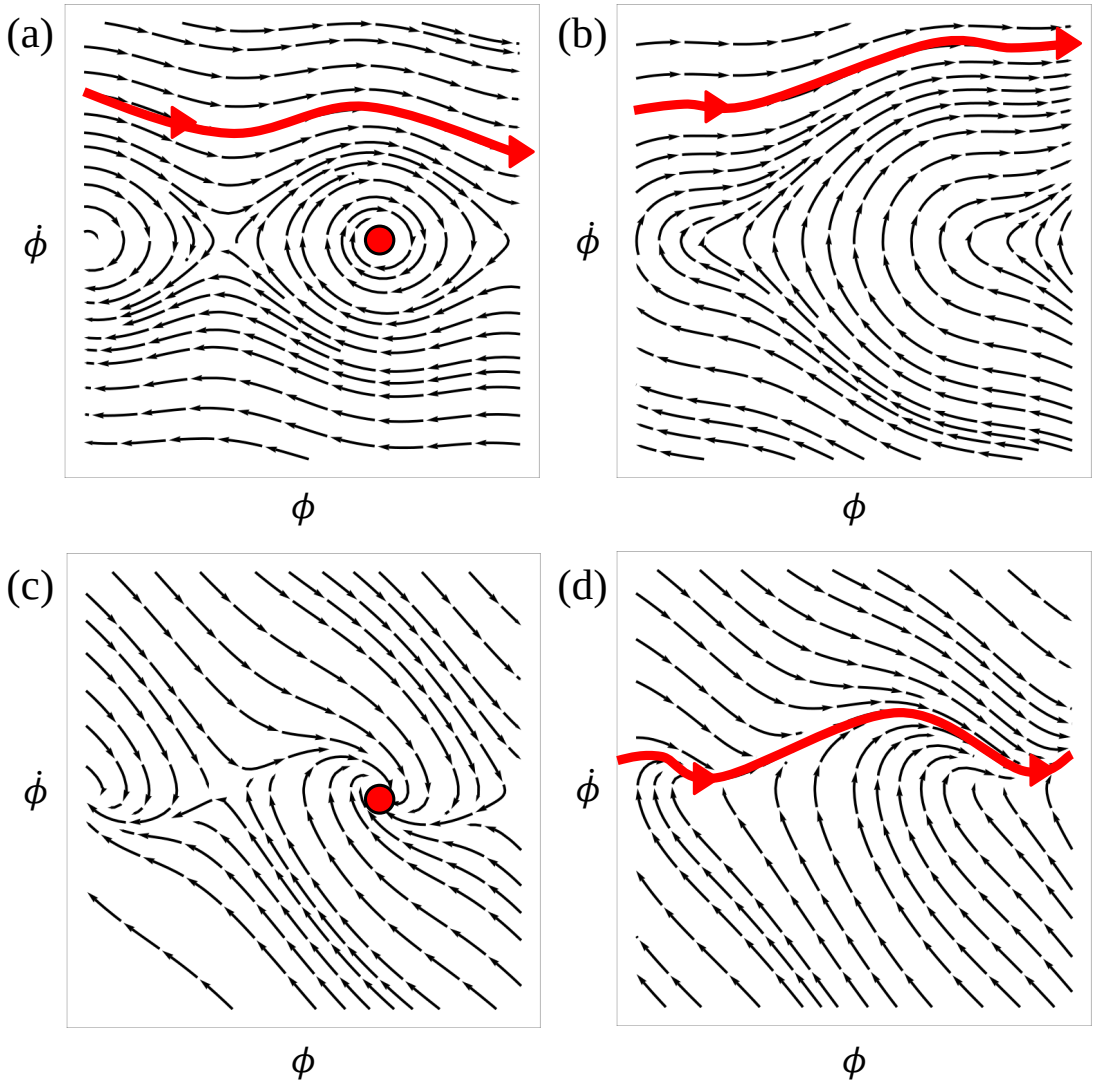

Figure 1.2: Phase portrait of RSJ model in the low damping limit when $I_c < I$ (a), the low damping limit when $I_c > I$ (b), the high damping limit when $I_c < I$ (c), and the high damping limit when $I_c >$ (d). The red dots indicate stable fixed points and red lines stable trajectories. Notice in particular the coexistence of a stable fixed point (S state) and trajectory (R state) in the low damping limit.

of the Cooper pairs into the metal exponentially decays over length scales proportional to $1/\sqrt{T}$ whereas the superconducting exponential recovers its bulk value over a characteristic length proportional to $1/\sqrt{T_c - T}$. These are known as the coherence length in both the superconducting and normal region.[3] Far below the critical temperature, the Ginzburg-Landau equations no longer provide an accurate physical model and microscopic equations of motion, known as the Usadel equations, must be appealed to. One finds that the proximity of the superconductor induces a "minigap" δ in the densities of states in the metal where δ is proportional to the transmission coefficient at the superconducting-normal interface.

Replacing a normal metal with a magnet at the interface with a conventional s-wave superconductor, one may expect a diminished effect as compared with the normal metal due to the Meissner effect on the superconducting side. Likewise, in the magnetic region, the exchange field tends to align the electrons that make up the Cooper pair which decreases their density. Broadly speaking, in homogeneous magnetic structures the correlation length no longer scales inversely with temperature or critical temperature but rather with the exchange field, which can be very large, and thus suppresses the proximity effects. Nonetheless, these structures exhibit properties that are unseen in the traditional proximity effect. The superconducting correlations leaked into the ferromagnet have both a singlet, as before, and a triplet component with zero spin projection along the axis of magnetization. The triplet component is a direct consequence of the exchange interaction in the magnet. As a result, superconducting order oscillates with wavelength equal to the decay length. Oscillatory behavior is a widely observed characteristic of magnetic-superconductor layers as the Berry phase accumulated by the electrons making up the Cooper pair sums rather than cancels. To this end, we note that the critical current in a superconductor|ferromagnet|superconductor (S|F|S)

[3]This is distinct from the so called Pippard length which reflects the coherence length of a Cooper in a superconductor and is constant with respect to temperature.

structure, i.e. a magnetic Josephson junction, oscillates with thickness of the ferromagnetic layer and can facilitate a π-junction. Conversely, the penetration of the exchange field into the superconductor induces a finite total momentum in the Cooper pairs which generates an inhomogeneous gap. This causes an oscillation in the critical temperature as a function of ferromagnetic layer thickness.

A structure consisting of inhomogeneous magnetization allows a "triplet odd" superconductivity which facilitates a long-range triplet component that can penetrate deep into a ferromagnetic layer. Recall that the exchange interaction induced a triplet component of superconductivity whose projection was zero along the axis of magnetization. When two noncollinear magnets are separated by a superconductor, each exchange interaction creates a triplet pairing, neither of which individually has a projection along their axis of magnetization. However, the superposition of these components contains all possible projections of the spin. Thus there is a triplet component of the superconducting wavefunction which is projected along either magnetization axis. Because these are energetically favored by the exchange interaction, they will penetrate deeper into the magnet. The coherence length thus goes as $\sqrt{1/T}$, similar to the normal proximity effect, which is typically much bigger than $\sqrt{1/H_{\text{xc}}}$ where H_{xc} is the magnitude of the exchange field. Experiments on magnetic multilayers have found signature current-voltage relations persistent for large magnetic thicknesses [KGK06, KKP10]

The case of spin valve with superconducting leads, i.e. a S|F|I|F|S structure where I is a thin insulating region, is considered in chapter 3. The critical current of this magnetic Josephson junction changes as a function of the relative orientation of the ferromagnets and is maximized, showing an enhancement of the critical current compared with that in absence of exchange, when they are antiparallel. To understand this, note that the pairing making up Cooper pairs in the superconducting leads is between opposite spins. When the magnets are parallel to each other, one of the spins is in the wrong direction and the Cooper

pair near that region is energetically disfavored. Suppose the Pippard length and the penetration depth in the ferromagnet are both larger than the thicknesses of the superconducting and ferromagnetic layers. When the magnets are antiparallel, the individual spins may localize to their energetically favorable ferromagnet. This can locally increase the density of the Cooper pairs and may increase the critical current. The critical current increases from the bare critical current logarithmically in the exchange field [BVE01]. Experimental indications of this effect have been found by varying thicknesses of spiral magnetically ordered substances to control orientation [RWB10].

1.4 Keldysh Formulation of Nonequilibrium Green's Functions

Although the S-matrix formulation of scattering is useful in describing equilibrium phenomenon, more complex machinery is necessary to analyze nonequilibrium properties of quantum mechanical systems. In this section we highlight the major results and reasoning that leads to them. A detailed account of this methodology, often called Keldysh formalism, and its applications can be found in [HJ08]. The relations derived in this section will be of special use to us when we consider voltage, spin, and temperature biasing magnetic systems in chapter 5.

1.4.1 Equilibrium Green's Function Expansion

Because we, in principal, know how to evaluate equilibrium Green's functions, our basic strategy will be to make nonequilibrium Green's functions obey similar rules to equilibrium Green's functions and evaluate in a similar way. We recall the salient points in calculating observables in equilibrium.

Consider a Hamiltonian $H = H_0 + V$ that can be broke up into a noninter-

acting quadratic part, H_0, and an interacting piece, V. We work in the interaction picture of quantum mechanics where the wavefunctions evolve in time according to the interacting piece of the Hamiltonian $\exp[iH_0t]\exp[-iHt]|\psi(0)\rangle = |\psi(t)\rangle$ and the observables evolve according to the noninteracting part $\mathcal{O}(t) = \exp[iH_0t]\mathcal{O}(0)\exp[-iH_0t]$. The basic quantity of interest is the time-ordered Green's function, which is the overlap of an observable $A(t)$ at time t and another observable $B(t')$ at time t' with respect to the exact groundstate of our Hamiltonian: $G^t_{BA} = -i\langle\mathcal{T}\{A(t)B(t')\}\rangle$. $\mathcal{T}\{\cdots\}$ denotes the time-ordering of $\cdots$ and G^t. However, we do not know the the exact groundstate. Conveniently, the Gellman-Low theorem states that infinitely far in the past or future the groundstate wave function is the noninterating groundstate. That is, defining the S matrix $\mathcal{S}(t,t') = \mathcal{T}\exp\left[-i\int_{t'}^{t} dt_1\hat{V}(t_1)\right]$ we can write our expression for the Green's function as $\langle 0|\mathcal{T}\{\mathcal{S}(-\infty,\infty)A(t)B(t')\}|0\rangle$. The prescription is to expand $\mathcal{S}(-\infty,\infty)$ in powers of the interaction and, because our ground state is noninteracting, use Wick's theorem to evaluate the Green's function.

There are a few Green's functions to note, but in equilibrium, when one is known the all others can be extracted. We enumerate them below

$$\begin{aligned}
G^t(t,t')_{AB} &= -i\theta(t-t')\langle A(t)B(t')\rangle \mp i\theta(t'-t)\langle B(t')A(t)\rangle\ ,\\
G^{\bar{t}}(t,t')_{AB} &= -i\theta(t'-t)\langle A(t)B(t')\rangle \mp i\theta(t-t')\langle B(t')A(t)\rangle\ ,\\
G^r(t,t')_{AB} &= -i\theta(t-t')\langle[A(t),B(t')]_{\mp}\rangle\ ,\\
G^a(t,t')_{AB} &= i\theta(t'-t)\langle[A(t),B(t')]_{\mp}\rangle\ ,\\
G^<_{AB} &= -i\langle A(t)B(t')\rangle\ ,\\
G^>_{AB} &= \mp i\langle B(t')A(t)\rangle
\end{aligned} \tag{1.15}$$

where $\theta(t)$ is the Heaviside theta function and $[\cdot,\cdot]_{\mp}$ denote the commutator and anticommutator, respectively, in which the latter is used only if both $A(t)$ and $B(t')$ are fermionic. From top to bottom, these are known as the time-ordered, antitime-ordered, retarded, advanced, lesser, and greater Green's functions.

1.4.2 Nonequilibrium Green's Functions

In equilibrium, the ground state wavefunctions at $t = -\infty, +\infty$ are guaranteed to be the same. The idea is to go into the noninteracting infinite past, slowly turn on interactions in the future, evaluate the Green's functions when the system is interacting, and continue to the infinite future to the same noninteracting ground state. However, when subjected to a nonequilibrium interaction there is no guarantee that the ground states at the ends of time are the same. Consequently, the system is slightly more complicated. Instead of going infinitely far into the future where we do not know the noninteracting groundstate, we take path in imaginary time from the infinite past, to the time when the interactions are turned on, and back to the infinite past. This insures that initial and final ground states are identical. However our philosophy remains essentially the same: write down the Green's functions, insert an operator so that we can evaluate the Green's function in a noninteracting ground state, expand that operator using Dyson's equation, and evaluate using Wick's theorem.

We consider a Hamiltonian $H = H_0 + V + H'(t)$ where H_0 is noninteracting, V contains the many-body interactions, and $H'(t)$ captures the nonequilibrium contributions. One may show that the time evolution of some operator $A_H(t) = \mathcal{T}_C\{\exp[-i\int_C \mathrm{d}\tau H'_h(\tau)]A_h(t)\}$ where $\mathcal{T}_C$ is contour-ordering over contour C that comes from infinitely far in the past, passes through t, and goes back to the infinite past. Contour ordered operator products position the operator furtherest along the the contour to the left. Operators with the subscript h denote time dependence with respect to $h = H_0 + V$ and those subscript H denote time dependence with respect to the full Hamiltonian. We now define the contour-ordered Green's function $G_{AB}(t,t') \equiv -i\langle\mathcal{T}_C\{A_H(t)B_H(t)\}\rangle$ where C is the contour depicted in Fig.1.3(a). One may show that this equivalent to $G_{AB}(t,t') = -i\langle\mathcal{T}_C\{\mathcal{S}_C A_{H_0}(t)B_{H_0}(t')\}\rangle$ where $\mathcal{S}_C$ is a time evolution operator, similar to the S matrix, over the contour. The operators are time dependent ac-

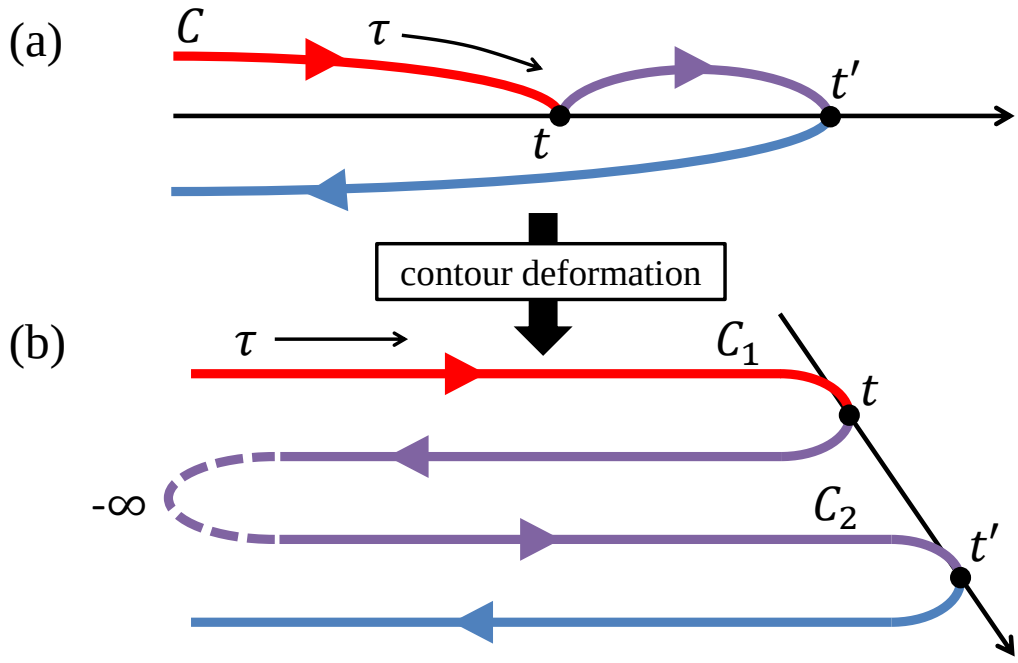

Figure 1.3: Contour of over which a contour-ordered Green's function is defined before (a) and after (b) deformation.

cording to the noninteracting Hamiltonian H_0 while the many body and nonequilibrium contributions reside in $\mathcal{S}_C$, completely analogous to the equilibrium case. The subtlety comes from the position of time coordinates on the contour, and must be kept track of. Because there are two branches of C corresponding to positive and negative direction, the contour-ordered Green's function can be written as a matrix in "Keldysh space"

$$G(t,t') = \begin{pmatrix} G^t(t,t') & G^>(t,t') \\ G^<(t,t') & G^{\bar{t}}(t,t') \end{pmatrix} . \tag{1.16}$$

The location in the matrix corresponds to t and t' residing on the same branch (diagonal entries) or on a combination of branches (off diagonal entries). After expanding $\mathcal{S}_C$, we obtain the Dyson's equation for the contour-ordered Green's

function

$$G(t,t') = G_0(t,t') + \int_C \mathrm{d}\tau G_0(t,\tau)U(\tau)G(\tau,t') + \int_C \mathrm{d}\tau \int_C \mathrm{d}\tau' G_0(t,\tau)\Sigma(\tau,\tau')G(\tau',t')\,, \tag{1.17}$$

where the nonequilibrium contribution, contained in the potential U, is assumed to be a single body potential. The many-body interaction is contained in the self-energy Σ.

Formally, this is the solution. However for this to be of use, the imaginary time must be analytically continued onto the real time axis. To continue, products of the form $D(t,t') = \int_C \mathrm{d}\tau A(t,\tau)B(\tau,t')$ must be evaluated. The following procedure is an archetype for this evaluation [LD76]. Suppose we want to evaluate the lesser than Green's function of contour ordered path integral, $D^<$. We deform the contour C into two parts, C_1 and C_2 [Fig. 1.3(b)] to obtain

$$D^<(t,t') = \int_{C_1} \mathrm{d}\tau A(t,\tau)B^<(\tau,t') + \int_{C_2} \mathrm{d}\tau A^<(t,\tau)B(\tau,t')\,. \tag{1.18}$$

In the integration along the first path C_1 we have identified B with $B^<$ by the rules of contour-ordering because all of C_1 is traversed before the position of t'. Similarly in the second integral. Evaluating the first path integral

$$\begin{aligned}\int_{C_1} \mathrm{d}\tau A(t,\tau)B^<(\tau,t') &= \int_{-\infty}^{t} \mathrm{d}t A(^>t,\tau)B^<(\tau,t') + \int_{t}^{-\infty} \mathrm{d}t A(^<t,\tau)B^<(\tau,t') \\ &= \int_{-\infty}^{\infty} \mathrm{d}t_1 A^r(t,t_1)B^<(t_1,t')\,,\end{aligned} \tag{1.19}$$

where we have again used the properties of contour ordering and the definition of the retarded Green's function. This method for analytic continuation is known as Langreth theorem. In chapter 5 will make use of Eq. (1.19) but an exhaustive table of such identities can be found in [HJ08].

CHAPTER 2

Spin-torque ac Impedence Shift in Magnetic Junctions

Subjecting a magnetic tunnel junction (MTJ) to a spin current and/or electric voltage induces magnetic precession, which can reciprocally pump current through the circuit. This results in an ac impedance, which is sensitive to the magnetic field applied to the MTJ. Measuring this impedance can be used to characterize the coupling between the magnetic free layer and the electric current as well as a read-out of the magnetic configuration of the MTJ.

2.1 Background

The development of the next generation of computer memory and logic can be made possible by current-driven effects through magnetic multilayers by utilizing the mechanisms of tunnel magnetoresistance [Jul75] and spin-transfer torque [Slo96, Ber96]. These effects have been demonstrated to efficiently read and write bits as furnished by magnetic domains [IHL07, CAD10]. Somewhat less utilized are the recently discovered torques due to the voltage-induced anisotropy [WFM07, MSN09]. The applied voltage induces a charge build up at the tunnel-barrier interface with the transition-metal ferromagnet. The strong electric field at the interface modifies electronic structure along with the local occupation of the *d*-character bands in the transition metal. Due to spin-orbit coupling, this results in the anisotropic interaction between the local excess charge and the magnetiza-

tion. Conventional MTJ spin-torque devices can benefit from the voltage-induced anisotropy by reducing the critical switching current for a fixed thermal stability [WLH11]. Recently, it has been shown that this voltage-controlled magnetic anisotropy (VCMA) can induce ferromagnetic resonance [NSM12, ZKR12] or reverse the magnetic direction [SNB11].

Here, we include the reciprocal backaction of magnetic dynamics on the circuit. Applying an ac voltage drives precession of the magnet that in turn pumps current, contributing to the ac impedance. In order to illustrate two physically distinct mechanisms of voltage-induced spin torques, we consider two special MTJ structures: (a) a ferromagnet (F)|insulator (I) bilayer with interfacial spin-orbit interaction and (b) an F|I|F heterostructure where one of the ferromagnetic layers is pinned and the other free. See Fig. 2.1 for schematics. In Fig. 2.1(a), the ferromagnet is agitated by voltage-induced anisotropy [WFM07][MSN09], while in Fig. 2.1(b) the free magnetic layer is driven by spin-transfer torque [Slo96][Ber96]. In practice, these two scenarios can be accessed by varying the thickness of the spacer: for thicker spacers that are Ohmically opaque the VCMA must ultimately dominate, while for thinner spacers the spin-transfer torque should become progressively more important. In the former case, within our model, the impedance vanishes when the equilibrium magnetization is parallel or perpendicular to the direction of induced anisotropy. In the latter case, we find that the impedance is enhanced when the magnetic equilibrium is nearly perpendicular to the direction of polarization of the spin current. If the magnitude of the VCMA and spin-transfer torque are comparable, we can tune between these effects by applying a magnetic field. The resultant impedance shift can be used to characterize the magnitude and the nature of the coupling between ferromagnet and circuit, as well as to probe magnetic configuration.

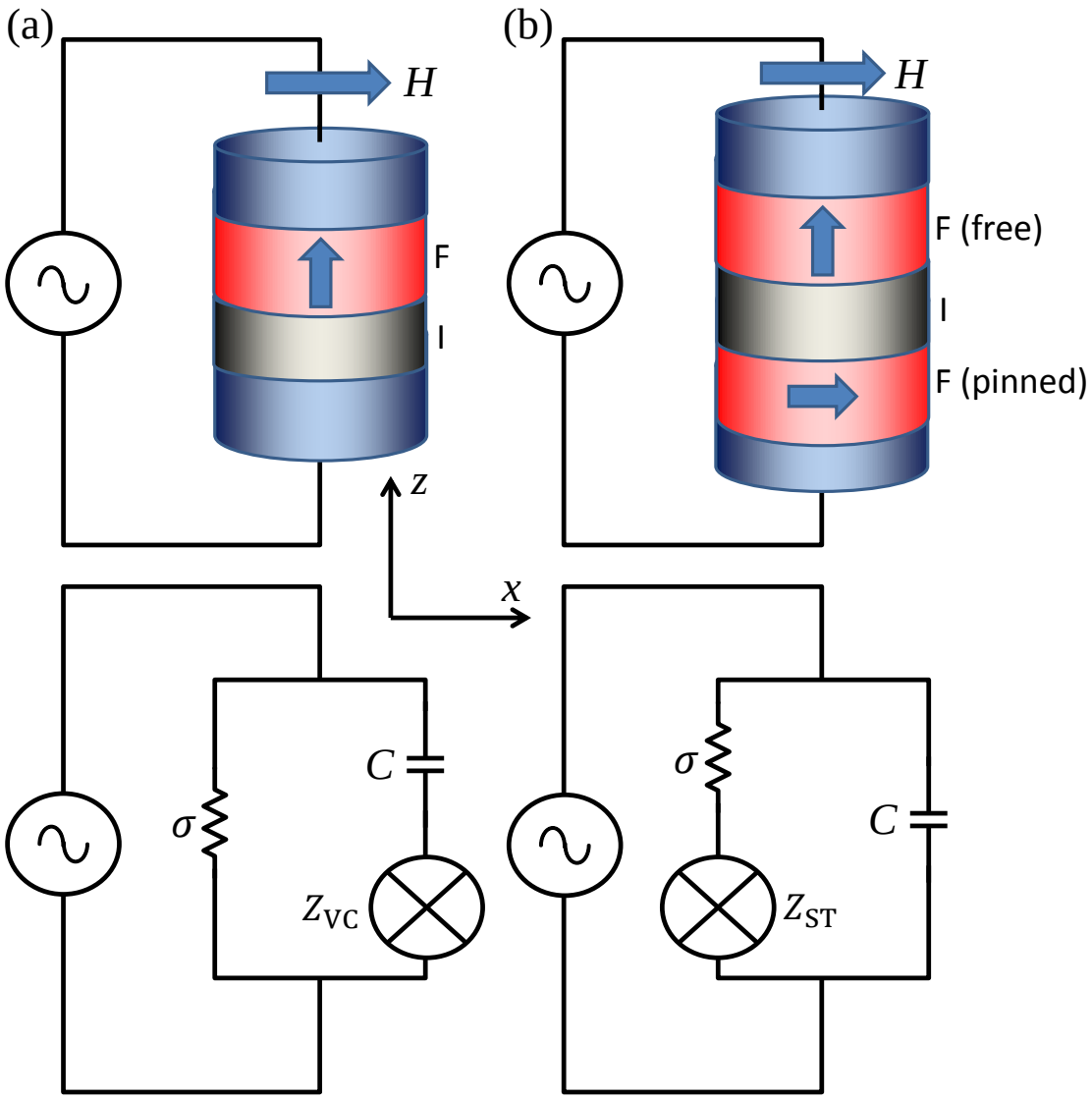

Figure 2.1: Schematics of magnetic tunnel junction subjected to a magnetic field, as part of an ac circuit that drives magnetic precession by VCMA (a) or Slonczewski torque (b), and the equivalent circuit diagrams (below) showing the additional impedance due to pumping by magnetic dynamics.

2.2 Voltage-Controlled Magnetic Anisotropy

The following analysis of voltage-controlled magnetic anisotropies [Fig. 2.1(a)] applies to a general class of MTJ's that break mirror symmetry normal to the face of the magnetic layer, inducing Rashba-type spin-orbit interaction [BR84]. Consider an F|I bilayer subjected to a voltage V in the external circuit, wherein the free energy of the transferred charge Q is $F[Q] = -QV$. We treat the ferromagnetic layer to be monodomain with free-energy density

$$F[\mathbf{M}]/\mathcal{V} = \frac{1}{2}(N_x M_x^2 + N_y M_y^2 + N_z M_z^2 - K M_z^2) - H M_x \,, \tag{2.1}$$

where $\mathcal{V}$ is the volume of the ferromagnetic layer and $\mathbf{M} = (M_x, M_y, M_z)$ is the magnetization vector. To be specific, we take the xy cross section of the magnet to be an ellipse elongated in the x direction. $N_x + N_y + N_z = 4\pi$ are the demagnetization factors (with $N_y > N_x$), H is the applied field along the semimajor (x) axis, and K is the perpendicular anisotropy that can be induced by the insulating layer in the absence of voltage. We consider a geometry wherein the perpendicular anisotropy overcomes the long-range dipole field such that $N_x > N_z - K$ and, when no magnetic field or voltage is applied, the equilibrium orientation of the magnet is perpendicular to the interface (z axis). Under application of a magnetic field along the semimajor axis of the ellipse, the equilibrium magnetization tilts away from the z axis as $\bar{\mathbf{M}} = (H/\tilde{N}_x, 0, \sqrt{M_s^2 - (H/\tilde{N}_x)^2})$, where $M_s = |\mathbf{M}|$ is the saturated magnetization, $\tilde{N}_x = N_x - N_z + K$ and $\tilde{N}_y = N_y - N_z + K$. Note that $\tilde{N}_x, \tilde{N}_y > 0$ are guaranteed by $N_y > N_x > N_z - K$. For simplicity, we restrict $|H| < M_s \tilde{N}_x$.

The tunneling layer is treated as a parallel plate capacitor of capacitance C, storing energy $F[q] = q^2/2C$ where q is the charge on the surface of the insulator. The structure of the device breaks mirror symmetry in the direction perpendicular to the interface. We treat the lateral dimensions of the device macroscopically, as compared with the microscopic spin-orbit interactions inducing VCMA, and thus

require the coupling to be rotationally symmetric around the z axis. Subject to these symmetries, the anisotropy controlled by voltage must be induced in the direction of the broken mirror symmetry. To satisfy time reversal symmetry, the free energy must be of even order in magnetization. Since there are no Ohmic losses associated with tunneling through the junction, we suppose the dominant interaction between the magnetization and the electric circuit to be nondissipative. Dissipative corrections could be taken into account similarly to Ref. [HBT12]. Because this torque is induced by the electric field at the interface, we take the energy to be proportional to electric flux in the insulating layer. The coupling, up to quadratic order in magnetization, is $F[\mathbf{M}, q] = -\nu q m_z^2/2$ where ν is the phenomenological coupling between the projection of the magnetic direction along the z axis, $m_z = M_z/M_s$, and the circuit. The full free energy is the sum of these individual components $F = F[\mathbf{M}] + F[Q] + F[q] + F[\mathbf{M}, q]$.

The equation of motion of the ferromagnet is described by the Landau-Lifshitz-Gilbert (LLG) equation [PL80, Gil04]

$$\dot{\mathbf{m}} = -\gamma \mathbf{m} \times \mathbf{H} + \alpha \mathbf{m} \times \dot{\mathbf{m}}\,, \tag{2.2}$$

where γ is the gyromagnetic ratio and α is the dimensionless Gilbert damping. The magnetic direction vector is $\mathbf{m} = \mathbf{M}/M_s$ and $\mathbf{H} = -\mathcal{V}^{-1}\partial F/\partial \mathbf{M}$ is the effective field. To solve it, it is convenient to rotate by Λ to a set of magnetic coordinates, $\mathbf{m}'$ where the equilibrium is along $\bar{\mathbf{m}}' = (0, 0, 1)$. We find

$$\bar{\mathbf{m}}' = \Lambda \begin{pmatrix} \bar{m}_x \\ 0 \\ \bar{m}_z \end{pmatrix} = \begin{pmatrix} \bar{m}_z & 0 & -\bar{m}_x \\ 0 & 1 & 0 \\ \bar{m}_x & 0 & \bar{m}_z \end{pmatrix} \begin{pmatrix} \bar{m}_x \\ 0 \\ \bar{m}_z \end{pmatrix} = \begin{pmatrix} 0 \\ 0 \\ 1 \end{pmatrix}, \tag{2.3}$$

where $\bar{\mathbf{m}} = (\bar{m}_x, \bar{m}_y, \bar{m}_z)$ is the equilibrium magnetization direction in the unro-

tated coordinates. The new magnetization coordinates are

$$\mathbf{m}' = \begin{pmatrix} m'_x \\ m'_y \\ m'_z \end{pmatrix} = \begin{pmatrix} \bar{m}_z & 0 & -\bar{m}_x \\ 0 & 1 & 0 \\ \bar{m}_x & 0 & \bar{m}_z \end{pmatrix} \begin{pmatrix} m_x \\ m_y \\ m_z \end{pmatrix} = \begin{pmatrix} m_x\bar{m}_z - m_z\bar{m}_x \\ m_y \\ m_x\bar{m}_x + m_z\bar{m}_z \end{pmatrix} \tag{2.4}$$

and similarly, as will be useful for later,

$$\mathbf{m} = \begin{pmatrix} m_x \\ m_y \\ m_z \end{pmatrix} = \begin{pmatrix} \bar{m}_z & 0 & \bar{m}_x \\ 0 & 1 & 0 \\ -\bar{m}_x & 0 & \bar{m}_z \end{pmatrix} \begin{pmatrix} m'_x \\ m'_y \\ m'_z \end{pmatrix} = \begin{pmatrix} m'_x\bar{m}_z + m'_z\bar{m}_x \\ m'_y \\ \bar{m}_z m'_z - m'_x\bar{m}_x \end{pmatrix}. \tag{2.5}$$

Multiplying the LLG equation by Λ gives

$$\Lambda\dot{\mathbf{m}} = -\gamma\Lambda\mathbf{m} \times \Lambda\mathbf{H} + \alpha\Lambda\mathbf{m} \times \Lambda\dot{\mathbf{m}} = \dot{\mathbf{m}}' = -\gamma\mathbf{m}' \times \mathbf{H}' + \alpha\mathbf{m}' \times \dot{\mathbf{m}}'. \tag{2.6}$$

The rotated effective field is

$$\begin{aligned} \mathbf{H}' = -\frac{1}{\mathcal{V}M_s}\Lambda\partial_{\mathbf{m}}F = M_s \begin{pmatrix} \bar{m}_z & 0 & -\bar{m}_x \\ 0 & 1 & 0 \\ \bar{m}_x & 0 & \bar{m}_z \end{pmatrix} \begin{pmatrix} \left[h + (\tilde{N}_y - \tilde{N}_x)\right] m_x \\ 0 \\ (\tilde{N}_y + \nu q/M_s^2\mathcal{V})m_z \end{pmatrix} \\ = \begin{pmatrix} \left[h + (\tilde{N}_y - \tilde{N}_x)\right] \bar{m}_z - (\tilde{N}_y + \nu q/M_s^2\mathcal{V})\bar{m}_x m_z \\ 0 \\ \left[h + (\tilde{N}_y - \tilde{N}_x)\right] \bar{m}_x + (\tilde{N}_y + \nu q/M_s^2\mathcal{V})\bar{m}_z m_z \end{pmatrix} \end{aligned} \tag{2.7}$$

or, as a function of the new coordinate system,

$$\mathbf{H}' = M_s \begin{pmatrix} h\bar{m}_z + (\tilde{N}_y - \tilde{N}_x)\bar{m}_z(\bar{m}_z m'_x + \bar{m}_x m'_z) \\ \quad - (\tilde{N}_y + \nu q/M_s^2\mathcal{V})\bar{m}_x(\bar{m}_z m'_z - \bar{m}_x m'_x) \\ 0 \\ h\bar{m}_x + (\tilde{N}_y - \tilde{N}_x)\bar{m}_x(\bar{m}_z m'_x + \bar{m}_x m'_z) \\ \quad + (\tilde{N}_y + \nu q/M_s^2\mathcal{V})\bar{m}_z(\bar{m}_z m'_z - \bar{m}_x m'_x) \end{pmatrix}. \tag{2.8}$$

Because we are only interested in perturbations about equilibrium, we write $\mathbf{m}' =$

$(m'_x, m'_y, 1)$ and retain terms linear in m'_x, m'_y, and q

$$\mathbf{H}' = M_s \begin{pmatrix} -m'_x \left[(\tilde{N}_x - \tilde{N}_y)\bar{m}_z^2 - \tilde{N}_y \bar{m}_x^2 \right] - (\nu q / M_s^2 \mathcal{V}) \bar{m}_x \bar{m}_z \\ 0 \\ \tilde{N}_y - h\bar{m}_z m'_x + (\nu q / M_s^2 \mathcal{V}) \bar{m}_z^2 \end{pmatrix} \tag{2.9}$$

and take the cross product with $\mathbf{m}'$

$$\mathbf{m}' \times \mathbf{H}' = M_s \begin{pmatrix} \tilde{N}_y m'_y \\ \left[(\tilde{N}_y - \tilde{N}_x)\bar{m}_z^2 + \tilde{N}_y - \tilde{N}_y \bar{m}_x^2 \right] m'_x - (\nu q / M_s^2 \mathcal{V}) \bar{m}_x \bar{m}_z \\ 0 \end{pmatrix} . \tag{2.10}$$

The equations of motion for the magnetic components perpendicular to $\bar{\mathbf{m}}'$ are

$$\begin{aligned} \dot{m}'_x &= -\gamma \tilde{N}_y M_s m'_y - \alpha \dot{m}'_y \,, \\ \dot{m}'_y &= \gamma \tilde{N}_x \bar{m}_z^2 M_s m'_x + \alpha \dot{m}'_x + \gamma (\nu q / M_s \mathcal{V}) \bar{m}_x \bar{m}_z \,. \end{aligned} \tag{2.11}$$

Writing this in terms of a second order differential equation shows m'_x oscillates as a driven damped harmonic oscillator

$$\begin{aligned} &(1+\alpha^2)\ddot{m}'_x + \alpha\gamma(\tilde{N}_y + \bar{m}_z^2 \tilde{N}_x) M_s \dot{m}'_x + \gamma^2 \bar{m}_z^2 \tilde{N}_y \tilde{N}_x M_s^2 m'_x \\ &= -\gamma(\nu / M_s \mathcal{V}) \bar{m}_x \bar{m}_z (\alpha \dot{q} + \gamma \tilde{N}_y M_s q) \,. \end{aligned} \tag{2.12}$$

Applying a small ac voltage, the response is linear and therefore $\dot{q} = i\omega q$. When driving at the natural frequency $\omega_0 = \gamma M_s \sqrt{\bar{m}_z^2 \tilde{N}_x \tilde{N}_y}$, the solution is of the form $m'_x = \bar{m}'_x + A \exp[i(\omega_0 t + \pi/2)]$ where

$$A = \frac{\gamma(\nu / M_s \mathcal{V}) \bar{m}_x \bar{m}_z (i\alpha\omega_0 + \gamma \tilde{N}_y M_s)}{\omega_0 \left[\alpha\gamma M_s (\tilde{N}_y + \bar{m}_z^2 \tilde{N}_x) \right]} \tilde{q} \,. \tag{2.13}$$

Because the Gilbert damping is typically small in practice, the damped driving term will be small unless the system is driven at frequencies orders of magnitude greater than the resonance frequency. Suppressing higher-order terms in α, the amplitude of the magnetic oscillations is

$$A = \frac{\nu \bar{m}_x \bar{m}_z \gamma \tilde{N}_z}{\alpha \omega_0 M_s \mathcal{V} \left[\tilde{N}_y + \bar{m}_z^2 (\tilde{N}_z - \tilde{N}_x) \right]} \tilde{q} \,. \tag{2.14}$$

To obtain an expression of the current through the circuit $\dot{Q}$, we note that the difference in change in charge between the reservoir and the capacitor is the leakage current due to tunneling through the insulator $\dot{Q} - \dot{q} = \sigma V$ where σ is the junction conductance (disregarding magnetoconductance). Neglecting impedance in the external circuit, $\partial_Q F = -\partial_q F$, we find

$$\dot{Q} = C\dot{V} + \sigma V + \nu C m_z \dot{m}_z \,. \tag{2.15}$$

In addition to the resistor and capacitor in parallel, the precession of the magnet pumps current, which is reciprocal to the VCMA. Substituting the equation of motion of the magnet into the formula for current and using the relation for leakage current we find

$$\dot{Q}\left[1 + i\frac{\nu^2 C}{\alpha\omega_0 S}\frac{\bar{m}_x^2\bar{m}_z^2\gamma\tilde{N}_y}{\tilde{N}_y + \bar{m}_z\tilde{N}_x}\right] = C\dot{V} + \sigma V\left[1 + i\frac{\nu^2 C}{\alpha\omega_0 S}\frac{\bar{m}_x^2\bar{m}_z^2\gamma\tilde{N}_y}{\tilde{N}_y + \bar{m}_z\tilde{N}_x}\right] . \tag{2.16}$$

where $S = \mathcal{V}M_s/\gamma$ is the total spin angular momentum. Comparing this with the circuit diagram in Fig. 2.1(a), the impedance due to VCMA is

$$Z_{\mathrm{VC}} = \frac{\nu^2}{\alpha\omega_0^2 S}\frac{\bar{m}_x^2\bar{m}_z^2\tilde{N}_y}{\tilde{N}_y + \bar{m}_z^2\tilde{N}_x} \,, \tag{2.17}$$

Notice that on resonance Z_{VC} is real, but away from resonance it is generally complex valued. The impedance is second order in ν reflecting the VCMA driving of the magnet and subsequent self-consistent pumping by magnetic precession. Z_{VC} is proportional to the product of the equilibrium value of magnetization along the x and z axes, being maximized at an intermediate polar angle, and can therefore be modulated by applied magnetic field. The effect is larger for smaller Gilbert damping.

2.3 Spin-Transfer Torque

Let us now consider an MTJ wherein the torque is induced by spin current polarized along the direction of the pinned layer (x axis) [Slo96, Ber96], as sketched in Fig. 2.1(b). (Note that one can obtain a similar effect also in an F|I bilayer due to spin-orbit interaction [MZ08, COL09, HBT10].) The equation of motion of the magnet coupled to an external circuit by Slonczewski torque is

$$\dot{\mathbf{m}} = -\gamma \mathbf{m} \times \mathbf{H} + \alpha \mathbf{m} \times \dot{\mathbf{m}} + \mu(\dot{Q} - \dot{q}) \mathbf{m} \times \mathbf{x} \times \mathbf{m} \,, \tag{2.18}$$

where $\mu = S(\hbar/2e)P/(1 + \bar{m}_x P^2)$ [Slo05], as determined by microscopic considerations, characterizes the strength of the torque induced by current on the magnet. P is the tunneling spin polarization. The torque is proportional to the leakage current, $\dot{Q} - \dot{q}$, through the capacitor. The equation of motion for charge satisfying microscopic time-reversal symmetry consistent with Eq. (2.18) is [TMX08]

$$\dot{Q} = \sigma(V - \mu S \dot{\mathbf{m}} \cdot \mathbf{m} \times \mathbf{x}) + C\dot{V} \,. \tag{2.19}$$

In contrast to the above VCMA model, $\sigma = \sigma_0(1 + \bar{m}_x P^2)$, the tunnel magnetoconductance, depends on the relative orientation of the pinned and free magnetic layers. Similar manipulations to the LLG equation as in the previous section gives

$$\begin{aligned} \dot{m}'_x &= -\gamma \tilde{N}_y M_s m'_y - \alpha \dot{m}'_y + \mu \bar{m}_z (\dot{Q} - \dot{q}) \,, \\ \dot{m}'_y &= \gamma \tilde{N}_x \bar{m}_z^2 M_s m'_x + \alpha \dot{m}'_x \,, \\ \dot{Q} - \dot{q} &= \sigma \left(V - \mu \frac{M_s \mathcal{V}}{\gamma} \bar{m}_z \dot{m}'_y \right) \,. \end{aligned} \tag{2.20}$$

Similar to the previous case, we apply an ac voltage at resonance which drives magnetic dynamics and shifts the impedance due to the charge pumping from magnetic precession. Again neglecting terms higher-order in α, the associated impedance is

$$Z_{\mathrm{ST}} = -\frac{\mu^2 S}{\alpha} \frac{\bar{m}_z^4 \tilde{N}_x}{\tilde{N}_y + \bar{m}_z^2 \tilde{N}_x} \,. \tag{2.21}$$

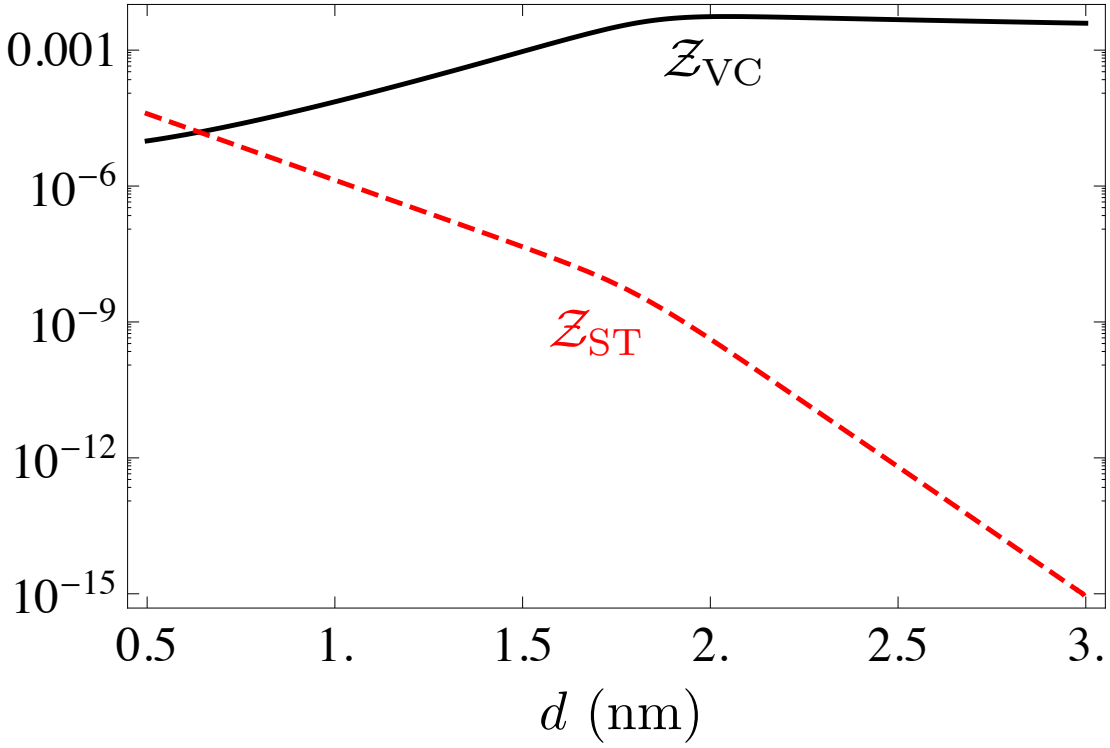

Figure 2.2: Relative change in impedance as a result of VCMA (black solid) or Slonczewski torque (red dashed) as a function of MgO spacer thickness, evaluated at $\bar{m}_x = 0.73$ and $\bar{m}_x = 0$, respectively. The kinks near $d \approx 2$ nm correspond to the crossover at $\sigma \sim \omega_0 C$.

Although at resonance $Z_{\rm ST}$ is real and negative, the second law of thermodynamics bounds the Slonczewski torque parameter $\mu^2 \leq \alpha/\sigma S$ [HBT12], ensuring positivity of $1/\sigma + Z_{\rm ST}$. Note that $Z_{\rm ST}$ vanishes when the equilibrium magnetization is perpendicular to the z axis.

2.4 Numerical Results

We now make an estimate of the effect for practical memory devices. Specifically, we consider a 150×70 nm^2 elliptical nanopillar of CoFeB/MgO, where the thickness of the magnetic layer is 1.6 nm, giving $N_x = 0.2$ and $N_y = 0.5$. The other rele-

vant parameters are taken from Ref. [ZKR12]: $\alpha = 3 \times 10^{-2}$, $M_s = 950$ emu/cm^3, $\nu = 2.8$ μerg statV^{-1} cm^{-1}, $K = 12$, $P = 0.5$, and $\sigma_0 = 1.6$ mS at the MgO thickness of $d = 0.86$ nm (with the exponential decay length as a function of d of 0.15 nm [AZL11]). Our figure of merit is the relative change in impedance as a result of VCMA or spin-transfer torque: $\mathcal{Z} \equiv |Z - Z_0|/|Z_0|$, where Z is the total impedance of the circuit in the presence of the magnetic dynamics and Z_0 is the impedance of the static junction (taking dielectric constant of MgO to be $\epsilon = 10$). To evaluate $\mathcal{Z}_{\rm VC}$ and $\mathcal{Z}_{\rm ST}$, we first choose the magnetic field H such that $\bar{m}_x$ maximizes the dimensionless geometric factors in Eq. (2.17) and Eq. (2.21): $\bar{m}_x = 0.73$ and $\bar{m}_x = 0$, respectively. Varying the tunnel barrier thickness d at a fixed magnetic field, we plot the corresponding $\mathcal{Z}$ in Fig. 2.2. $\mathcal{Z}_{\rm VC}$ increases exponentially reaching the maximum at $\sim 1\%$ near $d \approx 2$ nm. Past this thickness, the junction ac behavior crosses over from the resistive to capacitive regime, in which $\mathcal{Z}_{\rm VC}$ falls off inversely with d. Since spin-transfer torque is roughly proportional to conductance for thin barriers, $\mathcal{Z}_{\rm ST} \propto \sigma$ decreases exponentially with increasing spacer thickness, for $d \lesssim 2$ nm. For thicker barriers, $\mathcal{Z}_{\rm ST}$ becomes proportional to σ^2, doubling the logarithmic slope in its d dependence. For the smallest feasible spacer thickness of 0.5 nm, the relative change in impedance is $\sim 10^{-4}$.

Next, allowing the external magnetic field to vary, we plot $\mathcal{Z}_{\rm VC}$ and $\mathcal{Z}_{\rm ST}$ as a function of equilibrium value of magnetization in Fig. 2.3, fixing $d = 2$ nm and $d = 0.5$ nm, respectively. (These choices for d are motivated by the respective maxima in $\mathcal{Z}$ in Fig. 2.2.) In the case of Slonczewski torque, there is a small asymmetry in the function $\mathcal{Z}(\bar{m}_x)$ around zero due to variation of σ and μ with $\bar{m}_x$. Note that the functional dependences of $\mathcal{Z}_{\rm VC}$ and $\mathcal{Z}_{\rm ST}$ on $\bar{m}_x$ are qualitatively distinct (with the former having double-lobe and the latter single-lobe profiles), allowing for a clear experimental differentiation between VCMA and spin-transfer torque regimes by measuring ac impedance as a function of magnetic field.

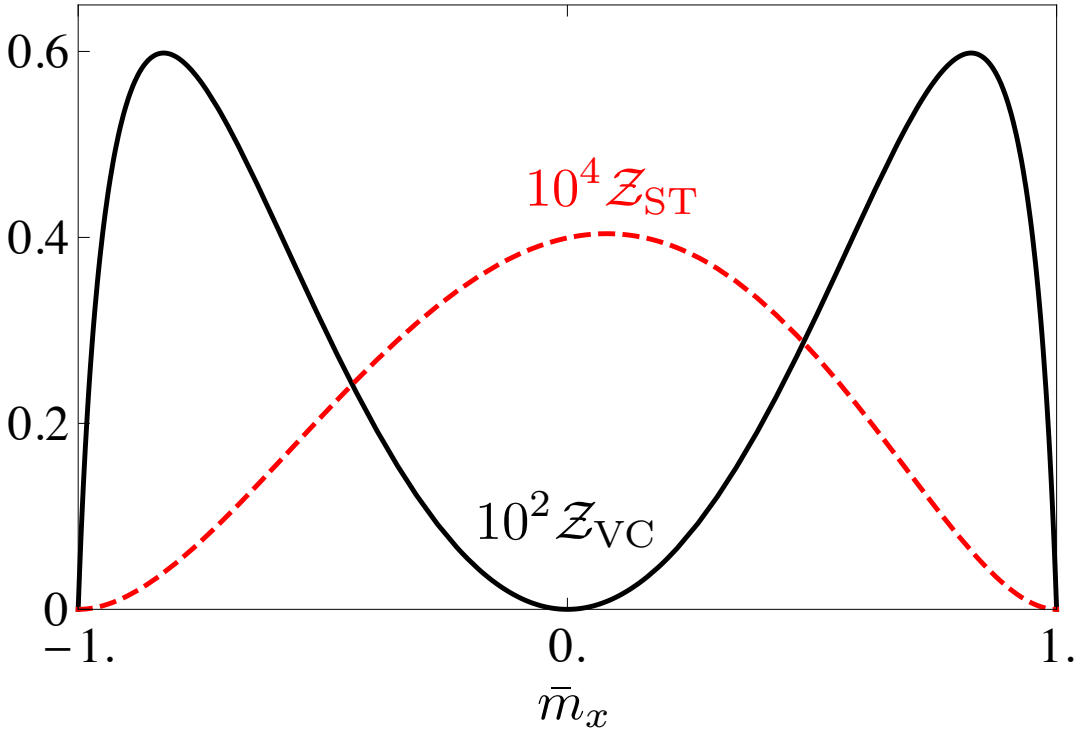

Figure 2.3: Relative change in impedance as a result of VCMA (black solid) or Slonczewski torque (red dashed) as a function of $\bar{m}_x$ at the MgO spacer thicknesses $d = 2$ nm and $d = 0.5$ nm, respectively. The voltage is assumed to be applied at the frequency of ferromagnetic resonance, ω_0, which depends on $\bar{m}_x$.

2.5 Outlook

Measuring the ac impedance shift due to resonant magnetic dynamics could be an efficient method for characterizing the magnitude of the coupling between voltage and ferromagnet (ν) and current and ferromagnet (μ), as well as distinguishing between the two scenarios. Furthermore, when the thickness of the spacer is large, and thus the conductance is prohibitively small to utilize tunnel magnetoresistance, one could envision that measuring the ac impedance may be used as a nondestructive low-dissipation bit read-out. Owing to the promising energy efficiency of VCMA and the reciprocal effect, we expect an active search for ferromagnet-insulator interfaces with higher values of ν, which could electrically control and read the direction of the magnet without tunneling current.

CHAPTER 3

Nonlinear Dynamics in a Magnetic Josephson Junction

We theoretically consider a Josephson junction formed by a ferromagnetic spacer with a strong spin-orbit interaction or a magnetic spin valve, i.e., a bilayer with one static and one free layer. Electron spin transport facilitates a nonlinear dynamical coupling between the magnetic moment and charge current, which consists of normal and superfluid components. By phenomenologically adding reactive and dissipative interactions (guided by structural and Onsager symmetries), we construct magnetic torques and charge pumping, whose microscopic origins are also discussed. A stability analysis of our coupled nonlinear systems generates a rich phase diagram with fixed points, limit cycles, and quasiperiodic states. Our findings reduce to the known phase diagrams for current-biased nonmagnetic Josephson junctions, on the one hand, and spin-torque driven magnetic films, on the other, in the absence of coupling between the magnetic and superconducting order parameters.

3.1 Introduction

Hybrid structures with ferromagnet (F)|normal-metal (N) interfaces have garnered much attention over the past few decades owing to their application in spintronic devices. Injecting a spin current into such a system exerts a torque on the magnet [Slo96, Ber96], which can induce precession and even reversal [TJB98, MRK99],

allowing for manipulation of the magnetic order parameter in nanoscale structures without an external magnetic field [RS08]. Because of the nonlinear nature of the ensuing magnetic dynamics, such devices offer observation of effects traditionally seen in nonlinear dynamical systems: phase locking, hysteresis, bifurcations, and chaos are readily observed [BMS09].

In consideration of a superconductor (S)|F|S heterostructure, one may expect the Josephson effect to be suppressed due to the rapid decay of a singlet pair inside the ferromagnet. Recent experiments [KGK06, KKP10, RWB10], however, observed superconducting transport through a strong ferromagnet between two conventional (s-wave) superconductors. With the expectation that the triplet component of the superconducting condensate can penetrate long distances into a ferromagnet, the preservation of this signal suggests a spin singlet-to-triplet conversion at the interfaces [BVE05]. The unexpected persistence of a supercurrent through the magnet forecasts a new kind of spintronic device that manipulates the Josephson junction by the ferromagnet and, conversely, ferromagnetic layer by the superconducting condensate [BB08, KB09, WB02, LY11, PAB09, CC10, BAP11].

Previous analyses [Buz08, BB08, LY11, PAB09] have considered *equilibrium* interactions between magnetic and superconducting order parameters, which naturally induce a reactive coupling. In contrast, in our description, we introduce *nonequilibrium* interactions consistent with the symmetries of the structure and obeying Onsager reciprocity [PL80]. This treatment allows the addition of both dissipative and reactive couplings between the magnet and superconductor that may in practice be crucial in the understanding of ferromagnetic Josephson junctions, analogous to the importance of Slonczewski [Slo96, TJB98, RS08] and spin-pumping [TBB05] terms in the theory of spin-transfer torques. Such effects cannot be fully captured by quasiequilibrium free-energy considerations. We expect the dissipation to be governed by the quasiparticle excitations in the superconductors in concert with the microscopic processes in the ferromagnet (due to magnon

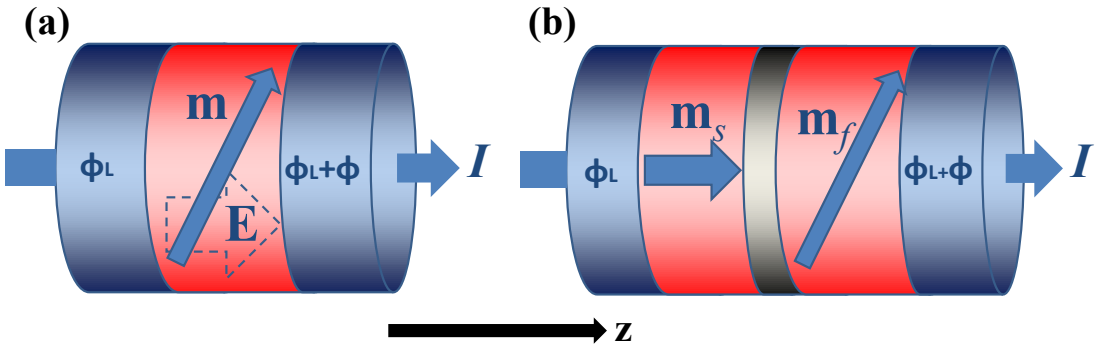

Figure 3.1: Schematics of our magnetic Josephson junctions. The directions of junction layering, applied current I, internal Rashba field $\mathbf{E}$ (a), and direction of the static ferromagnetic layer $\mathbf{m}_s$ (b) all lie along the z axis. ϕ is the phase difference between the superconducting leads.

interaction with electrons, phonons, or other magnons) that are responsible for their Gilbert damping (which, in turn, is known to persist down to very low temperatures [BL74]).

In order to provide specific examples, we consider (a) an S|F|S heterostructure with a Rashba spin-orbit interaction (SOI) in a thin ferromagnetic interlayer (neglecting the vector potential and associated phase shift caused by its magnetic moment [CC10]) and (b) S|F|N|F|S heterostructure wherein the SOI is replaced by a pinned ferromagnetic layer, $\mathbf{m}_s$. See Fig. 3.1. The corresponding spin-dependent Hamiltonians mix the singlet and triplet superconducting components [BVE05], allowing the superfluid to penetrate into the magnet and exert spin torque and carry spin pumping (since a triplet Cooper pair is a spin-1 object) that are analogous to those associated with normal quasiparticles (spin-1/2 objects). In particular, as a simple model to demonstrate proof of concept, we take the device geometry to be rotationally symmetric along the axis associated with the Rashba interaction, as sketched in Fig. 3.1(a), or along the direction of the fixed magnetic layer, as sketched in Fig. 3.1(b). By analyzing the stability and dynamics of our model, we outline a phase diagram of the coupled system as a

function of applied magnetic field and current bias.

3.2 Model

The phenomenological equation of motion of an isolated ferromagnet sufficiently well below the Curie temperature is given by the Landau-Lifshitz-Gilbert (LLG) equation [PL80, Gil04]

$$\dot{\mathbf{m}} = -\gamma \mathbf{m} \times \mathbf{H} + \alpha \mathbf{m} \times \dot{\mathbf{m}} \,, \tag{3.1}$$

where γ is the gyromagnetic ratio and α is the dimensionless Gilbert damping. We use a normalized form of this equation, in which the (unit) magnetic direction vector $\mathbf{m} = \mathbf{M}/M_s$, $M_s = |\mathbf{M}|$ (saturation magnetization), is dimensionless. $\mathbf{H} = -\mathcal{V}^{-1}\partial F/\partial \mathbf{M}$ is the effective magnetic field and F, $\mathbf{M}$, and $\mathcal{V}$ are the free energy, magnetization vector, and volume, respectively. In the spin-valve model, Fig. 3.1(b), $\mathbf{m}$ will denote the free layer $\mathbf{m}_f$.

We consider the resistively-shunted junction (RSJ) model for the Josephson junction, wherein the device is composed of conventional superconductors with some Ohmic conductance σ in the junction [Lik86]. Additionally, we take the capacitance to be zero, which precludes RC-type delays in the coupled dynamics. The corresponding Josephson relations (for a static magnetization) are

$$\dot{Q} = I_c \sin\phi + \sigma V \,, \quad \dot{\phi} = \frac{2e}{\hbar} V \,, \tag{3.2}$$

where V is the voltage drop across the junction. ϕ is the phase difference between the superconducting reservoirs and Q is the charge transported by the junction. The supercurrent is proportional to the critical current, $I_c = (2e/\hbar)E_J$, where E_J parametrizes the Josephson energy $-E_J \cos\phi$. We note that Eq. (3.2) is dictated by gauge symmetry and, in anticipation of the arguments to follow, is a manifestation of Onsager reciprocity in the dynamics of Q and ϕ.

Under time reversal, $\dot{\mathbf{m}} \to \dot{\mathbf{m}}$ and $\alpha \mathbf{m} \times \dot{\mathbf{m}} \to -\alpha \mathbf{m} \times \dot{\mathbf{m}}$. The term proportional to α in the LLG equation thus reflects irreversible processes. We characterize such terms as dissipative. σ, likewise, parametrizes Ohmic dissipation of normal fluid. All other terms thus considered so far are reactive. Couplings between the free ferromagnet and superconductor at the level of the free energy, induced by the static magnetic layer or SOI, are restricted by the symmetries of our structure. Our device geometries, shown in Fig. 3.1, are assumed to be structurally invariant under arbitrary rotations about the z axis as well as a parity transformation followed by π rotation about the x (or y) axis. Because both the exchange interaction between the magnetic layers of our spin-valve device and the Josephson energy are individually preserved under the symmetries of the combined system, the product of these interactions must also be permitted [LY11]. However, the interlayer F|N|F spin-valve exchange is usually very small (except for the thinnest N spacers) [RS08], and will be disregarded in our study. One may, furthermore, show that any (time-reversal symmetric) bilinear cross term involving $\mathbf{m}$, Q, and ϕ does not respect the symmetries of our device geometry (keeping in mind that $\phi \to -\phi$ under time reversal and $\mathbf{m}$ is a pseudovector under improper rotations). In particular, an interaction of the type [Buz08] $\cos(\phi + \Gamma m_z)$ is forbidden in our geometry. Thus neglecting interactions of $\mathbf{m}$, Q, and ϕ beyond quadratic order, the free energy remains uncoupled:

$$F[\mathbf{m}, Q, \phi] = F[\mathbf{m}] + F[Q] + F[\phi]\,, \tag{3.3}$$

where $F[\mathbf{m}] = \mathcal{V} K M_z^2/2 - \mathcal{V}\mathbf{M} \cdot \mathbf{H}_a$, $F[Q] = -QV$, and $F[\phi] = -E_J \cos\phi$. The sign of the anisotropy constant, K, defines an easy plane or easy axis and is determined by the geometry of the device and crystalline anisotropies. $\mathbf{H}_a$ is an applied external magnetic field.

The LLG equation of motion of the magnet is now complemented with interactions that are quasistationary (i.e., first order in frequency), up to quadratic order in the components of $\mathbf{m}$, preserving the magnitude of $\mathbf{m}$, and consistent

with the structural symmetry of the device:

$$\begin{aligned}\dot{\mathbf{m}} = &-\gamma \mathbf{m} \times \mathbf{H} + \alpha \mathbf{m} \times \dot{\mathbf{m}} \\ &+ (\mu \dot{Q} + \lambda \dot{\phi}) \mathbf{m} \times \mathbf{z} \times \mathbf{m} + (\nu \dot{Q} + \kappa \dot{\phi}) \mathbf{m} \times \mathbf{z} \,. \end{aligned} \tag{3.4}$$

Hereafter, we are focusing on the spin-valve case, Fig. 3.1(b), where the phenomenological coupling coefficients μ, λ, ν, and κ may be taken to be angle-independent constants if we identify $\mathbf{z} \equiv \mathbf{m}_s$. [For the SOI device, Fig. 3.1(a), structural symmetries dictate these coefficients to be odd functions in m_z, similar to voltage-controlled torques at CoFeB/MgO interfaces [MSN09], which are due to magnetic anisotropy induced by broken inversion symmetry.] Constants μ and ν characterize the strength of the coupling between the magnet and the total current $\dot{Q}$. Similarly, the strength of the coupling between the magnet and the dynamics of the superfluid condensate $\dot{\phi}$ is characterized by λ and κ. To the reader familiar with spin valves [RS08], Eq. (3.4) is reminiscent of the Landau-Lifshitz-Gilbert equation with the so-called Slonczewski and field-like torques, respectively, added on the second line of the right-hand side. In this case, sketched in Fig. 3.1(b), current is spin polarized by passing through the fixed magnetic layer. The resulting spin-polarized current impinging on a free ferromagnet induces torque due to conservation of angular momentum. In the case of a single magnetic layer with SOI, Fig. 3.1(a), a spin torque is generated via SOI inside this layer itself [MZ08, HBT10]. Because the leads in our system are superconducting, we additionally generate a torque as a result of the dynamics of the superfluid condensate. Loosely speaking, the torque induced by both currents, normal current and supercurrent, through the junction produce two channels for driving magnetization dynamics (and thus two sets of terms, as compared to the usual normal-metal spin torques). Appropriately, above the critical temperature of the superconductor, we recover the normal-metal limit, in which torque is generated by the Ohmic current (or, equivalently, voltage) alone [MSN09, MZ08, HBT10].

The reaction of the current and superconducting phase dynamics to the mag-

net are not captured by the Josephson relations, Eq. (3.2), which would not be consistent with Eq. (3.4). One must extend Eq. (3.2) to include the pumping terms satisfying Onsager reciprocity, in order to obtain equations of motion for our coupled system that obey microscopic time-reversal symmetry [PL80]. Because the magnet flips under time reversal (upon invoking Onsager symmetry), one must additionally use the symmetries of the structure to relate the time-reversed state to the original. After straightforward manipulations, that are analogous to [HBT10] for normal junctions, we construct the following equations in lieu of Eq. (3.2):

$$\begin{aligned}\dot{Q} &= \frac{2e}{\hbar}\left[E_J \sin\phi - \mathcal{S}(\lambda \dot{\mathbf{m}} \cdot \mathbf{m} \times \mathbf{z} + \kappa \dot{\mathbf{m}} \cdot \mathbf{z})\right] + \frac{\hbar\sigma}{2e}\dot{\phi}\,, \\ \dot{\phi} &= \frac{2e}{\hbar}\left[V - \mathcal{S}(\mu \dot{\mathbf{m}} \cdot \mathbf{m} \times \mathbf{z} + \nu \dot{\mathbf{m}} \cdot \mathbf{z})\right] - \rho \dot{Q}\,, \end{aligned} \tag{3.5}$$

where $\mathcal{S} = \mathcal{V} M_s/\gamma$ is the total spin angular momentum of the ferromagnetic layer. We disregard TMR, keeping σ constant with respect to magnetization. These equations of motion now include both normal and superfluid pumping, which are Onsager reciprocal to the driving effects introduced in the generalized LLG equation, Eq. (3.4). Our theory includes two types of pumping as a result of the non-Ohmic relationship between current and voltage. The term with coefficient ρ causes current to drag phase across the device; ρ is a measure of the viscosity between the current and superfluid condensate. Although this term is not needed for consistency with Onsager reciprocity, we will see that it would generally have to be included in order to satisfy the second law of thermodynamics. We could also immediately notice that the coefficients ρ, ν, and μ should vanish in the limit of large superconducting reservoirs, recovering the ordinary ac Josephson effect (as expected based on the gauge invariance). Keeping these terms, on the other hand, would capture finite-size (mesoscopic) properties of the superconducting layers, which are of secondary interest to our ends.

We may write the equations of motion in a dimensionless form by measuring time, magnetic field, charge, voltage, and conductance in units of $\mathcal{S}/E_J$, $E_J/\gamma\mathcal{S}$,

$2e\mathcal{S}/\hbar$, $E_J\hbar/2e\mathcal{S}$, and $\mathcal{S}(2e/\hbar)^2$, respectively:

$$\begin{aligned}
\dot{\mathbf{m}} =& -\mathbf{m}\times\mathbf{H} + \alpha\mathbf{m}\times\dot{\mathbf{m}} + \dot{\phi}(\lambda\mathbf{m}\times\mathbf{z}\times\mathbf{m} + \kappa\mathbf{m}\times\mathbf{z}) \\
&+ \dot{Q}(\mu\mathbf{m}\times\mathbf{z}\times\mathbf{m} + \nu\mathbf{m}\times\mathbf{z})\,, \\
\dot{Q} =& \sin\phi - \lambda\dot{\mathbf{m}}\cdot\mathbf{m}\times\mathbf{z} - \kappa\dot{\mathbf{m}}\cdot\mathbf{z} + \sigma\dot{\phi}\,, \\
\dot{\phi} =& V - \mu\dot{\mathbf{m}}\cdot\mathbf{m}\times\mathbf{z} - \nu\dot{\mathbf{m}}\cdot\mathbf{z} - \rho\dot{Q}\,.
\end{aligned} \tag{3.6}$$

Additionally, allow us to absorb a factor of $\mathcal{V}M_s^2/E_J$ into the anisotropy constant, such that the free energy for the magnet reads $F[\mathbf{m}, Q, \phi] = E_J(Km_z^2/2 - \mathbf{m}\cdot\mathbf{H}_a - QV - \cos\phi)$. Under time reversal, the terms with coefficients ν and λ reverse sign in the LLG equation. Because $\dot{\mathbf{m}}$ does not change sign, these are dissipative. Likewise, the terms with coefficients μ and κ do not reverse sign and are thus nondissipative. σ is a dissipative coefficient, therefore ρ is as well.

Let us try to understand the microscopic origin of the dissipative terms in our theory. Consider momentarily only the RSJ subsystem: when enough energy is supplied (either thermally or by a bias), quasiparticles are able to overcome the superconducting gap and transport through the junction. Normal scattering of quasiparticles across the junction causes Ohmic resistance. Likewise, consider an isolated precessing ferromagnet. This is microscopically described by a coherent magnon state that can decay into phonons and incoherent magnons, processes which macroscopically give Gilbert damping. In the case of a metallic ferromagnet, the additional decay channel into the electron-hole continuum enhances further its Gilbert damping. Upon coupling these subsystems, energy is shared by the entire structure. Likewise, dissipation by microscopic mechanisms underlying Ohmic conductance and Gilbert damping can give rise to a dissipative (viscous) energy transfer between ferromagnetic and superconducting layers, as parametrized by new dissipative coefficients ν and λ. Phenomenologically, therefore, we may expect σ, α, and ρ to bound ν and λ, which is indeed verified below.

In the RSJ model, Eq. (3.2), if ϕ is static, we are in a superconducting (S)

state because only dissipationless current is passing through the junction. Likewise if ϕ is not constant, the circuit must have a finite voltage drop. This is called a resistive (R) state. Notice that in our generalized model, Eqs. (3.6), a choice of dynamics that leave ϕ static can still generate dissipative current due to magnetic pumping. We will, nonetheless, keep refering to the static and dynamic states of ϕ as the superconducting (S) and resistive (R) states, respectively, even though this terminology is, in general, abusive, in the presence of the new spin-torque/pumping terms in Eqs. (3.6).

We distinguish between two regimes governed by the superconducting coherence length ξ. When ξ is smaller than the thickness of superconducting layers, the bulk properties of the superconductors will be largely detached from physics at the interfaces. Thus for superconducting *reservoirs,* a change in phase difference cannot be induced by transport through the junction. We expect the corresponding coefficients μ, ν, and ρ to scale inversely with the volume of the smaller of the superconducting layers then; these are representative of mesoscopic effects, as has already been inferred above. Because charge is a conserved hydrodynamic quantity, on the other hand, the electric current should be maintained in the bulk far from the junction. In particular, λ, κ, and σ should not depend on the size of superconducting reservoirs; these coefficients parametrize the properties of the Josephson junction itself and are thus of central interest to us.

In what follows we consider a dc current biased junction, $\dot{Q} = I$, where the applied magnetic field is along the axis of symmetry, $\mathbf{H}_a = H_a\hat{\mathbf{z}}$, and K is positive (which is generically the case for films with magnetostatic energy dominating over crystalline anisotropy).

3.3 Decoupled Junction

In the special case where $\lambda = \kappa = 0$ in Eqs. (3.6), the current-biased magnetic and superconducting dynamics decouple. We take this opportunity to recall the properties of magnetic spin valves and the RSJ model of superconductors, to which the decoupled equations map. Ignoring λ and κ,

$$\begin{aligned} \dot{\mathbf{m}} &= -\mathbf{m} \times \mathbf{H} + \alpha \mathbf{m} \times \dot{\mathbf{m}} + I(\mu \mathbf{m} \times \mathbf{z} \times \mathbf{m} + \nu \mathbf{m} \times \mathbf{z}) \,, \\ \sigma \dot{\phi} &= I - \sin \phi \,. \end{aligned} \tag{3.7}$$

The equation of motion for the magnet is thus the LLG equation for a spin valve, including Slonczewski (μ) and field-like (ν) torques, in the case that a fixed magnetic layer points along the z axis. The superconductor is described by the RSJ model with zero capacitance.

There are three possible stable states of the current-biased magnet in the presence of a static field in the z direction: pinned parallel to the z axis, antiparallel to the z axis, or precessing around the z axis, labeled p, a, and o, respectively. A pinned state is stable when $|(\mu/\alpha - \nu)I/K + h_a| \geq 1$, where $h_a \equiv H_a/K$. If $|(\mu/\alpha - \nu)I/K + h_a| < 1$, the magnet precesses at frequency $\omega_M = \mu I/\alpha$. The corresponding stability diagram with Hopf bifurcation lines is shown in Fig. 3.2. In the dimensionless form of the RSJ description, when $-1 \leq I \leq 1$, the junction is in the S state and the phase is fixed at $\phi = \sin^{-1} I$. When the current is raised beyond the critical current, $I > 1$, the Josephson junction is in the R state and ϕ oscillates with frequency $\omega_J = \sqrt{I^2 - 1}/\sigma$ [Lik86]. For the RSJ model, a π junction is trivially impossible: $|\phi|$ cannot access values between $\pi/2$ and π. The inset of Fig. 3.2 displays the well-known phase diagram of the RSJ junction.

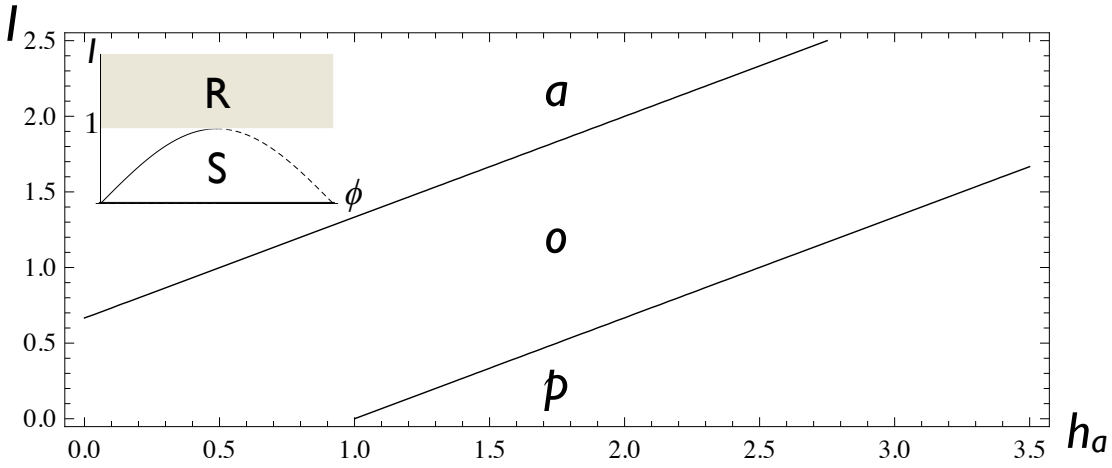

Figure 3.2: Stability diagram as a function of the current and applied magnetic field of the decoupled magnet. $\mu = -1.5$, $\nu, \lambda, \kappa = 0$, and $K = 1$. p and a label the parallel and antiparallel states of the magnet, respectively. Inset: decoupled Josephson junction. The S state (unshaded) and R state (shaded) are separated by the line $I = 1$. Solid line is the value of ϕ for a 0 junction and dashed for the unstable π junction.

3.4 Coupled Junction

Neglecting mesoscopic effects, we set ρ, ν, μ to zero:

$$\begin{aligned}\dot{\mathbf{m}} &= -\mathbf{m}\times\mathbf{H} + \alpha\mathbf{m}\times\dot{\mathbf{m}} + \dot{\phi}(\lambda\mathbf{m}\times\mathbf{z}\times\mathbf{m} + \kappa\mathbf{m}\times\mathbf{z})\,,\\ \sigma\dot{\phi} &= I - \sin\phi + \lambda\dot{\mathbf{m}}\cdot\mathbf{m}\times\mathbf{z} + \kappa\dot{\mathbf{m}}\cdot\mathbf{z}\,.\end{aligned} \tag{3.8}$$

Thermodynamic self consistency of our theory requires for the dissipation power $P = (E_J^2/\mathcal{S})(\alpha\dot{\mathbf{m}}^2 - 2\lambda\dot{\mathbf{m}}\cdot\mathbf{m}\times\mathbf{z}\dot{\phi} + \sigma\dot{\phi}^2) \geq 0$. This bounds our phenomenological constant λ as $\lambda^2 \leq \alpha\sigma$ (while, clearly, $\alpha \geq 0$ and $\sigma \geq 0$). To proceed with the analysis, notice that, according to Eq. (3.8), the dynamics of m_z and ϕ decouple from the transverse dynamics ($m = m_x + im_y$), which can, in turn, be expressed in terms of (m_z, ϕ):

$$\begin{aligned}\dot{m}_z =& (1-m_z^2)\left[\bar{\alpha}(H_a - Km_z) + \bar{\lambda}\dot{\phi}\right]\,,\\ \dot{\phi} =& \frac{I - \sin\phi - \bar{\lambda}(H_a - Km_z)(1-m_z^2)}{\sigma - (\lambda\bar{\kappa} + \kappa\bar{\lambda})(1-m_z^2)}\,,\\ m =& \sqrt{1-m_z^2}\exp\left[-\frac{i}{\alpha}\left(\lambda\phi + \frac{1}{2}\ln\frac{1-m_z}{1+m_z}\right) + i\varphi\right]\,,\end{aligned} \tag{3.9}$$

where $\bar{\lambda} \equiv (\lambda - \alpha\kappa)/(1+\alpha^2)$, $\bar{\kappa} \equiv (\kappa + \alpha\lambda)/(1+\alpha^2)$, $\bar{\alpha} \equiv \alpha/(1+\alpha^2)$ and φ determined by initial conditions. Consequently, the fixed points of the equations of motion for m_z and ϕ immediately determine the state of the full system.

When the current is below the critical current, $I \leq 1$, one can show that there are three stable fixed points: p_0, a_0, and o_0 which correspond to a Josephson 0-junction (defining a junction with $|\phi| < \pi/2$ to be in the "0 phase" and $\pi/2 < |\phi| < \pi$ in the "π phase") and magnetic direction parallel, antiparallel, and away from the z axis, respectively. In all these states ϕ is fixed by the applied current such that $\sin\phi = I$. As indicated by our stability diagram, Fig. 3.3, the state of our device is determined by the applied magnetic field. When $|h_a| \leq 1$, $m_z = h_a$ and m is fixed by initial conditions. By applying a sufficiently large external magnetic field, $|h_a| \geq 1$, o_0 is annihilated under a saddle-node bifurcation [GH83], and the

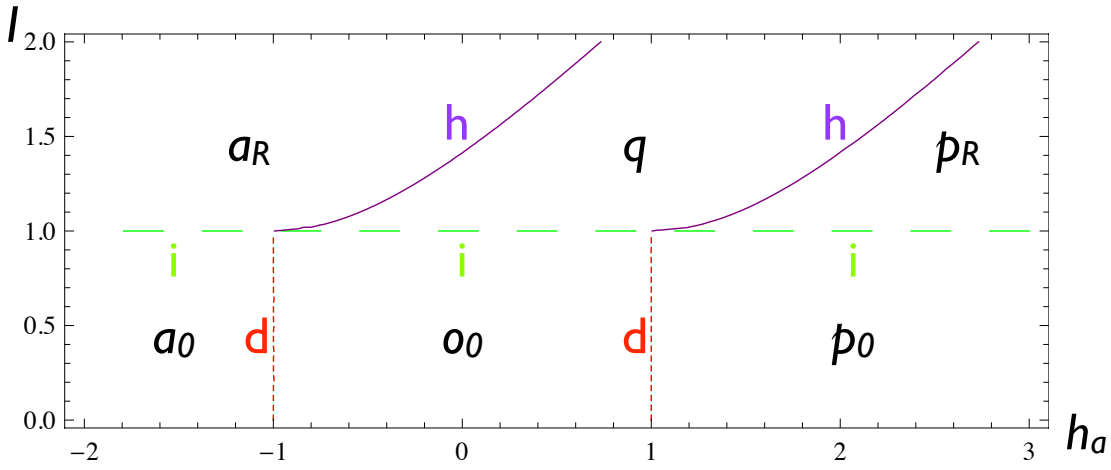

Figure 3.3: Stability diagram as a function of the current, I, and applied magnetic field h_a. $\lambda = -0.1$, $\mu, \nu, \kappa = 0$, $K = 1$, $\alpha = 1$, and $\sigma = 0.1$. h labels the Hopf bifurcation (solid lines), i labels the infinite-period bifurcation (long-dashed lines), and d labels the saddle-node bifurcation (short-dashed lines).

sole stable state is p_0 or a_0 for positive or negative applied field, respectively, pinning the magnet along the z axis.

If the current exceeds its critical value, $I > 1$, the superconducting phase and z component of the magnet become dynamic. This disappearance of all the fixed points is an infinite-period bifurcation [GH83]. Because no fixed points exist, the Poincaré-Bendixson theorem implies any closed orbit on the cylinder, parameterized by m_z and ϕ, is periodic and must go around the circumference of this cylinder. Supposing the frequency of this periodic motion is Ω_J, m_z may be written as a constant plus terms periodic in Ω_J. Likewise, we may express $\phi = n\Omega_J t$ (with nonzero $n \in \mathbb{Z}$) plus terms periodic in Ω_J. Therefore, the characteristic frequency of the system is given by the time average of $\dot{\phi}$. According to the equation for transverse component of the magnet, Eqs. (3.9), we find it undergoes rotations at frequency $n(\lambda/\alpha)\Omega_J$ that are superimposed with Ω_J oscillations. Therefore the magnet in general undergoes quasiperiodic motion, a state we label q.

To determine the full expression for Ω_J when $I > 1$ would require solving

the system of differential equations Eqs. (3.9). For simplicity, consider the limit of small λ and κ, so that we can neglect quadratic terms in λ and κ. In this case, the characteristic frequency of the Josephson junction is given by the usual RSJ frequency $\omega_J = \sqrt{I^2-1}/\sigma$ [Lik86]. In region q of our stability diagram, Fig. 3.3, m_z oscillates with frequency ω_J around the average value $\mathrm{sign}(I)(\lambda/\alpha - \kappa)\omega_J + h_a/K$. Near the point $|\mathrm{sign}(I)(\lambda/\alpha-\kappa)\omega_J + h_a/K| = 1$, a Hopf bifurcation [GH83] (labeled h) is induced wherein the quasiperiodic orbit disappears and the magnet is parallel or antiparallel to the z axis, labeled p_R and a_R respectively, and the phase is dynamic. We anticipate the higher-order coupling in λ and κ to modify the frequency dependence on current. Furthermore, we expect that, near the line defining the Hopf bifurcation, there exists a phase of bimodal stability wherein the magnet can orient along the z axis or precess quasiperiodically, subject to the initial conditions. This is a natural consequence of the reciprocity of current-driven magnetic dynamics and pumping and persists even in the absence of any superconductivity (i.e., $E_J = 0$). Details of these rich coupled nonlinear dynamics are, however, beyond the scope of the present paper.

3.5 Mesoscopic Junction

Finally, we analyze the properties of the general junction wherein we do not restrict any phenomenological parameters in Eqs. (3.6) to be zero, thus including mesoscopic effects. After dc biasing, we obtain the equations of motion for $\mathbf{m}$ and ϕ:

$$\begin{aligned}\dot{\mathbf{m}} =& -\mathbf{m}\times\mathbf{H} + \alpha\mathbf{m}\times\dot{\mathbf{m}} + \dot{\phi}(\lambda\mathbf{m}\times\mathbf{z}\times\mathbf{m} + \kappa\mathbf{m}\times\mathbf{z}) \\ &+ I(\mu\mathbf{m}\times\mathbf{z}\times\mathbf{m} + \nu\mathbf{m}\times\mathbf{z})\,, \\ \sigma\dot{\phi} =& I - \sin\phi + \kappa\dot{m}_z + \lambda\dot{\mathbf{m}}\cdot\mathbf{m}\times\mathbf{z}\,, \end{aligned} \tag{3.10}$$

where $I = \dot{Q}$ is fixed. If the applied magnetic field is strictly along the axis of rotational symmetry of our junction, $\mathbf{H} = H_a\hat{\mathbf{z}}$, the transverse equations of motion

decouple from (m_z, ϕ) and we obtain:

$$\begin{aligned}\dot{m}_z =&(1-m_z^2)\left[\bar{\alpha}(H_a - Km_z) + \bar{\lambda}\dot{\phi} + \bar{\mu}I\right], \\ \Sigma\dot{\phi} =&I - \sin\phi - \left[\bar{\lambda}(H_a - Km_z) - I(\bar{\mu}\kappa + \bar{\nu}\lambda)\right](1-m_z^2), \end{aligned} \tag{3.11}$$

where $\bar{\mu} \equiv (\mu - \alpha\nu)/(1+\alpha^2)$, $\bar{\nu} \equiv (\nu + \alpha\mu)/(1+\alpha^2)$ and $\bar{\lambda} \equiv (\lambda - \alpha\kappa)/(1+\alpha^2)$, $\bar{\kappa} \equiv (\kappa + \alpha\lambda)/(1+\alpha^2)$, $\bar{\alpha} \equiv \alpha/(1+\alpha^2)$, as before. Note that $\Sigma \equiv \sigma - (\lambda\bar{\kappa} + \kappa\bar{\lambda})(1-m_z^2)$ is guaranteed to be nonnegative by the thermodynamic bound $\lambda^2 \leq \alpha\sigma$. We see this by setting κ to be λ/α, which maximizes the quantity $\lambda\bar{\kappa} + \kappa\bar{\lambda}$ at $\lambda^2/\alpha \leq \sigma$. Furthermore, according to Sylvester's criterion, the thermodynamic bound requires the additional condition $\alpha\rho\sigma - \nu^2\sigma - \lambda^2\rho \geq 0$ in the general mesoscopic regime.

One can show that the general solution for transverse components is (up to an arbitrary phase shift φ)

$$m = \sqrt{1-m_z^2}\exp\left[-\frac{i}{\alpha}\left(\mu I t + \lambda\phi + \frac{1}{2}\ln\frac{1-m_z}{1+m_z}\right)\right]. \tag{3.12}$$

The fixed points in the (m_z, ϕ) plane are

$$(\bar{m}_z, \bar{\phi}) = \begin{cases} (\pm 1, \sin^{-1} I), \ \ (\pm 1, \pi - \sin^{-1} I) \\ \left((\mu/\alpha - \nu)I/K + h_a, \sin^{-1} I'\right) \\ \left((\mu/\alpha - \nu)I/K + h_a, \pi - \sin^{-1} I'\right) \end{cases}, \tag{3.13}$$

where we have introduced

$$I' \equiv I\left[1 + (\mu/\alpha)\lambda\left(1 - \bar{m}_z^2\right)\right] \tag{3.14}$$

with $\bar{m}_z = (\mu/\alpha - \nu)I/K + h_a$ that itself depends on the current bias I. At the first four fixed points, the magnet is pinned parallel or antiparallel to the z axis and can be either a 0 or π junction. Hence we label these fixed points p_0, a_0, p_π, and a_π. The final two fixed points [which are possible when $|(\mu/\alpha - \nu)I/K + h_a| < 1$] are labeled by o_0 and o_π. These o_0 and o_π points are stationary in the (m_z, ϕ)

plane but the transverse components of the magnet follow a circular orbit of radius $\sqrt{1-\bar{m}_z^2}$ at frequency $\omega_M = \mu I/\alpha$.

The salient differences between these fixed points and those found studying the fixed points of Eqs. (3.9) are in the properties of o_0 and o_π. First, the transverse component of the ferromagnet is dynamic when $\mu \neq 0$. Second, the static value of $\sin\phi$ is a nonlinear function of the current. This results in a change in shape of the boundary separating the S and R states of the superconductor: see, for example, Fig. 3.4, where the phase diagram develops a "foldover region." Consider the current increase at fixed magnetic field along the dashed line in Fig. 3.4. The system undergoes changes from (1) S to R, (2) R to S, and (3) S to R again. Unlike in a conventional Josephson junction, our model has multiple values of the current for which the junction changes between superconducting and resistive states. Thus the junction has three 'critical currents.' Likewise at a particular fixed value of current, we can induce a change from R to S then S to R by increasing or decreasing the applied magnetic field. This has no analogy in the RSJ model.

We study the stability of the fixed points in Eq. (3.13) by linearizing Eq. (3.11) around $(\bar{m}_z, \bar{\phi})$

$$\begin{aligned}
\dot{m}_z =&(\bar{m}_z^2 - 1)(\bar{\alpha}Km_z - \bar{\lambda}\dot{\phi}) \\
&+ 2m_z\bar{m}_z(\bar{\alpha}K\bar{m}_z - \bar{\alpha}H_a - \bar{\mu}I)\,, \\
\bar{\Sigma}\dot{\phi} =& -\phi\cos\bar{\phi} + \bar{\lambda}Km_z(1-\bar{m}_z^2) \\
&- 2m_z\bar{m}_z\left[\bar{\lambda}(K\bar{m}_z - H_a) + \lambda\bar{\nu}I + \kappa\bar{\mu}I\right]\,,
\end{aligned} \tag{3.15}$$

where we have introduced $\bar{\Sigma}$ as Σ evaluated at the fixed point $\bar{m}_z$. Recall that the stability properties of a system of linear differential equations, $\dot{\mathbf{x}} = \hat{\mathbf{A}}\mathbf{x}$, around a fixed point, $\bar{\mathbf{x}}$, of a pair variables, $\mathbf{x} = \{x_1, x_2\}$, are classified according to the following criteria: (1) $\det\hat{\mathbf{A}} < 0$, $\bar{\mathbf{x}}$ is a saddle point, (2) $\det\hat{\mathbf{A}} > 0$ and $\mathrm{tr}\hat{\mathbf{A}} < 0$, $\bar{\mathbf{x}}$ is stable, and (3) $\det\hat{\mathbf{A}} > 0$ and $\mathrm{tr}\hat{\mathbf{A}} > 0$, $\bar{\mathbf{x}}$ is unstable [BMS09]. The matrix

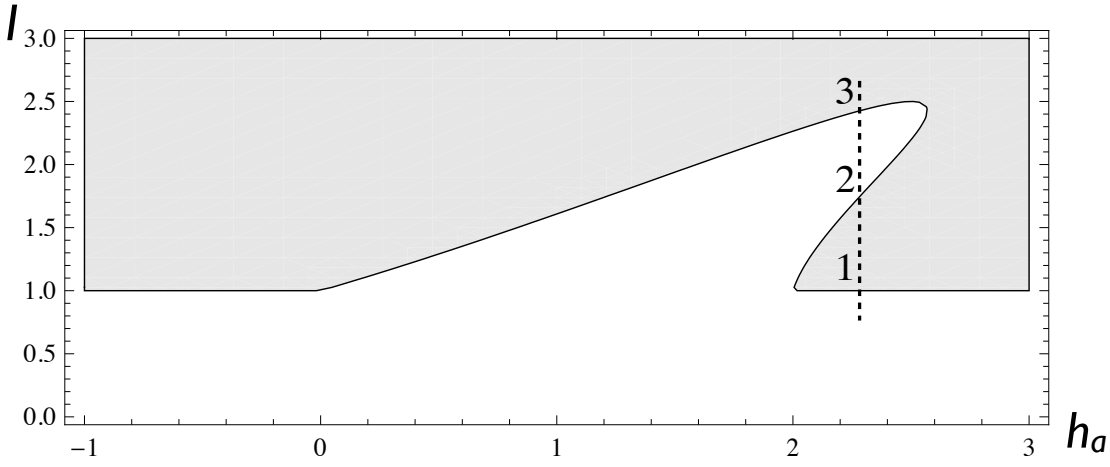

Figure 3.4: Separation of the S state (white) and R state (grey) of the superconductor by a nonlinear function defined by $I' = 1$. The parameters of this system are $\mu = -1$, $\lambda = 0.6$, $\nu, \kappa = 0$, $K = \alpha = 1$, and $\sigma = 2$. The $1, 2, 3$ labels along the dashed line show the three places where the Josephson junction switches between superconducting and resistive states.

defining the linearization around the fixed points with $\bar{m}_z = \pm 1$ is

$$\begin{bmatrix} 2[\bar{\alpha}K \mp (\bar{\alpha}H_a + \bar{\mu}I)] & 0 \\ -2/\sigma\left[\bar{\lambda}K \pm (\lambda\bar{\nu}I + \kappa\bar{\mu}I - \bar{\lambda}h_a)\right] & -\sigma^{-1}\cos\bar{\phi} \end{bmatrix}. \tag{3.16}$$

Because only the diagonal terms of the matrix in Eq. (3.16), which are independent of λ and κ, contribute to the trace and determinant, the stability analysis proceeds as in the decoupled regime. Specifically, if the current and magnetic field are not large enough to overcome the anisotropy, $\bar{\alpha}K > |\bar{\alpha}H_a + \bar{\mu}I|$, then these points are unstable π-junctions or saddle point 0-junctions. If the external sources are large enough to overcome the anisotropy, $\bar{\alpha}K < |\bar{\alpha}H_a + \bar{\mu}I|$, the π-junction is a saddle point and the 0-junction is stable node. When $\bar{m}_z = (\mu/\alpha - \nu)I/K + h_a$, the linearization matrix

$$\hat{\mathbf{A}} = \begin{bmatrix} (\bar{m}_z^2 - 1)\bar{\alpha}K - \bar{\lambda}\bar{\Sigma}^{-1}(\bar{m}_z^2 - 1)\Gamma & \bar{\lambda}\bar{\Sigma}^{-1}(\bar{m}_z^2 - 1)\cos\bar{\phi} \\ \bar{\Sigma}^{-1}\Gamma & -\bar{\Sigma}^{-1}\cos\bar{\phi} \end{bmatrix}, \tag{3.17}$$

where we have defined $\Gamma \equiv \left[\bar{\lambda}K(1-\bar{m}_z^2) - 2\mu\lambda I\bar{m}_z/\alpha\right]$ for brevity. One may show that the determinant of the this matrix is equal to that of an uncoupled junction and, because we have chosen $K > 0$, π-junctions are always saddle nodes and therefore cannot be realized in this device geometry.

We point out, however, that for $K < 0$ a π-junction can be stable or unstable subject to the trace of the above matrix. Because $\bar{\alpha} > (1-\bar{m}_z^2)\bar{\lambda}^2/\bar{\Sigma}$ as a result of the thermodynamic bound on λ, a stable π-junction is precluded in the absence of mesoscopic effects. However, in general, there is an additional term that contributes to stability in Eq. (3.17): $2\bar{m}_z(\bar{m}_z^2-1)\mu\lambda\bar{\lambda}I/\alpha\bar{\Sigma}$. We find that for sufficiently large κ and conductance, and thereby sufficiently large λ, an applied magnetic field and current can stabilize a π-junction in the mesoscopic regime.

Away from the fixed points, a rich variety of the coupled dynamics generally emerges, as seen in Fig. 3.5, where we have plotted the stereographic projection of the magnetic direction. A detailed analysis of this motion is deferred to a future study.

3.6 Summary and Outlook

We have introduced a model of S|F|S and S|F|N|F|S heterostructures coupling the dynamics of the magnets to that of the superconductor via a Rashba SOI in single-layer junctions and via magnetic misalignment in spin-valve junctions. We expect such structures to be highly adaptable to uses in spintronics due to the versatility with which one can in principle influence both the magnet and superconductor.

The S|F|S structures deposited on topological insulators (engendered by strong SOI) were studied in [TYN09, BL11]. With an appropriate modification of the Josephson effect in the presence of Majorana modes and, if necessary, revision of the structural symmetries, such systems can also be amenable to our phenomenol-

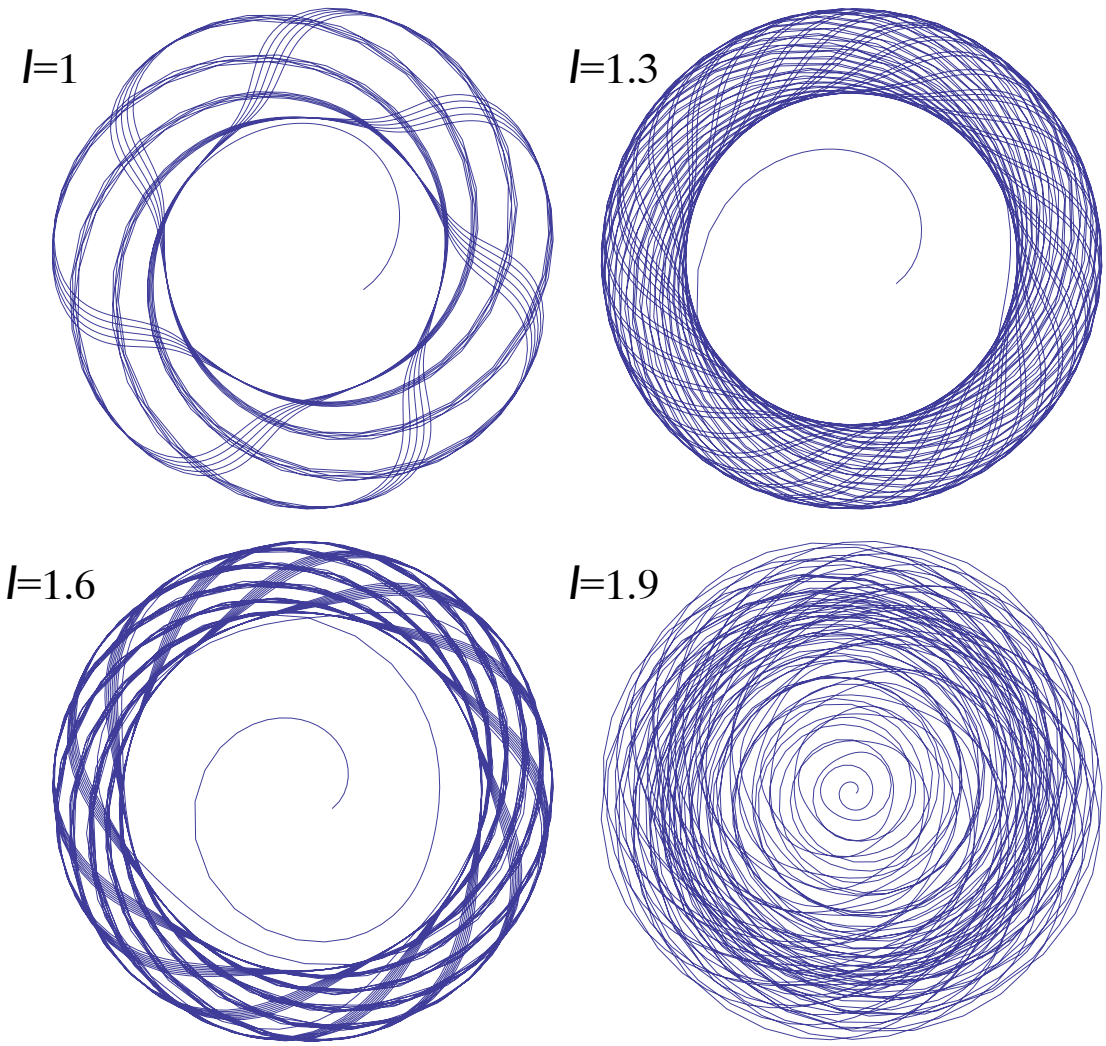

Figure 3.5: Stereographic projection of the magnetization at different currents. Here, $\mu = 0.1$, $\lambda = 0.5$, $\nu, \kappa = 0$, $K = 1$, $\alpha = 1$, and $\sigma = 1$.

ogy.

Chaos in ferrites and magnetic thin films is often attributed to spatially nonuniform magnetizations [BMS09]. Perhaps a simpler route towards chaos in our model is by applying a magnetic field perpendicular to the axis of cylindrical symmetry. As a result, the dynamic equations become three dimensional and thus no longer restricted by the Poincaré-Bendixson theorem to periodic orbits or fixed points.

CHAPTER 4

Texture Effects on Magnetic Bit Stability

We numerically study the thermal stability properties of computer memory storage realized by a magnetic ellipse. In the case of practical magnetic random-access memory devices, the bit can form a spin texture during switching events. To study the energy barrier for thermally-induced switching, we develop a variational procedure to force the bit to traverse a smooth path through configuration space between the points of stability. We identify textured configurations realizing domain-wall propagation, which may have an energy barrier less than that of the corresponding monodomain model. We contrast the emergence of such micromagnetic effects in thermal versus field-induced switching.

4.1 Background

The mechanisms of tunnel magnetoresistance [Jul75] and spin-transfer torque [Slo96, Ber96] offer a simple and localized method in which to read and write computer memory by applying electric currents rather than magnetic fields [IHL07, CAD10]. The corresponding devices have the potential to improve write energy and speed and decrease bit area. Equally as important is the lifetime of the bit; that is, the robustness of the bit against thermal fluctuations between the "on" and "off" states. This is furnished by the energy barrier, E_b, separating the points of bimodal stability and typically characterized by the dimensionless thermal-stability parameter, $\Delta = E_b/k_BT$, wherein k_B is Boltzmann constant and T ambient temperature.

Experimentally, the thermal barrier can be extracted using either a stochastic or deterministic approach. In stochastic methods, the thermal barrier is extrapolated from the thermal fluctuations of the magnet between the bistable points. Because these fluctuations are of the order of the bit lifetime at room temperature, switching is in practice assisted by a large temperature, a spin-transfer torque, or a magnetic field [KKS04, LKS04, YTF04, HYO05]. However, at large temperatures, the system parameters, such as magnetic saturation and anisotropies, become difficult to extrapolate making this method unreliable. Likewise, although the thermal stability can be extrapolated accurately at low voltages upon the application of a spin-transfer torque, at high voltages the local temperature may be too high to rely on the equilibrium parameters of our system due to the injection of "hot" electrons and the associated Ohmic losses. For deterministic field-induced switching, one applies an external magnetic field in the easy plane [UAK11]. By determining the magnitude of the magnetic field at which the system is no longer bimodally stable, the energy barrier can be ascertained. Following this procedure for all directions in the easy plane, one obtains a Stoner-Wohlfarth astroid curve [SW48, TG08]. In order to be viable, all these methods generally assume a single-domain model of the magnet. In this model, there is only one planar path through configuration space between one point of stability and the other. However, when the characteristic length scale of the spin texture becomes comparable to the major axis of the elliptical bit, a richer configuration space becomes energetically accessible, opening the possibility for a textured path with a lower energy barrier between the stable points [LDR04, LD06, RML06, SCA08]. As a result, extraction of the thermal barrier can be ambiguous.

In our analysis, we consider a magnetic ellipse of typical dimensions and material properties as those expected to be used as memory. For these values, we find that the exchange energy is of the order of the demagnetization energy. By applying slowly rotating local magnetic fields, which guide certain variationally

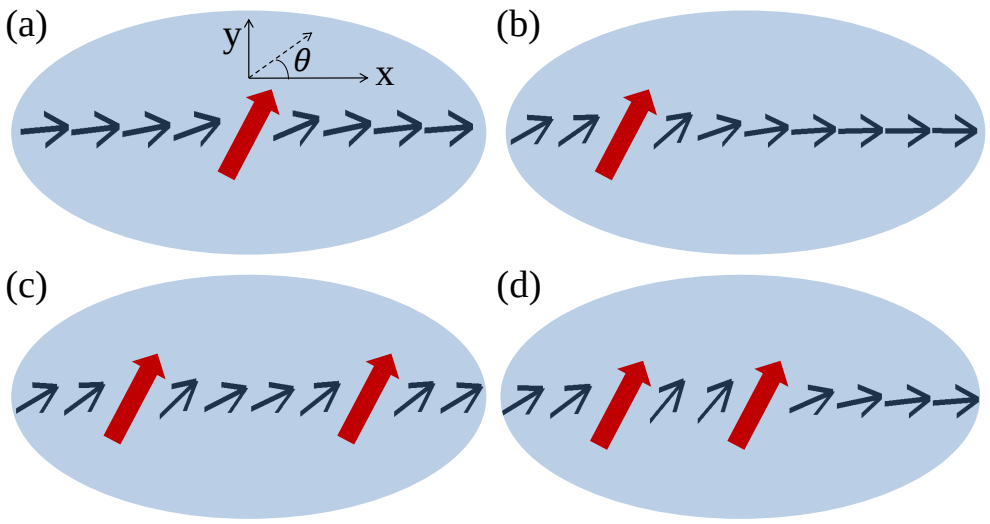

Figure 4.1: Application of the local pinning fields (thick arrows) and schematic of the resulting magnetic textures (thin arrows): (a) Center pinning, (b) left off–center, (c) simultaneous left-off-center and right-off-center, and (d) simultaneous center and left-off-center. We find that (b) produces the lowest energy barrier.

preselected points along the major axis (see Fig. 4.1), we force the bit into a series of textured configurations through phase space that continuously evolve one stable minimum into the other. We find a path between the bistable points, resembling domain-wall propagation, whose energy barrier is smaller than that of a single domain. We stress that the applied magnetic field is only a tool to elicit a magnetic configuration of which the details are, therefore, irrelevant to this study. For a concrete numerical demonstration, we start by modeling our bit as a $V = 150 \times 50 \times 2$ nm^3 thin-film ellipse with saturation magnetization of $M_s = 1100$ emu/cm^3 and exchange stiffness $A = 2$ μerg/cm. We choose to focus on magnetic tunnel junctions whose shape anisotropy is larger than the crystalline anisotropy (which is the case in many practical situations). Our axes are oriented such that the xy plane is in the plane of the ellipse and the easy (major) axis is along x. See Fig. 4.1. The energy of the bit is written as sum of the exchange

and demagnetization contributions:

$$F = E_{\rm xc} + E_{\rm dm}\,, \tag{4.1}$$

where $E_{\rm xc} = A\int dV(\nabla\mathbf{m})^2$, $\mathbf{m}$ is the unit magnetization vector, and $E_{\rm dm}$ is the dipole-dipole interaction. Note that the locally applied magnetic field here is only a theoretical tool to elicit a magnetic configuration, and in the following we are not including the associated contribution to the total energy. (This is in contrast to the experimentally relevant uniform applied fields included in Fig. 3 below and the pertinent discussion.) In the single-domain limit, $E_{\rm xc} = 0$ and $E_{\rm dm} = (N_x m_x^2 + N_y m_y^2 + N_z m_z^2)VM_s^2$, where the demagnetization factors $N_x + N_y + N_z = 2\pi$. The energy barrier is then simply given by $E_b = (N_y - N_x)VM_s^2$, corresponding to the xy-plane magnetization rotation. We define the characteristic length of the texture to be $\ell \sim \sqrt{A/N_y M_s^2}$. Because for our structure $\ell \sim 30$ nm, less than the major axis of our ellipse, micromagnetic (i.e., spin-texture) effects can be important.[1]

4.2 Results and Discussion

To find a continuous path through configuration space from one stable point to the other, we apply a single or a pair of localized (8×8 nm^2) pinning fields that force the magnet into a particular configuration, as sketched in Fig. 4.1. Initially oriented along the easy axis, we slowly rotate the pinning field in the xy plane, allowing the (twisted) texture to equilibrate, and calculate the internal energy. In order to variationally find an optimal path, we studied four different methods of applying the pinning field, which are depicted in Fig. 4.1. Calculating the internal energy as a function of angle of the pinning fields, we are able to plot the energy of the system as the bit flips. The principal results of our work can be found

[1] In order to simulate micromagnetic effects we use Michael Scheinfein's *LLG Micromagnetic Simulator*.

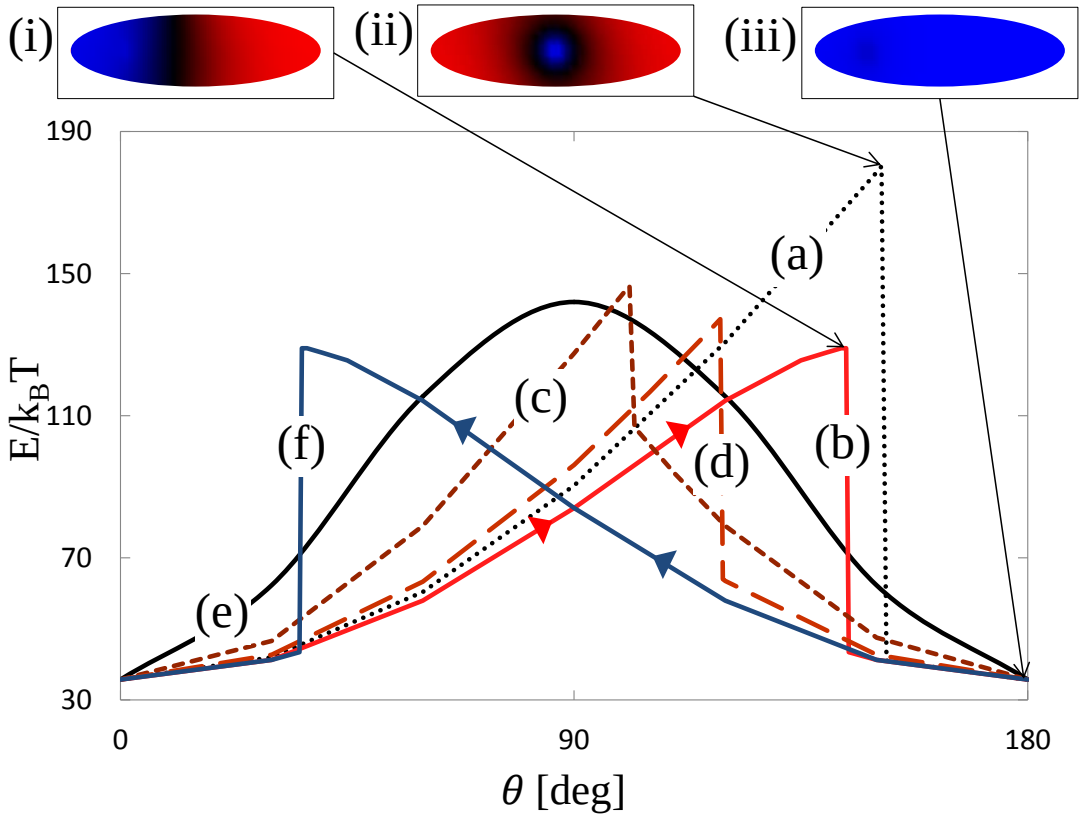

Figure 4.2: Energy as a function of angle for different pinning prescriptions: (a), (b), (c), (d) of Fig. 4.1, monodomain (e), and left off-center pinning while initializing the bit at $\theta = 180°$ (f). Insets (i)-(iii) show m_x at several critical points along the curves, with red corresponding to positive and blue negative magnetizations.

in Fig. 4.2: under application of a single off-center pinning, the energy barrier, $\Delta \approx 90$, is less than that of a monodomain, $\Delta \approx 110$. Since the thermal energy barrier is lowered by micromagnetic effects, the bit will follow a textured path in phase space when thermally flipping. Underlying the seemingly small change of $\lesssim 20\%$ between energy barriers is thus a fundamental change in the mode of thermal switching. The Arrhenius thermal transition rate $\propto e^{-\Delta}$ is, furthermore, greatly reduced. Upon examining the texture dynamics, one finds that the left off-center pinning field nucleates a domain wall, while rotating the pinning field pushes the domain wall to the right along the x axis. This is most apparent at about 145°, where, as illustrated in inset (i) of Fig. 4.2, the two domains each occupy approximately half the area of the magnet. At this point, the total internal energy is at a maximum, held in place only by the pinning field. After moving the domain wall past this point, there is a precipitous drop in internal energy as result of the domain-wall propagating to the right side of the magnet. This rapid drop in energy reflects a hysteretic process, wherein initially orienting the magnet at 0° or 180° with respect to the x axis, the energy will respectively follow the (b) or (f) curve of Fig. 4.2. We conclude that it is the domain-wall nucleation and propagation process that thermally flips the bit in our example.

To investigate the micromagnetic effects in the field-induced extraction of the thermal barrier, we apply a uniform magnetic field antiparallel to the direction of initialization of the bit. Our magnetic bit flips at between 600 and 650 Oe, which is close to the value predicted by the single-domain anisotropy: 680 Oe. Closely examining the texture, we indeed see the magnet flips like a monodomain. Analogous to the case of thin rectangular magnetic strips, wherein the coercivity field increases as the lateral width decreases, we suggest that the energetic bottleneck for domain-wall switching under application of an external field is at the tip of the bit where the domain wall nucleates. In contrast, the Arrhenius barrier for thermal domain-wall switching corresponds to the domain wall at the

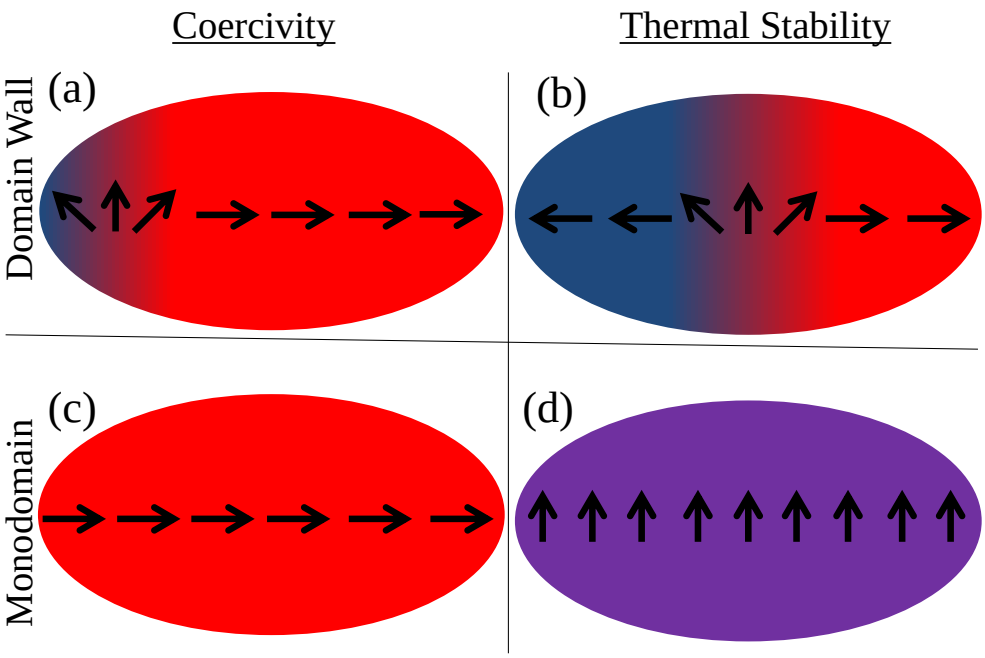

Figure 4.3: Schematic illustration of the "bottleneck" magnetic configurations for switching under the application of magnetic field, (a) and (c), and during thermal fluctuations, (b) and (d).

center of the magnet. We can thus distinguish three principal scenarios subject to the characteristics of the bit: First, the bit flips like a monodomain under both thermal fluctuations and application of a coercivity field (as in the case of infinite stiffness), illustrated schematically in Figs. 4.3(c) and (d), respectively. Second, the bit flips thermally via domain-wall propagation [Fig. 4.3(b)] but like a monodomain under application of a coercive field [Fig. 4.3(d)] (as in our example above). Third, the bit flips through domain-wall propagation both thermally and under application of a coercive field [Figs. 4.3(a),(b)]. We find this third case in our simulations on more elongated ellipses, e.g., with dimensions $400 \times 80 \times 2$ nm^3 (and the same material parameters). In this extreme example, we variationally guide, using a different pinning prescription from the previous case,[2] a domain wall along the major axis and find, expectedly, the most significant discrepancy in barrier height with the monodomain switching (top left Fig. 4.4). Conversely when considering a smaller aspect ratio of 80×40 nm^2, nucleating a domain wall is not energetically favorable and the value of the energy barrier of the left off-center pinning and monodomain converge (top right Fig. 4.4), essentially realizing the aforementioned first scenario (lower panels in Fig. 4.3). We further propose that if the minor axis of the ellipse is much greater than ℓ, two-dimensional textures such as vortex injection may compete with domain wall nucleation for the most energetically favorable path [LDR04, LD06, RML06, SCA08].

Since the exchange energy scales linearly with bit thickness while long-ranged dipolar interactions quadratically, upon increasing (decreasing) the thickness the texture effects should be enhanced (reduced), and, therefore, the disparity in the thermal barrier between different modes of switching sketched in Fig. 1 should increase (decrease). Particularly, we increase (decrease) the thickness to 3 nm

[2]Because of the quasi-one-dimensional nature of the most elongated ellipse in our calculation ($400 \times 80 \times 2$ nm^3), rotating a pinning field at a single point nucleates a domain wall but cannot propagate it to the other side to complete the switching process. We therefore must choose a different pinning prescription as follows: first a local field is applied as per our original method, nucleating a domain wall, which is then further moved by shifting the position of the pinning field along the major axis of the ellipse.

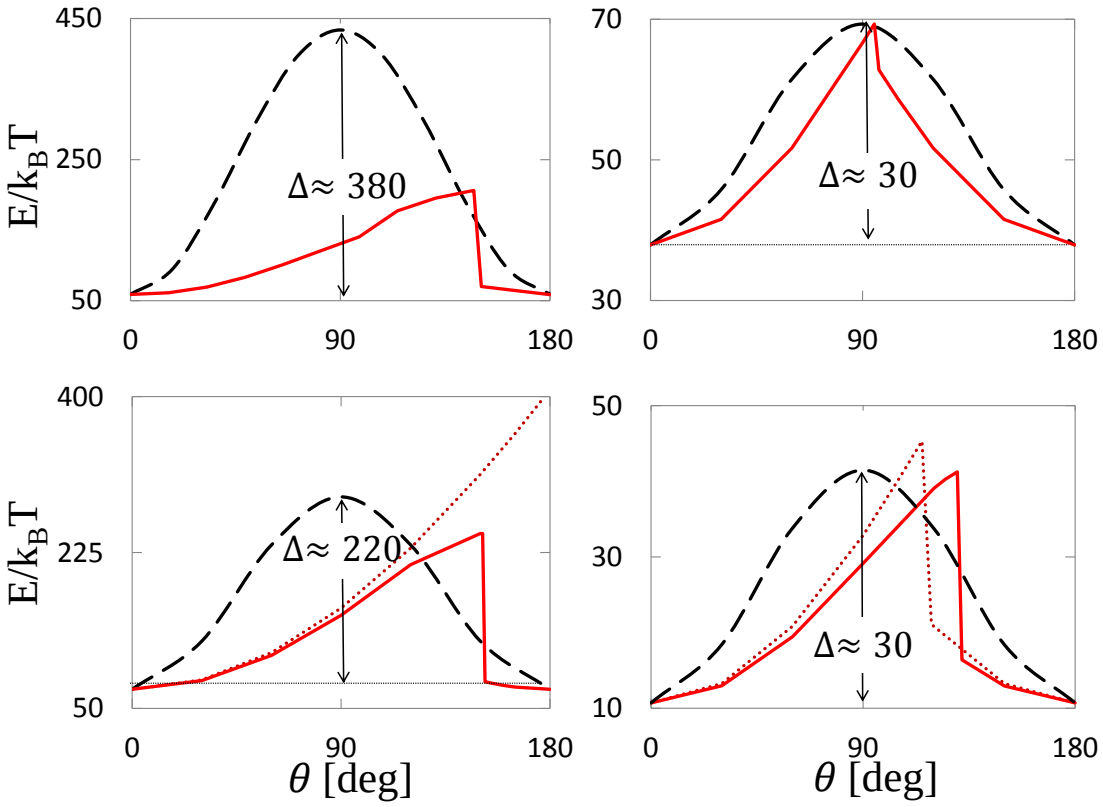

Figure 4.4: Energy profiles of four bit geometries: $400 \times 80 \times 2$ nm^3 (top left), $80 \times 40 \times 2$ nm^3 (top right), $150 \times 50 \times 3$ nm^3 (bottom left), and $150 \times 50 \times 1$ nm^3 (bottom right). The dashed curve shows single-domain, solid curve switching by domain wall nucleation, and dotted curve micromagnetic switching under application of a center pinning field.

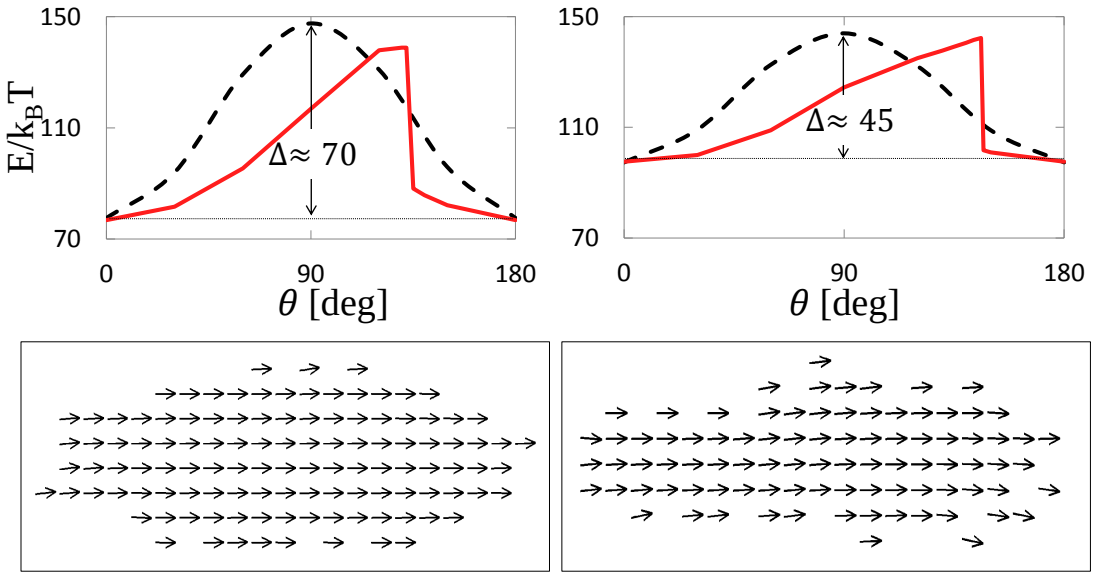

Figure 4.5: Energy profile of $150 \times 50 \times 2$ nm^3 bit with (left) edge roughness of amplitude 10 nm and wavelength 20 nm and (right) further enhanced roughness, where the dashed curve shows single-domain and the solid curve micromagnetic switching obtained under application of a local pinning field to the left off-center. The corresponding equilibrium bit textures are shown below.

(1 nm), keeping other parameters unmodified, and find that the monodomain thermal barrier is $> 20\%$ ($< 1\%$) larger than the micromagnetic barrier as graphed in the bottom left (bottom right) of Fig. 4.

We may expect random impurities and edge roughness to accentuate texture of the device and therefore affect the relative size of the thermal barrier in micromagnetic versus monodomain models. As an example, we model roughness as a crude edge modulation with wavelength 20 nm and amplitude 10 nm, as depicted in the left half of Fig. 4.5. While this is perhaps larger than the characteristic edge roughness of a typical device, we take this as a somewhat exaggerated case. Such edge modulation may be used to represent a generic structural or material disorder that introduces a random defect and could therefore promote domain wall nucleation. Including surface anisotropies could further distinguish the magneti-

zation textures between the smooth and rough bit models by emphasizing such defects, but are not considered in this analysis. We find that the thermal energy associated with both modes (thermal and field-induced) of switching is diminished by disorder, while the relative difference between the single-domain and textured behavior, $\lesssim 20\%$, is essentially unaffected for the $150 \times 50 \times 2$ nm^3 bit. Further distorting the edge (right half of Fig. 4.5), the thermal barriers become nearly equal. By way of roughening the edge, the aspect ratio of the elliptical bit has decreased, decreasing the xy demagnetization factors and thus favoring monodomain switching. A systematic analysis of geometric and material imperfections falls outside the scope of this work.

4.3 Outlook

As a result of our variational optimization of the path taken through the configuration space, there may be a trajectory of states with even a lower associated thermal barrier. In other words, the domain-wall type of propagation discussed here produces the upper bound for the thermal barrier. Finding at least one micromagnetic path, however, whose thermal barrier is smaller than that of the monodomain, suggests a qualitatively different scenario of thermal flipping and a lower thermal barrier, compared to the monodomain. We find such effects (along with their two-dimensional texture generalizations), with regard to both thermal stability and astroid diagrams, ubiquitous in practical devices.

CHAPTER 5

Nonequilibrium Spin Current Through a Quantum Dot

We develop an expression for spin current between two angled magnetic leads tunneling through a quantum dot with arbitrary interaction in and out of equilibrium. Specifically, we consider biasing by voltage, temperature, or spin pumping. We explicitly separate the equilibrium and nonequilibrium contributions to the current, both of which can be written in terms of the full retarded Green's function of the dot.

5.1 Introduction

Equilibrium spin current between two magnets characterizes their exchange interaction. When separated by an insulator, this interlayer exchange coupling (IEC), and likewise spin current, was found to be bigger than and opposite in sign [FTB02] from theoretical predictions [Slo89]. Impurities may assist enhancing the magnitude and explain the thickness dependence of the IEC [ZTV05, ZVV06]. We model this as two magnetic metal leads separated by a quantum dot with arbitrary on-site interaction and calculate the equilibrium and nonequilibrium spin current from which we can extract the IEC.

We extend the known expression of the Landauer-like formula for charge current through a quantum dot due to voltage difference between two normal metallic leads [MW92] by calculating the spin current between two canted ferromagnetic

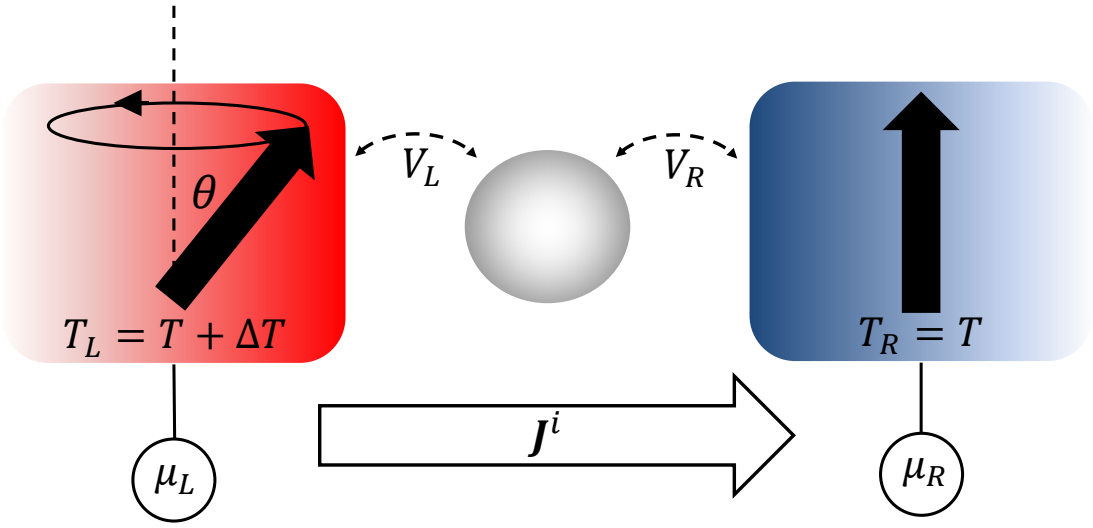

Figure 5.1: The model we consider in which two magnetic leads oriented at an angle θ with respect to each other are held at separate temperatures (T_L and T_R), chemical potentials (μ_L and μ_R) and spin biases. When in contact with a quantum dot tunneling (with probability $|V_L|^2$ and $|V_R|^2$) facilitates an equilibrium and nonequilibrium spin current, J^i.

conducting leads sandwiching a quantum dot. See Fig. 5.1. In addition to biasing by voltage, we consider spin biasing this system [BTB02, TMX08] and, due recent observation of the spin Seebeck effect [UTH08] we further extend our expression for spin current to accommodate temperature bias. We find that the expression for spin current can be written in terms of geometric coefficients and the fully interacting retarded Green's functions of the dot.

5.2 General Spin Current Expression

Consider a Hamiltonian of the form $H = H_L + H_D + H_T$ which describes non-interacting leads (H_L) coupled to a quantum dot (H_D) by tunneling (H_T). We

define these quantities as follows

$$
\begin{aligned}
H_L &= \sum_{k\sigma\gamma} \varepsilon_{k\sigma\gamma} c^\dagger_{k\sigma\gamma} c_{k\sigma\gamma} \,, \\
H_D &= (\{d^\dagger_i\}\{d_j\}) \,, \\
H_T &= \sum_{k\sigma\sigma\prime\gamma} V_{k\sigma\sigma\prime\gamma} d^\dagger_\sigma c_{k\sigma\prime\gamma} + V^\dagger_{k\sigma\sigma\prime\gamma} c^\dagger_{k\sigma\prime\gamma} d_\sigma \,.
\end{aligned} \tag{5.1}
$$

The summation in the lead part of the Hamiltonian is over momentum (k), spin quantized along the z axis ($\sigma = \uparrow, \downarrow$), and left ($\gamma = L$) and right ($\gamma = R$) leads. $\varepsilon_{k\sigma\gamma}$ is the energy of an electron with momentum k and spin σ created (annihilated) by $c^\dagger_{k\sigma\gamma}$ ($c_{k\sigma\gamma}$) in lead γ. $V_{k\uparrow\gamma}$ ($V_{k\downarrow\gamma}$) is the matrix element for a spin (down) up electron tunneling from lead γ to the dot. The dot Hamiltonian is a general Hermitian function of dot creation and annihilation operators $d^\dagger_i$ and d_j, respectively, that furnish a complete basis for the dot Fock space. The indices i and j of these operators may contain any quantum numbers but we consider the simplest case where a single spin-1/2 on site energy level: $d^\dagger_i \to d^\dagger_\sigma$ and $d_j \to d_{\sigma'}$ with $\sigma, \sigma' = \uparrow\downarrow$. Because we are interested in two leads canted with respected to one another, we rotate lead γ by θ_γ in the plane defined by the axis of quantization and direction of current

$$
\begin{aligned}
c_{\sigma\gamma} \to \tilde{c}_{k\sigma\gamma} &= R^\gamma_{\sigma\sigma\prime} c_{k\sigma\prime\gamma} \,, \\
c^\dagger_{k\sigma\gamma} \to \tilde{c}^\dagger_{k\sigma\gamma} &= (R^\gamma_{\sigma\sigma\prime} c_{k\sigma\prime\gamma})^\dagger = c^\dagger_{k\sigma\prime\gamma} (R^\dagger)^\gamma_{\sigma\prime\sigma} \,,
\end{aligned} \tag{5.2}
$$

where

$$
R^\gamma_{\sigma\sigma\prime} = \begin{pmatrix} \cos(\theta_\gamma/2) & -\sin(\theta_\gamma/2) \\ \sin(\theta_\gamma/2) & \cos(\theta_\gamma/2) \end{pmatrix} \tag{5.3}
$$

and $\theta_L = \theta$ and $\theta_R = 0$. Both the lead and dot Hamiltonians are invariant under this rotation, whereas the tunneling term of the Hamiltonian becomes

$$
H_T = \sum_{k\sigma\sigma\prime\gamma} V^*_{k\sigma\gamma} c^\dagger_{k\sigma\prime\gamma} (R^T)_{\sigma\prime\sigma} d_\sigma + V_{k\sigma\gamma} d^\dagger_\sigma R_{\sigma\sigma\prime} c_{k\sigma\prime\gamma} \,. \tag{5.4}
$$

We absorb this transformation into the tunneling probability which takes the matrix form

$$V^*_{k\sigma\gamma} \to V^*_{k\sigma\gamma}(R^T)_{\sigma\prime\sigma} = \begin{pmatrix} V^*_{k\uparrow\gamma}\cos(\theta_\gamma/2) & V^*_{k\uparrow\gamma}\sin(\theta_\gamma/2) \\ -V^*_{k\downarrow\gamma}\sin(\theta_\gamma/2) & V^*_{k\downarrow\gamma}\cos(\theta_\gamma/2) \end{pmatrix} \equiv V^\dagger_{k\sigma\prime\sigma\gamma}\,,$$
$$V_{k\sigma\gamma} \to V_{k\sigma\gamma}R_{\sigma\sigma\prime} = \begin{pmatrix} V_{k\uparrow\gamma}\cos(\theta_\gamma/2) & -V_{k\downarrow\gamma}\sin(\theta_\gamma/2) \\ V_{k\uparrow\gamma}\sin(\theta_\gamma/2) & V_{k\downarrow\gamma}\cos(\theta_\gamma/2) \end{pmatrix} \equiv V_{\sigma\sigma\prime\gamma}\,, \tag{5.5}$$

so that the tunneling Hamiltonian reads

$$H_T = \sum_{k\sigma\sigma\prime\gamma} V_{k\sigma\sigma\prime\gamma} d^\dagger_\sigma c_{k\sigma\prime\gamma} + V^\dagger_{k\sigma\sigma\prime\gamma} c^\dagger_{k\sigma\gamma} d_{\sigma\prime}. \tag{5.6}$$

Closely following the approach of [MW92], we begin calculating the spin current by taking the time derivative of $d^\dagger_\mu d_\nu$

$$\begin{aligned}\frac{d}{dt}(d^\dagger_\mu d_\nu) &= (i/\hbar)[H, d^\dagger_\mu d_\nu] = (i/\hbar)[H_T, d^\dagger_\mu d_\nu] = (i/\hbar)[H_T, d^\dagger_\mu]d_\nu + d^\dagger_\mu[H_T, d_\nu] \\ &= (i/\hbar)\sum_{k\alpha\gamma} V^\dagger_{k\alpha\mu\gamma} c^\dagger_{k\alpha\gamma} d_\nu - V_{k\nu\alpha\gamma} d^\dagger_\mu c_{k\alpha\gamma}\,. \end{aligned} \tag{5.7}$$

Owing to the continuity equation [CCN71], we equate the expectation value of Eq. (5.6) to the current

$$\begin{aligned} J^\gamma_{\mu\nu} &= \frac{i}{\hbar}\sum_{k\alpha} V^\dagger_{k\alpha\mu\gamma}\langle c^\dagger_{k\alpha\gamma} d_\nu\rangle - V_{k\nu\alpha\gamma}\langle d^\dagger_\mu c_{k\alpha\gamma}\rangle \\ &= \frac{1}{\hbar}\int\frac{d\omega}{2\pi}\sum_{k\alpha} V^\dagger_{k\alpha\mu\gamma} G^<_{\nu,k\alpha\gamma}(\omega) - V_{k\nu\alpha\gamma} G^<_{k\alpha\gamma,\mu}(\omega)\,, \end{aligned} \tag{5.8}$$

where we have defined $G^<_{\nu,k\alpha\gamma}(t) = i\langle c^\dagger_{k\alpha\gamma} d_\nu\rangle(t)$ and $G^<_{k\alpha\gamma,\mu}(t) = i\langle d^\dagger_\nu c_{k\alpha\gamma}\rangle(t)$ which are the lesser than Green's functions in the Keldysh formalism. Taking advantage of the noninteracting electrons in the leads, we use their equations of motion and Langreth's theorem to separate the lead and dot Green's functions

$$\begin{aligned} G^<_{k\alpha\gamma,\mu} &= \sum_\lambda V^\dagger_{k\alpha\lambda\gamma}\left(g^t_{k\alpha\gamma} G^<_{\lambda\mu} - g^<_{k\alpha\gamma} G^{\bar{t}}_{\lambda\mu}\right)\,, \\ G^<_{\nu,k\alpha\gamma} &= -\sum_\lambda V_{k\lambda\alpha\gamma}\left(g^{\bar{t}}_{k\alpha\gamma} G^<_{\nu\lambda} - g^<_{k\alpha\gamma} G^t_{\nu\lambda}\right)\,, \end{aligned} \tag{5.9}$$

where we have introduced the (anti-)time-ordered Green's functions on lead γ ($g^{\bar{t}}_{k\alpha\gamma}$) $g^{t}_{k\alpha\gamma}$ of momentum k and spin α and on the dot ($G^{\bar{t}}_{\mu\nu}$) $G^{t}_{\mu\nu}$ from spin μ to spin ν. Plugging this back into our equation for current we obtain

$$J^{\gamma}_{\mu\nu} = -\frac{1}{\hbar}\sum_{k\alpha}\int\frac{d\omega}{2\pi}\Big[V^{\dagger}_{k\alpha\mu\gamma}V_{k\lambda\alpha\gamma}\left(g^{\bar{t}}_{k\alpha\gamma}G^{<}_{\nu\lambda} - g^{<}_{k\alpha\gamma}G^{t}_{\nu\lambda}\right) + V_{k\nu\alpha\gamma}V^{\dagger}_{k\alpha\lambda\gamma}\left(g^{t}_{k\alpha\gamma}G^{<}_{\lambda\mu} - g^{<}_{k\alpha\gamma}G^{\bar{t}}_{\lambda\mu}\right)\Big]\,. \tag{5.10}$$

Using identities between Green's functions [Mah93] we rewrite the expression for the current, eliminating the time-ordered Green's functions in favor of retarded and advanced Green's functions

$$J^{\gamma}_{\mu\nu} = -\frac{1}{\hbar}\sum_{k\alpha}\int\frac{d\omega}{2\pi}\Big[-V^{\dagger}_{k\alpha\mu\gamma}V_{k\lambda\alpha\gamma}\left(g^{a}_{k\alpha\gamma}G^{<}_{\nu\lambda} + g^{<}_{k\alpha\gamma}G^{r}_{\nu\lambda}\right) + V_{k\nu\alpha\gamma}V^{\dagger}_{k\alpha\lambda\gamma}\left(g^{r}_{k\alpha\gamma}G^{<}_{\lambda\mu} + g^{<}_{k\alpha\gamma}G^{a}_{\lambda\mu}\right)\Big]\,, \tag{5.11}$$

where $G^{r}_{ij} = -i\Theta(t-t')\langle\{d_i(t), d^{\dagger}_j(t')\}\rangle$ and $G^{a}_{ij} = (G^{r})^{*}_{ji}$. After some tedious but straightforward manipulations one may show that

$$\sum_{\mu\nu\alpha\lambda}\left[-V^{\dagger}_{k\alpha\mu\gamma}V_{k\lambda\alpha\gamma}\left(g^{a}_{\alpha}G^{<}_{\nu\lambda} + g^{<}_{\alpha\gamma}G^{r}_{\nu\lambda}\right)\right]^{*}\sigma^{*}_{\mu\nu} = \sum_{\mu\nu\alpha\lambda}\left[V_{k\nu\alpha\gamma}V^{\dagger}_{k\alpha\lambda\gamma}\left(g^{r}_{\alpha\gamma}G^{<}_{\lambda\mu} + g^{<}_{\alpha\gamma}G^{a}_{\lambda\mu}\right)\right]\sigma_{\mu\nu} \tag{5.12}$$

and therefore that the spin current is real. Note that $g_{k\sigma\gamma}$, the free electron Green's function uncoupled to the dot, is

$$\begin{aligned} g^{<}_{k\sigma\gamma} &= 2\pi i\delta(\omega-\varepsilon_{k\sigma})f_{\sigma\gamma}(\omega)\,,\\ g^{r}_{k\sigma\gamma} &= \frac{1}{\omega-\varepsilon_{k\sigma}+i\eta} = -\pi i\delta(\omega-\varepsilon_{k\sigma}) + \mathcal{P}\frac{1}{\omega-\varepsilon_{k\sigma}}\,. \end{aligned} \tag{5.13}$$

where $\eta\to 0^{+}$ and $\mathcal{P}$ denotes the Cauchy principal value. We define

$$W^{r}_{\mu\nu\gamma} = -\frac{i}{2}\begin{bmatrix} \Gamma_{\uparrow\gamma}\cos^2(\theta_\gamma/2) + \Gamma_{\downarrow\gamma}\sin^2(\theta_\gamma/2) & -(\Gamma_{\uparrow\gamma}-\Gamma_{\downarrow\gamma})\sin(\theta_\gamma)/2 \\ -(\Gamma_{\uparrow\gamma}-\Gamma_{\downarrow\gamma})\sin(\theta_\gamma)/2 & \Gamma_{\downarrow\gamma}\cos^2(\theta_\gamma/2) + \Gamma_{\uparrow\gamma}\sin^2(\theta_\gamma/2) \end{bmatrix}, \tag{5.14}$$

where $\Gamma_{\sigma\gamma} = 2\pi \sum_k |V_{k\sigma\gamma}|^2 \delta(\omega - \varepsilon_{k\sigma\gamma}) = 2\pi \int |V_{k\sigma\gamma}|^2 \rho_{\sigma\gamma} \delta(\omega - \varepsilon_{k\sigma\gamma}) = 2\pi |V_{\sigma\gamma}|^2 \rho_{\sigma\gamma}$ so that $\sum_{k\alpha} V_{k\lambda\alpha\gamma} V^{\dagger}_{k\alpha\mu\gamma} \mathrm{Im}[g^r_{\alpha\gamma}] = -\sum_{k\alpha} V_{k\lambda\alpha\gamma} V^{\dagger}_{k\alpha\mu\gamma} \mathrm{Im}[g^a_{\alpha\gamma}] = W^r_{\lambda\mu\gamma}$. Likewise defining $W^<_{\lambda\mu\gamma} = \sum_{k\alpha} V_{k\lambda\alpha\gamma} V^{\dagger}_{k\alpha\mu\gamma} g^<_{\alpha\gamma}$ which has components

$$
\begin{aligned}
W^<_{\uparrow\uparrow\gamma} &= i \left[f_{\uparrow\gamma}(\omega) \Gamma_{\uparrow\gamma} \cos^2(\theta_\gamma/2) + f_{\downarrow\gamma}(\omega) \Gamma_{\downarrow\gamma} \sin^2(\theta_\gamma/2) \right] , \\
W^<_{\uparrow\downarrow\gamma} &= -(i/2)(f_{\uparrow\gamma}(\omega)\Gamma_{\uparrow\gamma} - f_{\downarrow\gamma}(\omega)\Gamma_{\downarrow\gamma}) \sin(\theta_\gamma) , \\
W^<_{\downarrow\uparrow\gamma} &= -(i/2)(f_{\uparrow\gamma}(\omega)\Gamma_{\uparrow\gamma} - f_{\downarrow\gamma}(\omega)\Gamma_{\downarrow\gamma}) \sin(\theta_\gamma) , \\
W^<_{\downarrow\downarrow\gamma} &= i[f_{\downarrow\gamma}(\omega)\Gamma_{\downarrow\gamma} \cos^2(\theta_\gamma/2) + f_{\uparrow\gamma}(\omega)\Gamma_{\uparrow\gamma} \sin^2(\theta_\gamma/2)] ,
\end{aligned}
\tag{5.15}
$$

reduces to $W^<_{\nu\lambda\gamma} = -2 f_\gamma W^r_{\nu\lambda\gamma}$ in the absence of spin biasing. $f_{\sigma\gamma}$ is the Fermi-Dirac distribution function in lead γ with spin σ. We take $\Gamma_{\sigma\gamma}$ to be independent of energy inside the electron band in the leads and zero otherwise. The principal part can be evuated as

$$
\begin{aligned}
&\sum_{k\alpha} \int \mathrm{d}\omega V_{k\lambda\alpha\gamma} V^{\dagger}_{k\alpha\mu\gamma} G^<_{\nu\lambda} \mathcal{P} \frac{1}{\omega - \varepsilon_{k\sigma}} = \sum_{k\alpha} \mathcal{P} \int \mathrm{d}\omega \mathrm{d}\omega' V_{k\lambda\alpha\gamma} V^{\dagger}_{k\alpha\mu\gamma} G^<_{\nu\lambda}(\omega) \frac{\delta(\omega' - \varepsilon_{k\sigma})}{\omega - \omega'} \\
&= \sum_{k\alpha} \mathcal{P} \int \mathrm{d}\omega \mathrm{d}\omega' V_{k\lambda\alpha\gamma} V^{\dagger}_{k\alpha\mu\gamma} G^<_{\nu\lambda}(\omega') \frac{\delta(\omega' - \varepsilon_{k\sigma})}{\omega' - \omega} = W^r_{\lambda\mu\gamma} \int \mathrm{d}\omega \mathcal{P} \int \frac{\mathrm{d}\omega'}{-i\pi} \frac{G^<_{\nu\lambda}(\omega')}{\omega' - \omega} .
\end{aligned}
\tag{5.16}
$$

The spin current may be written in the compact form

$$
\begin{aligned}
J^i_\gamma &= S^i_{\mu\nu} J^\gamma_{\mu\nu} = \frac{\hbar}{2} \sigma^i_{\mu\nu} J^\gamma_{\mu\nu} \\
&= \sum_{\mu\nu\lambda} \int \frac{\mathrm{d}\omega}{2\pi} \mathrm{Re} \left[-W^r_{\lambda\mu\gamma} \sigma^i_{\mu\nu} G^<_{\nu\lambda} + W^<_{\lambda\mu\gamma} \sigma^i_{\mu\nu} G^r_{\nu\lambda} + i W^r_{\lambda\mu\gamma} \sigma^i_{\mu\nu} \mathcal{P} \int \frac{\mathrm{d}\omega'}{\pi} \frac{G^<_{\nu\lambda}}{\omega' - \omega} \right] \\
&= \mathrm{Re} \left\{ \int \mathrm{d}\omega \mathbf{Tr} \left[\mathbf{W}^<_\gamma \sigma^i \mathbf{G}^r - \mathbf{W}^r_\gamma \sigma^i \left(\mathbf{G}^< - \frac{i}{\pi} \mathcal{P} \int \mathrm{d}\omega' \frac{\mathbf{G}^<(\omega')}{\omega' - \omega} \right) \right] \right\} ,
\end{aligned}
\tag{5.17}
$$

where $\mathbf{G} \equiv G_{\mu\nu}$ and $\mathbf{W} \equiv W_{\mu\nu}$. This general expression for charge and spin current under voltage, temperature, or spin bias is the principal result of our work. A similar expression was derived by [ZZY09] but there was no discussion of temperature biasing. Moreover, their result does not facilitate spin biasing of the system.

A serious barrier in the calculation of the current out of equilibrium is determining the on-site lesser than Green's function. One may use Dyson's equation and Keldysh formalism to show $\mathbf{G}^{<} = \mathbf{G}^{r}\Sigma^{<}\mathbf{G}^{a}$ out of equilibrium. However, because $\Sigma^{<}$ is a functional of $\mathbf{G}^{<}$, it is in general difficult to obtain an analytic expression for $\mathbf{G}^{<}$. Consequently, extending, Ng's ansatz [Ng96], we take

$$\Sigma^{<} = -(\mathbf{W}_L^{<} + \mathbf{W}_R^{<})(\mathbf{W}_L^{r} + \mathbf{W}_R^{r})^{-1}[(\mathbf{G}^{r})^{-1} - (\mathbf{G}^{a})^{-1}]/2\,. \tag{5.18}$$

The advantage of this ansatz is that we recover the exact expression for $\mathbf{G}^{<}$ when either no bias is applied or there is no interaction on the dot. Although this does not simplify the general form of the current, consider only voltage and temperature biasing from which it follows $\mathbf{W}^{<} = -2f_\gamma \mathbf{W}^{r}$ in which the lesser than Green's function simplifies to

$$\mathbf{G}^{<} = \mathbf{G}^{r}(f_L\mathbf{W}_L^{r} + f_R\mathbf{W}_R^{r})(\mathbf{W}_L^{r} + \mathbf{W}_R^{r})^{-1}[(\mathbf{G}^{r})^{-1} - (\mathbf{G}^{a})^{-1}]\mathbf{G}^{a} \tag{5.19}$$

and the spin current takes the form

$$\begin{aligned} J_\gamma^i = \int d\omega \mathrm{Re}\Big[\mathbf{Tr}\Big[\mathbf{W}_\gamma^{a}\sigma^i\mathbf{G}^{r}(f_L\mathbf{W}_L^{r} + f_R\mathbf{W}_R^{r})(\mathbf{W}_L^{r} + \mathbf{W}_R^{r})^{-1}[(\mathbf{G}^{r})^{-1} - (\mathbf{G}^{a})^{-1}]\mathbf{G}^{a} \\ -f_\gamma\mathbf{W}_\gamma^{r}\sigma^i(\mathbf{G}^{r} - \mathbf{G}^{a}) - f_\gamma\mathbf{W}_\gamma^{r}\sigma^i(\mathbf{G}^{r} + \mathbf{G}^{a}) + \mathbf{W}_\gamma^{r}\sigma^i\frac{i}{\pi}\mathcal{P}\int \mathrm{d}\omega'\frac{\mathbf{G}^{<}(\omega')}{\omega' - \omega})\Big]\Big]\,. \end{aligned} \tag{5.20}$$

Using $[\mathbf{G}^{r} - \mathbf{G}^{a}] = \mathbf{G}^{r}[(\mathbf{G}^{a})^{-1} - (\mathbf{G}^{r})^{-1}]\mathbf{G}^{a}$ and inserting the identity $1 = (\mathbf{W}^{L} + \mathbf{W}^{R})(\mathbf{W}^{L} + \mathbf{W}^{R})^{-1}$

$$\begin{aligned} J_\gamma^i = -\int d\omega(f_{\bar\gamma} - f_\gamma)\mathrm{Re}\left[\mathbf{Tr}\left[\mathbf{W}_\gamma^{r}\sigma^i\mathbf{G}^{r}\mathbf{W}_{\bar\gamma}^{r}(\mathbf{W}_L^{r} + \mathbf{W}_R^{r})^{-1}[(\mathbf{G}^{r})^{-1} - (\mathbf{G}^{a})^{-1}]\mathbf{G}^{a}\right]\right] \\ + f_\gamma\mathrm{Re}\left[\mathbf{Tr}\left[\mathbf{W}_\gamma^{r}\sigma^i\left(\mathbf{G}^{r} + \mathbf{G}^{a}\right) - \mathbf{W}_\gamma^{r}\sigma^i\frac{i}{\pi}\mathcal{P}\int \mathrm{d}\omega'\frac{\mathbf{G}^{<}(\omega')}{\omega' - \omega}\right]\right]\,. \end{aligned} \tag{5.21}$$

where lead $\bar\gamma$ is the opposite to lead γ. We can directly extract the equilibrium and nonequilibrium spin current and evaluate the differential spin conductance and the spin Seebeck coefficient.

5.3 Anderson Green's Function

A natural candidate for the dot interaction is the Anderson Hamiltonian with strong on-site interaction below the Kondo temperature. Only a many-body formalism, such as Keldysh used to calculate the spin current, can capture Kondo physics. We proceed to calculate the Anderson Green's function of a single quantum dot coupled to a reservoir with infinite on-site interaction. Recall that the Anderson Hamiltonian for single level is $H_D = \sum_\sigma \varepsilon_\sigma d_\sigma^\dagger d_\sigma + U n_\downarrow n_\uparrow$, where U modulates the strength of Coulomb interaction on the dot. We proceed by using the equation of motion (EoM) technique to obtain an expression for the Green's function after using a decoupling scheme [MWL93] that, although neglecting divergent correlations, captures some features of the Kondo effect.

The retarded Green's function on the dot is by definition

$$D_{ij}^r = -i\Theta(t-t')\langle\{d_i(t), d_j^\dagger(t')\}\rangle\,. \tag{5.22}$$

where $\Theta(t)$ is the Heaviside step function and $\langle\cdots\rangle$ is the thermal average of $\cdots$. Using the fact that

$$[d_i, H] = \epsilon_i d_i + V_{i\sigma} c_\sigma + U d_i n_{\bar{i}}\,, \tag{5.23}$$

where we have introduced $n_i = d_i^\dagger d_i$ and $\bar{\bar{i}} = -i$, we follow the equation of motion method of determining the Green's function by taking the time derivative

$$\begin{aligned} i\partial_t D_{ij}^r(t-t') &= \delta(t-t')\delta_{ij} - i\Theta(t-t')\langle\{[d_i, H](t), d_j^\dagger(t')\}\rangle \\ &= \delta(t-t')\delta_{ij} - i\Theta(t-t')\langle\{[\epsilon_i d_i + V_{i\sigma}c_\sigma + U d_i n_{\bar{i}}](t), d_j^\dagger(t')\}\rangle \\ &= \delta(t-t')\delta_{ij} + \epsilon_i D_{ij}^r(t-t') + \sum_{k\sigma} V_{i\sigma} G_{\sigma j}^r(t-t') + U\Gamma_i\,, \end{aligned} \tag{5.24}$$

where $G_{\sigma j}^r(t-t') = -i\Theta(t-t')\left\langle\{c_\sigma(t), d_j^\dagger(t')\}\right\rangle$ and $\Gamma_i = \langle\langle d_i n_{\bar{i}}, d_j^\dagger\rangle\rangle$. We have implicitly included the indices, and subsequent summation, of the leads and momentum in the spin index of the lead creation (annihilation) operators. We adopt the notation that $\langle\langle A, B\rangle\rangle = -i\Theta(t-t')\,\langle\{A(t), B(t')\}\rangle$. We further differentiate

the unknown functions, as is practice in the EoM technique. Further differentiating $G^r_{\sigma j}$

$$i\partial_t G^r_{\sigma j} = \varepsilon_\sigma G^r_{\sigma j} + \sum_{\sigma'} V^\dagger_{\sigma\sigma'} D^r_{\sigma' j}\,, \tag{5.25}$$

or after Fourier transforming

$$(\omega + i\eta - \varepsilon_\sigma) G^r_{\sigma j} = \sum_{\sigma'} V^\dagger_{\sigma\sigma'} D^r_{\sigma' j}\,, \tag{5.26}$$

where we have used the commutation relation $[c_\sigma, H] = \varepsilon_\sigma c_\sigma + V^\dagger_{\sigma\sigma'} d_{\sigma'}$ and added an infinitesimal η as is necessary procedure to ensure convergence for a retarded Green's function. Finally solving the Green's function

$$G^r_{\sigma j} = \frac{\sum_{\sigma'} V^\dagger_{\sigma\sigma'} D^r_{\sigma' j}}{\omega + i\eta - \varepsilon_{k\sigma}}\,. \tag{5.27}$$

The equation of motion for Γ_i is

$$\langle\langle d_i n_{\bar{i}}, d^\dagger_j \rangle\rangle = \delta(t-t')\{d_i n_{\bar{i}}, d^\dagger_j\} + \langle\langle [d_i n_{\bar{i}}, H], d^\dagger_j \rangle\rangle\,. \tag{5.28}$$

Further taking these (anti-)commutation relations gives

$$\begin{aligned}
\{d_i n_{\bar{i}}, d^\dagger_j\} =& \delta_{ij} n_{\bar{i}} - \delta_{\bar{i}j} d^\dagger_{\bar{i}} d_i\,, \\
[d_i n_{\bar{i}}, H] =& (\epsilon_i + U) d_i n_{\bar{i}} + \sum_\sigma d_i d^\dagger_{\bar{i}} V_{\bar{i}\sigma} c_\sigma - d_i V^\dagger_{\sigma\bar{i}} c^\dagger_\sigma d_{\bar{i}} + V_{i\sigma} c_\sigma n_{\bar{i}}\,,
\end{aligned} \tag{5.29}$$

In order to time differentiate these new operators we will again need to commute them with the Hamiltonian

$$\begin{aligned}
[d_i d^\dagger_{\bar{i}} c_\sigma, H] =& (\epsilon_i - \epsilon_{\bar{i}} + \varepsilon_\sigma) d_i d^\dagger_{\bar{i}} c_\sigma + \sum_\mu d_i d^\dagger_{\bar{i}} d_\mu V^\dagger_{\sigma\mu} + V_{i\mu} c_\mu d^\dagger_{\bar{i}} c_\sigma - d_i V^\dagger_{\mu\bar{i}} c^\dagger_\mu c_\sigma\,, \\
[d_i c^\dagger_\sigma d_{\bar{i}}, H] =& (\epsilon_i + \epsilon_{\bar{i}} - \varepsilon_\sigma + U) d_i c^\dagger_\sigma d_{\bar{i}} + \sum_\mu -d_i d_{\bar{i}} V_{\mu\sigma} d^\dagger_\mu + d_i V_{\bar{i}\mu} c_\mu c^\dagger_\sigma + V_{i\mu} c_\mu d_{\bar{i}} c^\dagger_\sigma\,, \\
[c_\sigma n_{\bar{i}}, H] =& \varepsilon_\sigma c_\sigma n_{\bar{i}} + \sum_\mu n_{\bar{i}} V^\dagger_{\sigma\mu} d_\mu + d^\dagger_{\bar{i}} V_{\bar{i}\mu} c_\mu c_\sigma - V^\dagger_{\mu\bar{i}} c^\dagger_\mu d_{\bar{i}} c_\sigma\,.
\end{aligned} \tag{5.30}$$

Because of the step function implicit in the definition of the retarded Green's

function, we must evaluate the anticommutator of these operators with $d_j^\dagger$

$$\begin{aligned}
\{d_i d_{\bar{i}}^\dagger c_\sigma, d_j^\dagger\} =& \delta_{ij} d_{\bar{i}}^\dagger c_\sigma \,, \\
\{d_i c_\sigma^\dagger d_{\bar{i}}, d_j^\dagger\} =& \delta_{\bar{i}j} d_i c_\sigma^\dagger + \delta_{ij} c_\sigma^\dagger d_{\bar{i}} \,, \\
\{c_\sigma n_{\bar{i}}, d_j^\dagger\} =& \delta_{\bar{i}j} c_\sigma d_{\bar{i}}^\dagger \,.
\end{aligned} \tag{5.31}$$

Because a factor of U enters the equation of motion for the second term in Eq. (5.30), it will not contribute to the equation of motion for the full dot Green's function when the on-site interaction is large. Thus the time differentiation of the remaining operators' respective retarded Green's functions is

$$\begin{aligned}
(\omega + i\eta - \varepsilon_\sigma - \epsilon_i + \epsilon_{\bar{i}})\Gamma_{i\sigma}^{(1)} =& -\delta_{ij}\langle d_{\bar{i}}^\dagger c_\sigma\rangle - V_{\sigma\bar{i}}^\dagger \Gamma_i \\
&+ \sum_\mu V_{i\mu}\langle\langle d_{\bar{i}}^\dagger c_\mu c_\sigma, d_j^\dagger\rangle\rangle + V_{\mu\bar{i}}^\dagger \langle\langle d_i c_\mu^\dagger c_\sigma, d_j^\dagger\rangle\rangle \,, \\
(\omega + i\eta - \varepsilon_\sigma)\Gamma_{\bar{i}\sigma}^{(2)} =& -\delta_{\bar{i}j}\langle d_{\bar{i}}^\dagger c_\sigma\rangle \\
&+ V_{\sigma i}^\dagger \Gamma_i + \sum_\mu V_{\bar{i}\mu}\langle\langle d_{\bar{i}}^\dagger c_\mu c_\sigma, d_j^\dagger\rangle\rangle + V_{\mu\bar{i}}^\dagger \langle\langle d_{\bar{i}} c_\mu^\dagger c_\sigma, d_j^\dagger\rangle\rangle \,,
\end{aligned} \tag{5.32}$$

where we have made use of $(d_i)^2 = 0$ and defined $\Gamma_{i\sigma}^{(1)} = \langle\langle d_{\bar{i}}^\dagger d_i c_\sigma, d_j^\dagger\rangle\rangle$ and $\Gamma_{\bar{i}\sigma}^{(2)} = \langle\langle n_{\bar{i}} c_\sigma, d_j^\dagger\rangle\rangle$. We make the following decoupling [Lac81]

$$\begin{aligned}
\langle\langle c_\mu^\dagger c_\sigma d_i, d_j^\dagger\rangle\rangle \approx& \langle c_\mu^\dagger c_\sigma\rangle\langle\langle d_i, d_j^\dagger\rangle\rangle - \langle c_\mu^\dagger d_i\rangle\langle\langle c_\sigma, d_j^\dagger\rangle\rangle \,, \\
\langle\langle d_{\bar{i}}^\dagger c_\mu c_\sigma, d_j^\dagger\rangle\rangle \approx& \langle d_{\bar{i}}^\dagger c_\mu\rangle\langle\langle c_\sigma, d_j^\dagger\rangle\rangle - \langle d_{\bar{i}}^\dagger c_\sigma\rangle\langle\langle c_\mu, d_j^\dagger\rangle\rangle \,.
\end{aligned} \tag{5.33}$$

Recall that

$$\langle\langle c_\sigma, d_j^\dagger\rangle\rangle = \sum_\mu V_{\sigma\mu}^\dagger \frac{\langle\langle d_\mu, d_j^\dagger\rangle\rangle}{\omega + i\eta - \varepsilon_\sigma} \,, \tag{5.34}$$

and therefore

$$\sum_\sigma \frac{\langle\langle c_\sigma, d_j^\dagger\rangle\rangle}{\omega + i\eta - \varepsilon_\sigma - \epsilon_i + \epsilon_{\bar{i}}} = \sum_{\sigma\mu} \frac{V_{\sigma\mu}^\dagger \langle\langle d_\mu, d_j^\dagger\rangle\rangle}{(\omega + i\eta - \varepsilon_\sigma - \epsilon_i + \epsilon_{\bar{i}})(\omega + i\eta - \varepsilon_\sigma)} \tag{5.35}$$

Using the relation

$$\int \mathrm{d}\varepsilon \left(\frac{1}{\omega + i\eta - \varepsilon + a}\right)\left(\frac{1}{\omega' \pm i\eta - \varepsilon}\right) = \int \frac{\mathrm{d}\varepsilon}{\omega - \omega' + i\eta + a}$$
$$\left(\frac{1}{\omega' \pm i\eta - \varepsilon} - \frac{1}{\omega + i\eta - \varepsilon + a}\right) = -\frac{i\pi(1 \mp 1)}{\omega - \omega' + i\eta + a} \tag{5.36}$$

we may show that the sum in Eq. (5.35) vanishes and thus the relations in Eq. (5.33) reduce to

$$\begin{aligned}\langle\langle c_\mu^\dagger c_\sigma d_i, d_j^\dagger\rangle\rangle \approx & \langle c_\mu^\dagger c_\sigma\rangle\langle\langle d_i, d_j^\dagger\rangle\rangle\,, \\ \langle\langle d_{\bar{i}}^\dagger c_\mu c_\sigma, d_j^\dagger\rangle\rangle \approx & -\langle d_{\bar{i}}^\dagger c_\sigma\rangle\langle\langle c_\mu, d_j^\dagger\rangle\rangle\,.\end{aligned} \tag{5.37}$$

Although these terms are singular, in previous analyses [MWL93, SWW06] these expectation values were assumed to be $\langle c_\mu^\dagger c_\nu\rangle = \delta_{\mu\nu} f(\varepsilon_\mu)$ and $\langle d_\mu^\dagger c_\nu\rangle = 0$ and Kondo physics was still apparent. Upon making this approximation[1]

$$\begin{aligned}(\omega - \varepsilon_\sigma - \epsilon_i + \epsilon_{\bar{i}})\langle\langle d_i d_{\bar{i}}^\dagger c_\sigma, d_j^\dagger\rangle\rangle &= V_{\sigma\bar{i}}^\dagger\langle\langle d_i n_{\bar{i}}, d_j^\dagger\rangle\rangle - V_{\sigma\bar{i}}^\dagger f_\sigma\langle\langle d_i, d_j^\dagger\rangle\rangle\,, \\ (\omega - \varepsilon_\sigma)\langle\langle c_\sigma n_{\bar{i}}, d_j^\dagger\rangle\rangle &= V_{\sigma i}^\dagger\langle\langle d_i n_{\bar{i}}, d_j^\dagger\rangle\rangle + V_{\sigma\bar{i}}^\dagger f_\sigma\langle\langle d_{\bar{i}}, d_j^\dagger\rangle\rangle\,.\end{aligned} \tag{5.38}$$

Plugging this back into the equation of motion for Γ_i

$$\begin{aligned}\omega\Gamma_i = \delta_{ij}\langle n_{\bar{i}}\rangle - \delta_{\bar{i}j}\langle d_{\bar{i}}^\dagger d_i\rangle + (\epsilon_i + U)\Gamma_i + \sum_\sigma \frac{V_{\bar{i}\sigma}V_{\sigma\bar{i}}^\dagger(\Gamma_i - f_\sigma D_{ij}^r)}{\omega - \varepsilon_\sigma - \epsilon_i + \epsilon_{\bar{i}}} \\ + \sum_\sigma \frac{V_{i\sigma}(V_{\sigma i}^\dagger\Gamma_i + f_\sigma V_{\sigma\bar{i}}^\dagger D_{\bar{i}j}^r)}{\omega - \varepsilon_\sigma}\,.\end{aligned} \tag{5.39}$$

Owning to the strength of the on-site interaction

$$U\Gamma_i = \delta_{\bar{i}j}\langle d_{\bar{i}}^\dagger d_i\rangle - \delta_{ij}\langle n_{\bar{i}}\rangle + \sum_\sigma \frac{f_\sigma V_{\bar{i}\sigma}V_{\sigma\bar{i}}^\dagger}{\omega - \varepsilon_\sigma - \epsilon_i + \epsilon_{\bar{i}}} D_{ij}^r - \sum_\sigma \frac{f_\sigma V_{i\sigma}V_{\sigma\bar{i}}^\dagger}{\omega - \varepsilon_\sigma} D_{\bar{i}j}^r\,, \tag{5.40}$$

which, in turn, is used to solve the expression for the original Green's function

$$(\omega - \epsilon_i)D_{ij}^r = \delta_{ij} + \delta_{\bar{i}j}\langle d_{\bar{i}}^\dagger d_i\rangle - \delta_{ij}\langle n_{\bar{i}}\rangle + \sum_\sigma(\Sigma_{i\sigma}^0 + \Sigma_{i\sigma}^1)D_{\sigma j}^r \tag{5.41}$$

[1]However, an approximation similar to [Lac81], although more complicated, gives more accurate results.

where we have defined the noninteracting (tunneling) self energy Σ^0 and the Anderson dot self energy Σ^1 as

$$\begin{aligned}
\Sigma^0_{ij} &= \frac{\sum_{k\sigma} V_{i\sigma} V^\dagger_{\sigma j}}{\omega + i\eta - \varepsilon_{k\sigma}}\,, \\
\Sigma^1_{ii} &= \sum_{k\sigma} \frac{f_\sigma(\varepsilon_{k\sigma}) V_{\bar{i}\sigma} V^\dagger_{\sigma\bar{i}}}{\omega + i\eta - \varepsilon_{k\sigma} - \epsilon_i + \epsilon_{\bar{i}}}\,, \\
\Sigma^1_{i\bar{i}} &= -\sum_{k\sigma} \frac{f_\sigma(\varepsilon_{k\sigma}) V_{i\sigma} V^\dagger_{\sigma\bar{i}}}{\omega + i\eta - \varepsilon_{k\sigma}}\,.
\end{aligned} \tag{5.42}$$

Equivalently, we may write this as

$$(\mathbf{d}_0^{-1} - \Sigma^0 - \Sigma^1)\mathbf{D}^r = \tilde{\mathbf{n}}\,, \tag{5.43}$$

where $d_{0ij} = \delta_{ij}(\omega - \epsilon_i)^{-1}$ is the free Green's function on the dot and $\tilde{n}_{ii} = 1 - \langle n_{\bar{i}} \rangle$ and $\tilde{n}_{i\bar{i}} = \langle d^\dagger_{\bar{i}} d_i \rangle$ which agrees with [SWW06]. $\tilde{\mathbf{n}}$ must determined self-consistently from the occupation number on the dot as defined by

$$\begin{aligned}
\langle n_i \rangle &= \mathrm{Im} \int \frac{\mathrm{d}\omega}{2\pi} D^<_{ii}(\omega)\,, \\
\langle d^\dagger_{\bar{i}i} \rangle &= -i\mathrm{Im} \int \frac{\mathrm{d}\omega}{2\pi} D^<_{i\bar{i}}(\omega)\,,
\end{aligned} \tag{5.44}$$

by definition of lesser Green's functions.

Because we may trivially identify $\Sigma^0 = W^r$, we need only evaluate Σ^1 which has the form

$$\sum_{k\sigma\gamma} \frac{f_{\sigma\gamma}(\varepsilon_{k\sigma}) V_{\bar{i}\sigma\gamma} V^\dagger_{\sigma\bar{i}\gamma}}{\omega + i\eta - \varepsilon_{k\sigma} - A} = \sum_{k\sigma\gamma} f_{\sigma\gamma}(\varepsilon_{k\sigma}) V_{\bar{i}\sigma\gamma} V^\dagger_{\sigma\bar{i}\gamma} \left[-i\pi\delta(\omega - \varepsilon_{k\sigma} - A) + \frac{1}{\pi}\mathcal{P}\frac{1}{\omega - \varepsilon_{k\sigma} - A} \right]. \tag{5.45}$$

Defining the functions $\mathcal{G}_{\sigma\gamma}(\omega) = (1/i\pi)\mathcal{P}\int \mathrm{d}\omega' f_{\sigma\gamma}(\omega')/(\omega - \omega')$,

$$\begin{aligned}
\Sigma^1_{ii} &= (i/2) \sum_\gamma \left[f_{i\gamma}(\omega - \epsilon_i + \epsilon_{\bar{i}}) + \mathcal{G}_{i\gamma}(\omega - \epsilon_i + \epsilon_{\bar{i}}) \right] \Gamma_{i\gamma} \cos^2(\theta_\gamma/2) \\
&\quad + \left[f_{\bar{i}\gamma}(\omega - \epsilon_{\bar{i}} + \epsilon_i) + \mathcal{G}_{\bar{i}\gamma}(\omega - \epsilon_{\bar{i}} + \epsilon_i) \right] \Gamma_{\bar{i}\gamma} \sin^2(\theta_\gamma/2)\,, \\
\Sigma^1_{\uparrow\downarrow} &= \Sigma^<_{\downarrow\uparrow} = -(i/4) \sum_\gamma \left\{ \left[f_{\uparrow\gamma}(\omega) + \mathcal{G}_{\uparrow\gamma}(\omega) \right] \Gamma_{\uparrow\gamma} - \left[f_{\downarrow\gamma}(\omega) + \mathcal{G}_{\downarrow\gamma}(\omega) \right] \Gamma_{\downarrow\gamma} \right\} \sin\theta_\gamma\,.
\end{aligned} \tag{5.46}$$

In the zero temperature limit we can evaluate this analytically

$$\mathcal{G}_{\sigma\gamma}(\omega) = \mathcal{P}\int_{-D}^{\mu_{\sigma\gamma}} \frac{\mathrm{d}\omega'}{i\pi}\frac{1}{\omega-\omega'} = -\frac{1}{\pi i}\ln\left|\frac{\omega-\mu_{\sigma\gamma}}{\omega+D}\right| . \tag{5.47}$$

5.4 Outlook

We envision further broadening the application of this methodology to insulating rather than metallic ferromagnetic leads in which only magnons can tunnel through the interlayer. Because the lead is insulating we expect no hybridization between the conduction electrons and a single electron quantum dot. The lack of a Kondo cloud should be indicative in a simplification of the many-body Green's function of the dot.

Bibliography

[AZL11] P. Khalili Amiri, Z. M. Zeng, J. Langer, H. Zhao, G. Rowlands, Y.-J. Chen, I. N. Krivorotov, J.-P. Wang, H. W. Jiang, J. A. Katine, Y. Huai, K. Galatsis, and K. L. Wang. "Switching current reduction using perpendicular anisotropy in CoFeB–MgO magnetic tunnel junctions." *Appl. Phys. Lett.*, **98**(11):112507, 2011.

[BAP11] SE Barnes, M. Aprili, I. Petković, and S. Maekawa. "Ferromagnetic resonance with a magnetic Josephson junction." *Superconductor Science and Technology*, **24**:024020, 2011.

[BB08] V. Braude and Ya. M. Blanter. "Triplet Josephson Effect with Magnetic Feedback in a Superconductor-Ferromagnet Heterostructure." *Phys. Rev. Lett.*, **100**(20):207001 2008.

[Ber96] L. Berger. "Emission of spin waves by a magnetic multilayer traversed by a current." *Phys. Rev. B*, **54**(13):9353–9358 1996.

[BL74] S. M. Bhagat and P. Lubitz. "Temperature variation of ferromagnetic relaxation in the 3*d* transition metals." *Phys. Rev. B*, **10**:179–185 1974.

[BL11] Annica M. Black-Schaffer and Jacob Linder. "Magnetization dynamics and Majorana fermions in ferromagnetic Josephson junctions along the quantum spin Hall edge." *Phys. Rev. B*, **83**:220511 2011.

[BMS09] G. Bertotti, I. Mayergoyz, and C. Serpico. *Nonlinear Magnetization Dynamics in Nanosystems.* Elsevier, 2009.

[BR84] Y.A. Bychkov and EI Rashba. "Oscillatory effects and the magnetic susceptibility of carriers in inversion layers." *J. Phys. C: Solid State Phys.*, **17**:6039, 1984.

[BTB02] A. Brataas, Y. Tserkovnyak, G.E.W. Bauer, and B.I. Halperin. "Spin battery operated by ferromagnetic resonance." *Phys. Rev. B*, **66**:060404, 2002.

[Buz08] A. Buzdin. "Direct Coupling Between Magnetism and Superconducting Current in the Josephson φ_0 Junction." *Phys. Rev. Lett.*, **101**(10):107005 2008.

[BVE01] F. S. Bergeret, A. F. Volkov, and K. B. Efetov. "Enhancement of the Josephson Current by an Exchange Field in Superconductor-Ferromagnet Structures." *Phys. Rev. Lett.*, **86**:3140–3143 2001.

[BVE05] F. S. Bergeret, A. F. Volkov, and K. B. Efetov. "Odd triplet superconductivity and related phenomena in superconductor-ferromagnet structures." *Rev. Mod. Phys.*, **77**(4):1321–1373 2005.

[CAD10] E. Chen, D. Apalkov, Z. Diao, A. Driskill-Smith, D. Druist, D. Lottis, V. Nikitin, X. Tang, S. Watts, S. Wang, S.A. Wolf, A.W. Ghosh, J.W. Lu, S.J. Poon, M. Stan, W.H. Butler, S. Gupta, C. Mewes, T. Mewes, and P.B. Visscher. "Advances and Future Prospects of Spin-Transfer Torque Random Access Memory." *Magnetics, IEEE Transactions on*, **46**(6):1873 –1878 2010.

[CC10] Liufei Cai and E. M. Chudnovsky. "Interaction of a nanomagnet with a weak superconducting link." *Phys. Rev. B*, **82**:104429 2010.

[CCN71] C. Caroli, R. Combescot, P. Nozieres, and D. Saint-James. "Direct calculation of the tunneling current." *J. Phys. C: Solid State Phys.*, **4**:916, 1971.

[COL09] A. Chernyshov, M. Overby, X. Liu, J. K. Furdyna, Y. Lyanda-Geller, and L. P. Rokhinson. "Evidence for reversible control of magnetization

in a ferromagnetic material by means of spin-orbit magnetic field." *Nature Phys.*, **5**:656–659 2009.

[FTB02] J. Faure-Vincent, C. Tiusan, C. Bellouard, E. Popova, M. Hehn, F. Montaigne, and A. Schuhl. "Interlayer Magnetic Coupling Interactions of Two Ferromagnetic Layers by Spin Polarized Tunneling." *Phys. Rev. Lett.*, **89**:107206 2002.

[GH83] J. Guckenheimer and P. Holmes. *Nonlinear Oscillations, Dynamical Systems and Bifurcations of Vector Fields*. Springer, 1983.

[Gil04] T.L. Gilbert. "A phenomenological theory of damping in ferromagnetic materials." *Magnetics, IEEE Transactions on*, **40**(6):3443 – 3449, 2004.

[HBT10] K. M. D. Hals, A. Brataas, and Y. Tserkovnyak. "Scattering theory of charge-currentinduced magnetization dynamics." *Europhys. Lett.*, **90**(4):47002, 2010.

[HBT12] Silas Hoffman, Ya. M. Blanter, and Yaroslav Tserkovnyak. "Nonlinear dynamics in a magnetic Josephson junction." *Phys. Rev. B*, **86**:054427 2012.

[HJ08] H. Haug and A.P. Jauho. *Quantum kinetics in transport and optics of semiconductors*, volume 6. Springer Verlag, 2008.

[HYO05] Y. Higo, K. Yamane, K. Ohba, H. Narisawa, K. Bessho, M. Hosomi, and H. Kano. "Thermal activation effect on spin transfer switching in magnetic tunnel junctions." *Appl. Phys. Lett.*, **87**:082502, 2005.

[IHL07] S. Ikeda, J. Hayakawa, Young Min Lee, F. Matsukura, Y. Ohno, T. Hanyu, and H. Ohno. "Magnetic Tunnel Junctions for Spintronic Memories and Beyond." *IEEE Trans. El. Dev.*, **54**(5):991 –1002 2007.

[Jul75] M. Julliere. "Tunneling between ferromagnetic films." *Phys. Lett. A*, **54**(3):225 – 226, 1975.

[KB09] F. Konschelle and A. Buzdin. "Magnetic moment manipulation by a Josephson current." *Phys. Rev. Lett.*, **102**(1):17001, 2009.

[KGK06] R.S. Keizer, S.T.B. Goennenwein, T.M. Klapwijk, G. Miao, G. Xiao, and A. Gupta. "A spin triplet supercurrent through the half-metallic ferromagnet CrO2." *Nature*, **439**(7078):825–827, 2006.

[KKP10] T.S. Khaire, M.A. Khasawneh, WP Pratt Jr, and N.O. Birge. "Observation of spin-triplet superconductivity in Co-based Josephson junctions." *Phys. Rev. Lett.*, **104**(13):137002, 2010.

[KKS04] R. H. Koch, J. A. Katine, and J. Z. Sun. "Time-Resolved Reversal of Spin-Transfer Switching in a Nanomagnet." *Phys. Rev. Lett.*, **92**:088302 2004.

[Lac81] C. Lacroix. "Density of states for the Anderson model." *J. Phys. F: Met. Phys.*, **11**:2389, 1981.

[LD76] DC Langreth and JT Devreese. "Linear and nonlinear electron transport in solids." In *NATO Advanced Study Institute Series B*, volume 17, 1976.

[LD06] Kyung-Jin Lee and Bernard Dieny. "Micromagnetic investigation of the dynamics of magnetization switching induced by a spin polarized current." *Appl. Phys. Lett.*, **88**(13):132506, 2006.

[LDR04] K.-J. Lee, A. Deac, O. Redon, J.-P. Nozières, and B. Dieny. "Excitations of incoherent spin-waves due to spin-transfer torque." *Nature Materials*, **3**:877–881 2004.

[Lik86] K.K. Likharev. *Dynamics of Josephson Junctions and Circuits.* CRC Press, 1986.

[LKS04] D. Lacour, JA Katine, N. Smith, MJ Carey, and JR Childress. "Thermal effects on the magnetic-field dependence of spin-transfer-induced magnetization reversal." *Appl. Phys. Lett.*, **85**:4681, 2004.

[LY11] J. Linder and T. Yokoyama. "Supercurrent-induced magnetization dynamics in a Josephson junction with two misaligned ferromagnetic layers." *Phys. Rev. B*, **83**(1):012501, 2011.

[Mah93] G.D. Mahan. *Many-Particle Physics.* Plenum, 1993.

[MRK99] EB Myers, DC Ralph, JA Katine, RN Louie, and RA Buhrman. "Current-induced switching of domains in magnetic multilayer devices." *Science*, **285**(5429):867–870, 1999.

[MSN09] T. Maruyama, Y. Shiota, T. Nozaki, K. Ohta, N. Toda, M. Mizuguchi, A. A. Tulapurkar, T. Shinjo, M. Shiraishi, S. Mizukami, Y. Ando, and Y. Suzuki. "Large voltage-induced magnetic anisotropy change in a few atomic layers of iron." *Nature Nanotechnology*, **4**:158–161 2009.

[MW92] Y. Meir and N.S. Wingreen. "Landauer formula for the current through an interacting electron region." *Phys. Rev. Lett.*, **68**(16):2512–2515, 1992.

[MWL93] Y. Meir, N.S. Wingreen, and P.A. Lee. "Low-temperature transport through a quantum dot: The Anderson model out of equilibrium." *Phys. Rev. Lett.*, **70**(17):2601–2604, 1993.

[MZ08] A. Manchon and S. Zhang. "Theory of nonequilibrium intrinsic spin torque in a single nanomagnet." *Phys. Rev. B*, **78**:212405 2008.

[Ng96] T.K. Ng. "AC response in the nonequilibrium Anderson impurity model." *Phys. Rev. Lett.*, **76**(3):487–490, 1996.

[NSM12] T. Nozaki, Y. Shiota, S Miwa, F. Murakami, Bonel, S. Ishibashi, H. Kubota, K. Yakushiji, T. Saruya, A. Fukushima, S. Yuasa, T. Shinjo, and Suzuki Y. "Electric-field-induced ferromagnetic resonance excitation in an ultrathin ferromagnetic metal layer." *Nature Phys.*, 2012.

[PAB09] I. Petković, M. Aprili, SE Barnes, F. Beuneu, and S. Maekawa. "Direct dynamical coupling of spin modes and singlet Josephson supercurrent in ferromagnetic Josephson junctions." *Phys. Rev. B*, **80**(22):220502, 2009.

[PL80] L.P. Pitaevskii and E.M. Lifshitz. *Statistical Physics, Part 2: Volume 9.* Butterworth-Heinemann, 1980.

[RML06] D. Ravelosona, S. Mangin, Y. Lemaho, J. A. Katine, B. D. Terris, and Eric E. Fullerton. "Domain Wall Creation in Nanostructures Driven by a Spin-Polarized Current." *Phys. Rev. Lett.*, **96**:186604 2006.

[RS08] D.C. Ralph and M.D. Stiles. "Spin transfer torques." *J. Magn. Magn. Mater.*, **320**(7):1190 – 1216, 2008.

[RWB10] J.W.A. Robinson, J.D.S. Witt, and M.G. Blamire. "Controlled injection of spin-triplet supercurrents into a strong ferromagnet." *Science*, **329**(5987):59–61, 2010.

[SCA08] J. P. Strachan, V. Chembrolu, Y. Acremann, X. W. Yu, A. A. Tulapurkar, T. Tyliszczak, J. A. Katine, M. J. Carey, M. R. Scheinfein, H. C. Siegmann, and J. Stöhr. "Direct Observation of Spin-Torque Driven Magnetization Reversal through Nonuniform Modes." *Phys. Rev. Lett.*, **100**:247201 2008.

[Slo89] J. C. Slonczewski. "Conductance and exchange coupling of two ferromagnets separated by a tunneling barrier." *Phys. Rev. B*, **39**(10):6995–7002 1989.

[Slo96] J. C. Slonczewski. "Current-driven excitation of magnetic multilayers." *J. Magn. Magn. Mater.*, **159**(12):L1 – L7, 1996.

[Slo05] J. C. Slonczewski. "Currents, torques, and polarization factors in magnetic tunnel junctions." *Phys. Rev. B*, **71**(2):024411, 2005.

[SNB11] Y. Shiota, T. Nozaki, F. Bonell, S. Murakami, T. Shinjo, and Y. Suzuki. "Induction of coherent magnetization switching in a few atomic layers of FeCo using voltage pulses." *Nature Materials*, **11**(1):39–43, 2011.

[SW48] E.C. Stoner and EP Wohlfarth. "A mechanism of magnetic hysteresis in heterogeneous alloys." *Philosophical Transactions of the Royal Society of London. Series A. Mathematical and Physical Sciences*, pp. 599–642, 1948.

[SWW06] R. Świrkowicz, M. Wilczyński, M. Wawrzyniak, and J. Barnaś. "Kondo effect in quantum dots coupled to ferromagnetic leads with noncollinear magnetizations." *Phys. Rev. B*, **73**(19):193312, 2006.

[TBB05] Yaroslav Tserkovnyak, Arne Brataas, Gerrit E. W. Bauer, and Bertrand I. Halperin. "Nonlocal magnetization dynamics in ferromagnetic heterostructures." *Rev. Mod. Phys.*, **77**(4):1375–1421 2005.

[TG08] C. Tannous and J. Gieraltowski. "The Stoner–Wohlfarth model of ferromagnetism." *Eur. J. Phys.*, **29**:475, 2008.

[TJB98] M. Tsoi, A. G. M. Jansen, J. Bass, W.-C. Chiang, M. Seck, V. Tsoi, and P. Wyder. "Excitation of a Magnetic Multilayer by an Electric Current." *Phys. Rev. Lett.*, **80**:4281–4284 1998.

[TMX08] Y. Tserkovnyak, T. Moriyama, and J.Q. Xiao. "Tunnel-barrier-enhanced dc voltage signals induced by magnetization dynamics in magnetic tunnel junctions." *Phys. Rev. B*, **78**(2):020401, 2008.

[TYN09] Yukio Tanaka, Takehito Yokoyama, and Naoto Nagaosa. "Manipulation of the Majorana Fermion, Andreev Reflection, and Josephson Current on Topological Insulators." *Phys. Rev. Lett.*, **103**:107002 2009.

[UAK11] P. Upadhyaya, P.K. Amiri, A.A. Kovalev, Y. Tserkovnyak, G. Rowlands, Z. Zeng, I. Krivorotov, H. Jiang, and K.L. Wang. "Thermal stability characterization of magnetic tunnel junctions using hard-axis magnetoresistance measurements." *J. Appl. Phys.*, **109**:07C708, 2011.

[UTH08] K. Uchida, S. Takahashi, K. Harii, J. Ieda, W. Koshibae, K. Ando, S. Maekawa, and E. Saitoh. "Observation of the spin Seebeck effect." *Nature*, **455**(7214):778–781, 2008.

[WB02] Xavier Waintal and Piet W. Brouwer. "Magnetic exchange interaction induced by a Josephson current." *Phys. Rev. B*, **65**:054407 2002.

[WFM07] M. Weisheit, S. Fähler, A. Marty, Y. Souche, C. Poinsignon, and D. Givord. "Electric field-induced modification of magnetism in thin-film ferromagnets." *Science*, **315**(5810):349–351, 2007.

[WLH11] W.G. Wang, M. Li, S. Hageman, and CL Chien. "Electric-field-assisted switching in magnetic tunnel junctions." *Nature Materials*, 2011.

[YTF04] K. Yagami, AA Tulapurkar, A. Fukushima, and Y. Suzuki. "Low-current spin-transfer switching and its thermal durability in a low-saturation-magnetization nanomagnet." *Appl. Phys. Lett.*, **85**(23):5634–5636, 2004.

[ZKR12] Jian Zhu, J. A. Katine, Graham E. Rowlands, Yu-Jin Chen, Zheng Duan, Juan G. Alzate, Pramey Upadhyaya, Juergen Langer, Pedram Khalili Amiri, Kang L. Wang, and Ilya N. Krivorotov. "Voltage-Induced Ferromagnetic Resonance in Magnetic Tunnel Junctions." *Phys. Rev. Lett.*, **108**:197203 2012.

[ZTV05] M. Ye. Zhuravlev, E. Y. Tsymbal, and A. V. Vedyayev. "Impurity-Assisted Interlayer Exchange Coupling across a Tunnel Barrier." *Phys. Rev. Lett.*, **94**:026806 2005.

[ZVV06] M.Y. Zhuravlev, J. Velev, AV Vedyayev, and E.Y. Tsymbal. "Effect of oxygen vacancies on interlayer exchange coupling in Fe/MgO/Fe tunnel junctions." *J. Magn. Magn. Mater.*, **300**(1):e277–e280, 2006.

[ZZY09] H. Zhang, G.M. Zhang, and L. Yu. "Spin transport properties of a quantum dot coupled to ferromagnetic leads with noncollinear magnetizations." *J. Phys.: Condens. Matter*, **21**(15):155501, 2009.